Functional Comparison of Human and Murine Equilibrative Nucleobase Transporter 1

by

Chan Sungchan Kim

A thesis submitted in partial fulfillment of the requirements for the degree of

Master of Science

Department of Pharmacology
University of Alberta

Abstract

6-Mercaptopurine (6-MP) maintenance therapy is the mainstay for various types of leukemia and inflammatory bowel disease (IBD). 6-MP is associated with numerous adverse effects including gastrointestinal intolerance, myelotoxicity and hepatotoxicity. This can lead to therapy discontinuation which is associated with a higher risk of relapse. Drug transporter expression is a known factor for patient variability in drug response and toxicity. We have established that SLC43A3-encoded equilibrative nucleobase transporter 1 (ENBT1) mediates the transport of 6-MP into human lymphocytes and human embryonic kidney 293 (HEK293) cell lines transfected with SLC43A3. ENBT1 is known to be expressed in the gastrointestinal tract, bone marrow, and the liver. However, the relationship between ENBT1 and 6-MP-associated adverse events, or 6-MP pharmacokinetics are not known. To validate the use of a novel slc43a3 knockout (KO) mouse for exploring this relationship, we assessed the functional similarities between human and murine ENBT1 using transfected-HEK293 cell lines, MOLT-4 and L1210 leukemia cell lines, and a FL83B hepatic cell line. Based on in silico analysis of structural similarities between transporters, we hypothesized that human and murine ENBT1 will have similar 6-MP transport/inhibition kinetics and mediate 6-MP effect on cell viability similarly. Our results show that recombinant and endogenous hENBT1 and mENBT1 are functionally similar in regards to ENBT1-mediated 6-MP cellular accumulation and mediating 6-MP deleterious effect on cell viability.

Overall, these findings support the utilization of a slc43a3 KO mouse model to explore the role of ENBT1 in 6-MP/6-MP metabolite absorption, cellular accumulation, and tissue biodistribution.

Preface

This thesis is an original work by Chan Sungchan Kim.

The creation and initial characterization of transfected-HEK293 cell models utilized in this thesis was started by Nicholas M Ruel, a Ph.D. candidate, and further work was aided by undergraduate students Aaron L Sayler and Hannah Dean, all from the Hammond laboratory. A version of chapters 4 and 5 will be published as Kim, C. S.; Ruel, N. M.; Sayler, A. L.; Dean, H.; Hammond, J. R.: *Functional Comparison of Recombinant and Endogenously Expressed Human and murine Equilibrative Nucleobase Transporter 1* (*Tentative title*). I was responsible for data collection, data analysis, and manuscript composition. Nicholas M Ruel was responsible for the creation of the transfected-HEK293 cell lines and for preliminary 6-MP transport kinetic assays in the HEK293-mslc43a3 cell line. Aaron L Sayler was responsible for 6-MP transport kinetic assays in leukemia cell lines. Hannah Dean was responsible for various 6-MP/6-MP metabolite cell viability assays in transfected-HEK293 cell lines. Dr. James R Hammond provided manuscript edits and was involved with concept formation, manuscript composition and submission.

All research work in this thesis received research ethics approval from the University of Alberta Animal Ethics Board, protocol AUP00002022.

DEDICATION

We are all here on Earth to help others;

what on earth the others are here for, I don't know.

- W. H. Auden and J. F. Hall

ACKNOWLEDGEMENTS

Dr. Maria Spavor and Colleagues.

This thesis would not exist without the tireless efforts of you and those at the 4E3 pediatric oncology/hematology clinic. My heartfelt gratitude for granting me the opportunity to realize my potential in life.

Dr. Bruce Dick and Kathy Reid.

Thank you for always pointing me towards the right path and for continuing to be an essential pillar of support. Words are inadequate to describe how your decades of counseling and encouragement have shaped me as an individual.

…

Dr. David Eisenstat.

Thank you for taking a chance on me and being my gateway into academia. I feel blessed for your introduction to a P.I. and project that perfectly reflect my research interests and personal passions.

Members of my supervisory committee, Dr. Elaine Leslie and Dr. John Seubert.

The significance of my scientific work was undoubtedly strengthened by your suggestions. Thank you for your thoughtful advice, expertise, and constructive criticism during this process.

Past and present members of the Hammond Lab.

It has been a pleasure working with such compassionate and knowledgeable people. Thank you for your assistance and support over the years, this thesis would not have been half as coherent without you all.

…

My supervisor, Dr. James R Hammond.

Thank you for welcoming me into a group that became my second family for the past 5 years and for always taking the time to listen to my concerns. Your continuous guidance and support have molded me into a wiser individual that can play gracefully with ideas.

…

My Father, YoungWook Kim.

For giving me the strength to move forward during the lowest points in my life; your tenacity and perspective on life truly inspire me. You are my superhero and good friend.

And finally, to my Mother, Iris Wee.

For your endless support, understanding, and affection during my endeavors. Your son is doing better than ever and is working on accomplishing his dreams. So please stop blaming yourself.

TABLE OF CONTENTS

LIST OF TABLES

Chapter 3. Materials and methods:

LIST OF FIGURES

Chapter 1. Introduction:

Chapter 3. Materials and methods:

Chapter 4. Recombinant ENBT1:

Chapter 5. Endogenous ENBT1:

Appendix:

Glossary of Abbreviations

ALL	acute lymphoblastic leukemia
AML	acute myelogenous leukemia
A_1AR	adenosine A1 receptor
$A_{2A}AR$	adenosine A2A receptor
$A_{2B}AR$	adenosine A2B Receptor
A_3AR	adenosine A3 receptor
ADP	adenosine diphosphate
AMP	adenosine monophosphate
ATP	adenosine triphosphate
aa	amino acid
ANOVA	analysis of variance
AUC	area under the curve
Asn	asparagine
bp	base pair
BCA	bicinchoninic acid
K_{on}	binding rate constant
BSA	bovine serum albumin
CML	chronic myelogenous leukemia
cDNA	complementary DNA
CNT	concentrative nucleoside transporters
CD	Crohn's disease
Ci	Curie
Ct	cycle threshold
D22	decynium-22
dATP	deoxyadenosine triphosphate
dGTP	deoxyguanosine triphosphate
DNA	deoxyribonucleic acid
DMSO	dimethyl sulfoxide
DY	dipyridamole
DPM	disintegrations per minute
K_{off}	dissociation rate constant
dH_2O	distilled water
DMEM	Dulbecco's modified Eagle's medium
DPBS	Dulbecco's phosphate buffered saline
EEG1	embryonic epithelia gene 1
ECL	enhanced chemiluminescence
EDTA	ethylenediaminetetraacetic acid
ENBT1	equilibrative nucleobase transporter 1
ENT	equilibrative nucleoside transporters
FBS	fetal bovine serum
Fwd	forward
Geneticin	G418 sulfate

Gln	glutamine
GDA	guanine deaminase
GMP	guanine monophosphate
GMPS	guanosine monophosphate synthetase
EC_{50}	Half maximal effective concentration
IC_{50}	Half maximal inhibitory concentration
HRP	horseradish peroxidase
HEK293	human embryonic kidney 293 cells
HD	Huntington's disease
HGPRT	hypoxanthine-guanine phosphoribosyl transferase
IBD	inflammatory bowel disease
IMP	inosine monophosphate
IMPDH	inosine monophosphate dehydrogenase
K_i	inhibition constant
KO	knockout
LDH	lactate dehydrogenase
MDCKII	Madin-Darby canine kidney cells
MFS	major facilitator superfamily
C_{max}	maximal 6-MP plasma concentration
V_{max}	maximal velocity of transport
6-MP	6-mercaptopurine
NMG	N-methyl-D-glucamine
6-MeMP	6-methylmercaptopurine
6-MeMPR	6-methylmercaptopurine ribonucleotide
6-MeTG	6-methylthioguanine
6-MeTGMP	6-methylthioguanine monophosphate
6-MeTIMP	6-methylthioinosine monophosphate
K_m	Michaelis constant
MMR	mismatch repair
MTT	3-(4,5-dimethylthiazol-2-yl)-2,5-diphenyltetrazolium bromide
NBMPR	nitrobenzylmercaptopurine
NDPK	nucleoside-diphosphate kinase
NMPK	nucleoside-phosphate kinase
NUDT15	nudix hydrolase 15
PRPP	phosphoribosyl pyrophosphate
PolyQ	polyglutamine
PCR	polymerase chain reaction
RIPA	radioimmunoprecipitation
Rac1	Ras-related C3 botulinum toxin substrate 1
k	rate constant
Rcf	relative centrifugal field
Rev	reverse
RNA	ribonucleic acid
ROUT	robust regression and outlier removal

RPMI-1640	Roswell Park Memorial Institute 1640
qPCR	semi-quantitative PCR
SNBT	sodium-dependent nucleobase transporter
SVCT	sodium-dependent vitamin C transporter
SDS	sodium dodecyl sulfate
SDS-PAGE	sodium dodecyl sulfate-polyacrylamide gel electrophoresis
NaOH	sodium hydroxide
SLC	solute carrier
SD	standard deviation
6-TdGTP	6-thio-deoxyguanine triphosphate
6-TG	6-thioguanine
6-TGDP	6-thioguanine diphosphate
6-TGMP	6-thioguanine monophosphate
6-TGN	6-thioguanine nucleotides
6-TGTP	6-thioguanosine triphosphate
6-TIMP	6-thioinosine monophosphate
TPMT	thiopurine methyltransferase
6-TU	6-thiouric acid
6-TX	6-thioxanthine
6-TXMP	6-thioxanthosine monophosphate
TMD	transmembrane domain
TBS-T	tris-buffered saline-Tween20
LAT	L-type amino acid transporter
UC	ulcerative colitis
XO	xanthine oxidase

GLOSSARY OF GENES

*Human genes are capitalized; mouse genes are lowercased

slc23a1	sodium-dependent vitamin C transporter-1	***SLC43A3_2***	equilibrative nucleobase transporter 1 isoform 2
slc23a2	sodium-dependent vitamin C transporter-2	***XO***	xanthine oxidase
slc23a4	sodium-dependent nucleobase transporter 1	***TPMT***	thiopurine methyltransferase
SLC23A4P	sodium-dependent nucleobase transporter 1 pseudogene	***HGPRT***	hypoxanthine-guanine phosphoribosyltransferase
SLC29A1	equilibrative nucleoside transporter 1	***IMPDH1***	inosine-5′-monophosphate dehydrogenase
SLC29A2	equilibrative nucleoside transporter 2	***GMPS***	guanosine monophosphate synthetase
SLC29A4	equilibrative nucleoside transporter 4	***NUDT15***	nudix hydrolase 15
SLC28A2	concentrative nucleoside transporter 2	***ACTB***	β-actin
SLC28A3	concentrative nucleoside transporter 3	***TUBA1A***	alpha tubulin
SLC43A1	L-type amino acid transporter 3	***GAPDH***	glyceraldehyde 3-phosphate dehydrogenase
SLC43A2	L-type amino acid transporter 4	***ABCC4***	multidrug resistance-associated protein 4
SLC43A3_1	equilibrative nucleobase transporter 1 isoform 1	***ABCC5***	multidrug resistance-associated protein 5

CHAPTER 1.

Introduction

1.1 General History of Nucleoside/Nucleobase Transporters

1.1.a Equilibrative Nucleoside Transporters

Equilibrative nucleoside transporters (ENTs) have an intriguing history in the field of molecular biology and cellular physiology. The first clues to the existence of ENTs came in the early 1970s when researchers observed nitrobenzylmercaptopurine riboside (NBMPR) sensitive transport of nucleosides across cell membranes, suggesting the presence of specialized transport proteins (Oliver and Paterson, 1971; Pickard and Paterson, 1972). It wasn't until the mid-1990s that the first ENT gene, *SLC29A1*/ENT1, was cloned and characterized in human and rat (Griffiths et al., 1997; Yao et al., 1997; Coe et al., 1997). This breakthrough led to the discovery of other members of the SLC29 family, notably *SLC29A2*/ENT2 (Yao et al., 1997; Crawford et al., 1998), which further expanded our knowledge of these transporters and their roles in various cellular processes. In the subsequent years, researchers delved deeper into the functions of ENT1 and ENT2 and found that these transporters play a crucial role in maintaining cellular nucleoside homeostasis by facilitating the bidirectional movement of purine and pyrimidine nucleosides and nucleobases at low affinities (Baldwin et al., 2004; Young et al., 2013), across cell membranes and thus are essential for DNA and RNA synthesis, energy transfer, and various signaling pathways (Griffiths et al., 1997; Jarvis and Young, 1987; Baldwin et al., 2004; Rose et al., 2010). The investigation of ENTs also revealed their significance in pharmacology, as they influence the accumulation/efficacy of anti-cancer and anti-viral nucleoside/nucleobase analog drugs (Coe et al., 1997; Crawford et al., 1998; Jarvis and Young, 1987; Baldwin et al., 2004), and are druggable targets for vasodilation (Lin and Buolamwini, 2007; Paproski et al., 2008) and cardio protection against ischemia-reperfusion injury (Yang and Leung, 2015; Ruan et al., 2023).

1.1.b **Concentrative Nucleoside Transporters**

The history of concentrative nucleoside transporters (CNTs) is equally interesting and has significantly contributed to our understanding of nucleoside transport mechanisms. The quest to uncover these transporters began in the 1970s when researchers observed the active transport of nucleosides against their concentration gradient in cells (Oliver and Paterson, 1971). However, it wasn't until the late 1990s that the CNT genes, *SLC28A1*/CNT1 (Huang et al., 1994; Ritzel et al., 1997) and *SLC28A2*/CNT2 (Ritzel et al., 1998; Patel et al., 2000), were first cloned and identified in humans and mice. Following the discovery, CNTs were classified as secondary active transporters, utilizing the electrochemical gradient of sodium ions or protons to facilitate the accumulation of nucleosides in cells (Ritzel et al., 1997; Gray et al., 2004). As research progressed, additional members of the CNT family, such as *SLC28A3*/CNT3 (Ritzel et al., 2001) were identified, each showing distinct substrate specificities; CNT1 is pyrimidine selective/ sodium dependent, CNT2 is purine selective/sodium dependent, and CNT3 is pyrimidine and purine selective/sodium or proton dependent (Huang et al., 1994; Ritzel et al., 1998; Patel et al., 2000; Gray et al., 2004; Young et al., 2013). Much like the ENTs, further exploration of CNTs revealed their importance in pharmacology as the transporters play a crucial role in determining the accumulation and efficacy of anti-cancer and anti-viral nucleobase/ nucleoside analog drugs (Ritzel et al., 2001; Gray et al., 2004; Young et al., 2013).

1.1.c **Sodium-Dependent Nucleobase Transporter 1**

Sodium-dependent nucleobase transporter (SNBTs) is a relatively recent discovery (Yamamoto et al., 2010) that has been neglected due to low clinical relevance in humans. For decades, a high affinity nucleobase transporter had eluded researchers, however, many candidates have been proposed over the years. In 1999 the *SLC23A1*/sodium-

dependent vitamin C transporter (SVCT) (Hogue and Ling, 1999) gene was identified, then predicted to be a human nucleobase transporter-like protein, however, *SLC23A1*/SVCT1 and *SLC23A2*/SVCT2 are now known to be a sodium-dependent vitamin C transporter (Tsukaguchi et al., 1999). In 2010, the *slc23a4*/SNBT1 gene was identified in rats and characterized as the first nucleobase transporters in mammals with specificity for uracil and guanine nucleobase and analogs (Yamamoto et al., 2010; Yuasa et al., 2020). However, *SLC23A4P* is a pseudogene in humans and higher primates (NCBI Gene: 641842), thus cannot be responsible for nucleobase flux in humans (Yuasa et al., 2020). *slc23a4*/SNBT1 (NCBI Gene: 243753) expression has been found in mouse intestinal cells, however, function has not yet been characterized in mice. *slc23a4*/SNBT1 is of concern as this transporter may be a confounding source of intestinal drug absorption in rodents that is not present in humans.

1.1.d **L-type Amino Acid Transporters and Equilibrative Nucleobase Transporter 1**

The discovery of L-type amino acid transporters (LAT) began in the early 1950s when researchers observed that certain cells had specific mechanisms to transport amino acids across cell membranes (Christensen et al., 1952; Christensen and Riggs, 1952; Oxender and Christensen, 1963). Initial studies focused on identifying and characterizing these transporters (Kanai et al., 1998; Yanagida et al., 2001), which led to the cloning and identification of several LAT isoforms, most relevantly *SLC43A1*/LAT3 (Babu et al., 2003) and *SLC43A2*/LAT4 (Bodoy et al., 2005). These transporters have been investigated in cancer, neurological disorders, and metabolic diseases, and have been found to contribute to the accumulation of specific amino acids, and serve as important regulators of amino acid homeostasis. The third member of the SLC43 family, *SLC43A3*/embryonic epithelia gene 1 (EEG1), was first identified as an orphan

gene due to displaying no specificity for amino acids (Stuart et al., 2001; Bodoy et al., 2013). At the time the physiological function of EEG1 was unknown, however, EEG1 and LAT3 were thought to have a role in early development and growth (Stuart et al., 2001; Bodoy et al., 2013). *SLC43A3*/EEG1, herein by referred to as *SLC43A3*/equilibrative nucleobase transporter 1 (ENBT1), is one of the newer entries in a long history of nucleoside and nucleobase transporters. As previously described, those in the field of nucleoside transporters were interested in discovering a human nucleobase transporter. However, this search was relatively unsuccessful for many years, leading to suggestions that low affinity ENTs and CNTs were responsible for nucleobase uptake (Baldwin et al., 2004; Zaza et al., 2010; Young et al., 2013). This was until 2007, when Dr. Hammond and colleagues observed dipyridamole (DY)-insensitive and purine nucleobase-sensitive, cellular accumulation of hypoxanthine (Bone and Hammond, 2007) at μM range affinity compared to ENTs mM range affinity (Boswell-Casteek and Hays, 2017), which ruled out ENTs as the unknown nucleobase transporter. Further characterization of this unknown nucleobase transporter also exhibited no dependence on sodium ions or protons, which then ruled out CNTs as the unknown nucleobase transporter (Bone and Hammond, 2007).

The molecular identity of this nucleobase transporter remained unknown until 2015 when *SLC43A3*/ENBT1 was characterized in canine cells as a purine-selective nucleobase transporter involved in purine salvage, and the transport of guanine, adenine, and hypoxanthine (Furukawa et al., 2015). In 2019, our lab further characterized human ENBT1 isoforms/splice variants (*SLC43A3_1*/ENBT1.1 and *SLC43A3_2*/ENBT1.2), which are functionally similar in facilitating the bidirectional flux of the anti-cancer drug, 6-mercaptopurine (6-MP) (Ruel et al., 2019), and thus will not be differentiated for the purposes of this thesis. ENBT1 is of particular interest because it is broadly expressed in most tissues in both disease and non-disease states. Most clinically notable tissues include the gastrointestinal tract and bone marrow/

lymphocytes (Furukawa et al., 2015; Takenaka et al., 2020) (Figure. 1). ENBT1 is also detected in many cancer cell lines, including leukemias (93/93 cell lines), lymphomas (72/76 cell lines), and in skin cancers (61/62 cell lines), which have the highest expression levels (Human Protein Atlas; https://www.proteinatlas.org/) (Uhlen et al., 2015; Thul et al., 2017).

Figure 1. *SLC43A3* RNA tissue distribution and expression in cancer ►

A: Non-disease state human tissue distribution of SLC43A3 RNA expression colour-coded by tissue groups. **B:** Disease state SLC43A3 RNA expression based on human cancer cell lines, sorted from highest to lowest expression levels. Presented is consensus RNA expression data obtained from The Human Protein Atlas (HPA) (Human Protein Atlas; https:// www.proteinatlas.org/) (Uhlen et al., 2015; Thul et al., 2017). The HPA obtained raw RNA expression data from internal HPA sources and from the Genotype-Tissue Expression (GTEx) Project. Data from the two sources were normalized to transcripts per million protein coding genes (nTPM) to obtain consensus RNA expression data.

Figure 1.

A

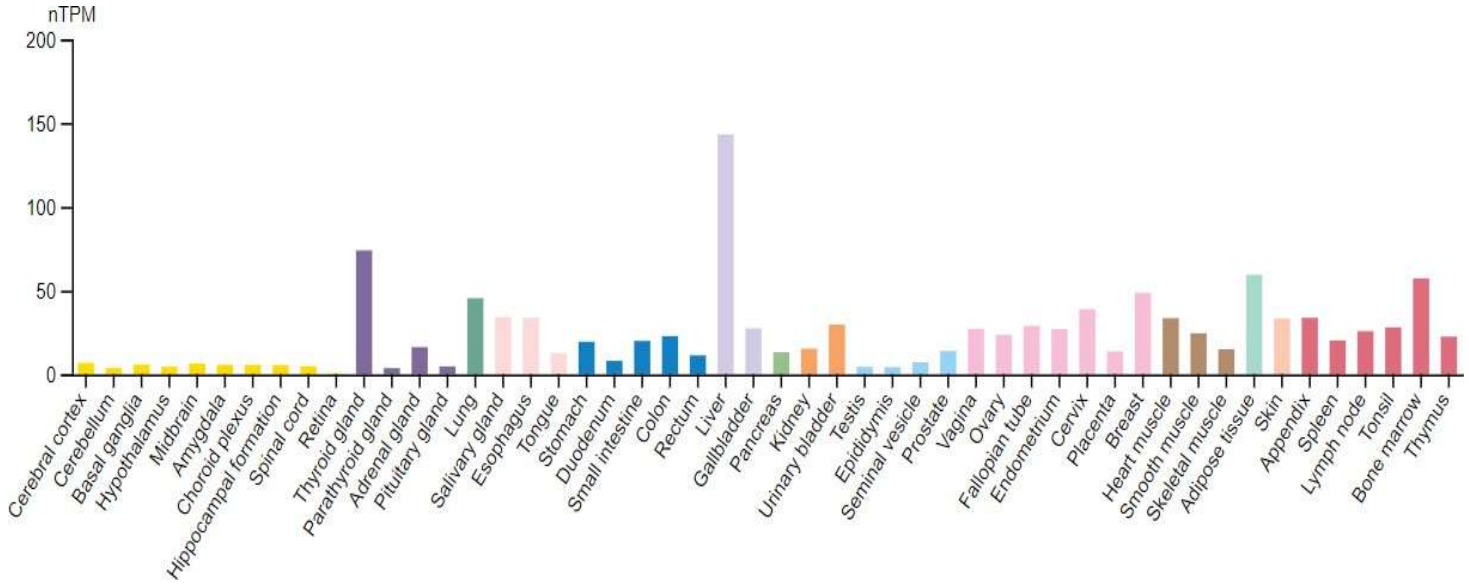
nTPM
200
150
100
50
0
Cerebral cortex
Cerebellum
Basal ganglia
Hypothalamus
Midbrain
Amygdala
Choroid plexus
Hippocampal formation
Spinal cord
Retina
Thyroid gland
Parathyroid gland
Adrenal gland
Pituitary gland
Lung
Salivary gland
Esophagus
Tongue
Stomach
Duodenum
Small intestine
Colon
Rectum
Liver
Gallbladder
Pancreas
Kidney
Urinary bladder
Testis
Epididymis
Seminal vesicle
Prostate
Vagina
Ovary
Fallopian tube
Endometrium
Cervix
Placenta
Breast
Heart muscle
Smooth muscle
Skeletal muscle
Adipose tissue
Skin
Appendix
Spleen
Lymph node
Tonsil
Bone marrow
Thymus

B

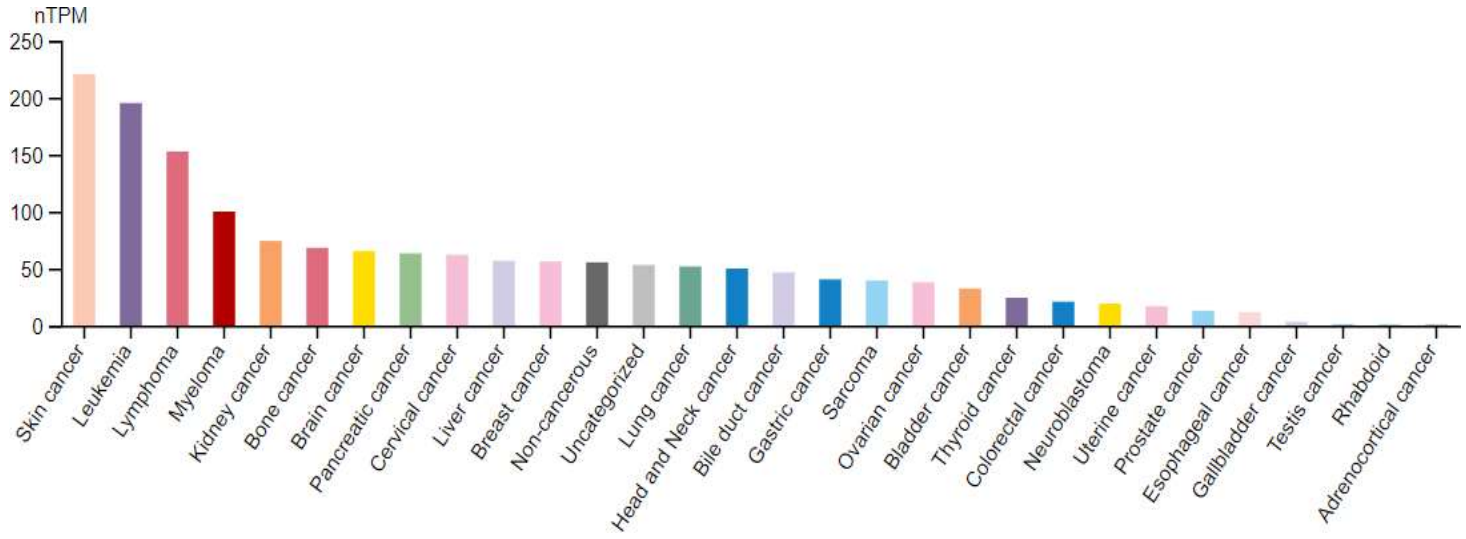
nTPM
250
200
150
100
50
0
Skin cancer
Leukemia
Lymphoma
Myeloma
Kidney cancer
Bone cancer
Brain cancer
Pancreatic cancer
Cervical cancer
Liver cancer
Breast cancer
Non-cancerous
Uncategorized
Lung cancer
Head and Neck cancer
Bile duct cancer
Gastric cancer
Sarcoma
Ovarian cancer
Bladder cancer
Thyroid cancer
Colorectal cancer
Neuroblastoma
Uterine cancer
Prostate cancer
Esophageal cancer
Gallbladder cancer
Testis cancer
Rhabdoid
Adrenocortical cancer

Figure 2. ENBT1 substrate structure ►

Chemical structures of relevant ENBT1 purine nucleobase and nucleobase analog substrates.

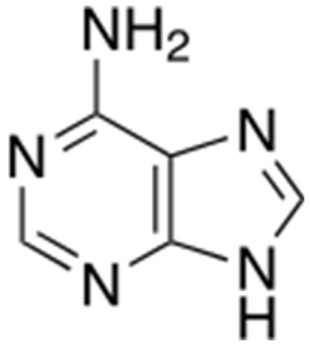

adenine

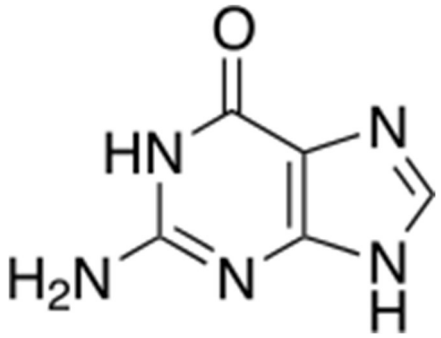

guanine

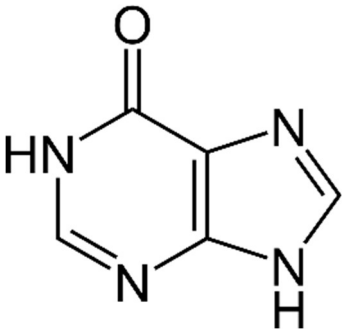

hypoxanthine

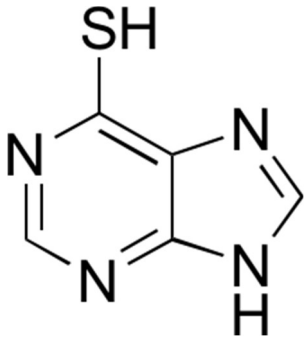

6-mercaptopurine

Table 1. Known ENBT1 substrate K_m values ►

Known published ENBT1 substrate K_m values. Adenine, hypoxanthine, and 6-MP K_m values were obtained by colleagues from the Hammond Lab (Bone and Hammond, 2007; Ruel et al., 2019). Guanine K_m values was obtained by an independent research group (Furukawa et al., 2015). * However, due to the selection of a 40 second time point, guanine K_m values obtained by Furukawa and colleagues, (2015) are likely inaccurate and more closely approximate enzyme kinetics for guanine and its downstream metabolite xanthine, rather than ENBT1 transport kinetics. Literature enzyme K_m values are as follows: guanine deaminase (GDA) guanine K_m = 0.20 mM - 1.66 mM (Kuman et al., 1967); xanthine oxidase (XO): xanthine K_m = 17 μM (Yang et al., 2021). More on the topic of selecting appropriate time points will be discussed in section 4.3.c.iii.

Table 1.

ENBT1 Substrate	**ENBT1 K_m (µM)**	**Citation**
adenine	37 ± 26	Ruel et al., 2019
guanine	1.70 *	Furukawa et al., 2015
hypoxanthine	96 ± 37	Bone and Hammond, 2007
6-mercaptopurine	163 ± 126	Ruel et al., 2019

1.1.e **Physiological Role of Nucleoside/Nucleobase Transporters**

Nucleobase and nucleoside transporters facilitate the bidirectional flux of nucleobases and nucleosides that would otherwise be unable to cross the plasma membrane due to their hydrophilic nature (Aymerich et al., 2005). These transporters are crucial for cell growth and proliferation, as they maintain intracellular concentrations of molecules that are involved in DNA, RNA, and nucleotide synthesis (Griffiths et al., 1997; Jarvis and Young, 1987; Baldwin et al., 2004; Rose et al., 2010). These transporters also play a key role in salvaging purine and pyrimidines from extracellular sources, which is an energy-efficient way for cells to maintain an adequate supply of nucleotides (Furukawa et al., 2015). This is especially crucial in rapidly dividing cells, such as immune cells and cancer cells, where the demand for nucleotides is high (Zhu and Thompson, 2019). Furthermore, nucleoside transporters regulate extracellular levels of adenosine, which is an agonist of 4 extracellular adenosine receptors (A_1AR, A_{2A}AR, A_{2B}AR, and A_3AR) that are known to have various regulatory functions in the central nervous system, cardiovascular system, and immune system (Eckle et al., 2007; Borea et al, 2018). An example in the cardiovascular system, is adenosine signaling acting as a cardioprotective mechanism in response to cardiovascular stress (Eckle et al., 2007; Headrick et al., 2011; Yang and Leung, 2015; Ruan et al., 2023); in times of reduced oxygen availability during tissue hypoxia, extracellular adenosine levels rise and act as a vasodilator, leading to increased blood flow/oxygen delivery to affected tissues (Eckle et al., 2007; Headrick et al., 2011; Yang and Leung, 2015). Adenosine can also slow heart rate by inhibiting impulse conduction generation in the sinoatrial node, the heart's natural pacemaker (Headrick et al., 2011). Finally, nucleobase and nucleoside transporters play a vital role in accumulating various nucleobase and nucleoside analog anti-cancer and anti-viral drugs (Coe et al., 1997; Crawford et al., 1998; Jarvis and

Young, 1987; Baldwin et al., 2004, Ritzel et al., 2001; Gray et al., 2004; Young et al., 2013; Ruel et al., 2019), making these transporters promising therapeutic targets in the treatment of various medical conditions.

1.2 6-Mercaptopurine and 6-thioguanine overview

1.2.a Clinical Usage

The history of the clinical usage of 6-MP dates back to 1951 when it was synthesized by Nobel Prize winners Gertrude Elion and George Hitchings (Elion G.B., 1986). By 1953, the drug was administered to the first pediatric patient with acute lymphoblastic leukemia (ALL), and remarkably induced remission and significantly prolonged survival rates (Burchenal et al., 1953; Hall et al., 1953; Hill and Lajous, 1954; Toksvang et al., 2022). Following its initial success in ALL, 6-MP gradually became an essential component of combination chemotherapy regimens and maintenance therapies for different types of leukemia, particularly ALL (Toksvang et al., 2022), chronic myelogenous leukemia (CML), and acute myelogenous leukemia (AML) (Fountain J.R., 1956; Curtis et al., 1975). As the understanding of its mechanisms of action improved, the clinical usage of 6-MP expanded to treat autoimmune disorders, such as rheumatoid arthritis (Mason et al., 1969; Suarez-Almazor et al, 2000), and Crohn's disease (CD) and ulcerative colitis (UC) (Brown and Achkar, 1970; Goldstein F. 1987), which are both colloquially referred to as inflammatory bowel disease (IBD). By the 1970s, 6-MP had become an indispensable drug in the field of oncology and immunology, playing a vital role in the management of these conditions. Around the 1980s, 6-thioguanine (6-TG), another drug in the same family as 6-MP, was found to have a more direct intracellular activation pathway than 6-MP and entered clinical trials for ALL (Lennard et al., 1993; Lancaster et al., 1998). To date, some cases have found that 6-TG has higher efficacy than 6-MP in the treatment of ALL (Stork

et al., 2010; Chen et al., 2020). However, the safety of 6-TG is often controversial as many studies have also observed higher adverse events (Lancaster et al., 1998; Stork et al., 2010; Toksvang et al., 2019; Chen et al., 2020), thus 6-TG usage in the clinic is not as common as 6-MP.

1.2.b **Mechanism of Action**

6-MP and 6-TG are a purine nucleobase analogue antimetabolite that belong to the thiopurine family of drugs, a group of compounds that is structurally similar to endogenous purine nucleobases, such as adenine, guanine, and hypoxanthine (Aarbakke et al., 1997; Giverhaug et al., 1999). Upon entering the cell, 6-MP and 6-TG undergo intracellular metabolism via various different pathways (Figure 3.), and is eventually metabolized into active metabolites such as **(1):** 6-Thioguanine nucleotides (6-TGN) disrupts DNA and RNA by self-incorporating into replicating DNA strands as false-nucleotides, leading to DNA damage/DNA lesions, and inducing DNA mismatch repair (MMR)-dependent G2 cell-cycle arrest or apoptosis (Aarbakke et al., 1997; Karran and Attard, 2008; Zaza et al., 2010; Shin et al., 2016; Fernandez-Ramos et al., 2017). **(2):** 6-Methylthioinosine monophosphate (6-MeTIMP) disrupts de novo nucleic acid synthesis by inhibiting phosphoribosyl pyrophosphate (PRPP) amidotransferase, which is the rate-limiting enzyme for purine synthesis (Skipper, H.E., 1954; Tay et al., 1969; Karran and Attard, 2008; Zaza et al., 2010; Fernandez-Ramos et al., 2017). Inhibition of de novo purine synthesis reduces supply of endogenous purine nucleotides and further exacerbates 6-TGN incorporation into DNA and RNA. 6-MeTIMP has not been confirmed to but is also likely linked to the depletion of intracellular adenosine monophosphate (AMP), adenosine diphosphate (ADP), and adenosine triphosphate (ATP), via inhibition of ATP synthesis, leading to energetic failure, altered cell metabolism, and overall decreased proliferative ability (Fernandez-Ramos et

al., 2017). **(3):** 6-Thioguanosine triphosphate (6-TGTP) complexes with Rac1 and blocks activation, which suppresses pro-survival pathways and promotes apoptosis in $CD4^+$ T-lymphocytes (Poppe et al., 2006; Zaza et al., 2010; Shin et al., 2016; Fernandez-Ramos et al., 2017). As a result of these mechanisms, cell division is impeded, leading to reduced proliferation and growth, and disproportionally affect rapidly dividing cells such as cancer cells and immune cells involved in autoimmune diseases.

1.2.c **Intracellular Metabolism**

The metabolic pathways of 6-MP are intricate and involve multiple enzymatic conversions that ultimately determine the drug's pharmacological activity (Figure 3.). Upon oral administration, 6-MP is absorbed into the bloodstream via the gastrointestinal tract, potentially by ENBT1 in humans and additionally by SNBT1 in rats (Yamamoto et al.,2010; Yuasa et al., 2020). Upon transport into cells, 6-MP undergoes extensive metabolism through three primary pathways, **(1):** the XO pathway, **(2):** the hypoxanthine-guanine phosphoribosyl transferase (HGPRT) pathway, **(3):** the thiopurine methyltransferase (TPMT) pathway (Aarbakke et al., 1997; Karran and Attard, 2008; Zaza et al., 2010). **(1):** In the XO pathway, 6-MP is oxidized by XO to form 6-thiouric acid (6-TU), a therapeutically inactive metabolite that is readily excreted via the urine (Jackson, P.J., 1983; Chan et al., 1990; Andersen et al., 1998; Bradford and Shih, 2011; Singh et al., 2017; Sheu et al., 2022). The XO pathway is considered the least significant of the three pathways in determining therapeutic outcome, as it is an excretion pathway that contributes to the inactivation of 6-MP. Additionally, most metabolism by XO occurs in the gastrointestinal tract and liver (Andersen et al., 1998; Ansari et al., 2008), and not in lymphocytes, which do not have measurable XO activity (Aarbakke et al., 1997).

(2): In the HGPRT pathway, 6-MP is converted to an intermediate metabolite, 6-thioinosine monophosphate (6-TIMP) by HGPRT. At this point 6-TIMP can either exit and enter the TPMT pathway or continue in the HGPRT pathway. Assuming 6-TIMP remains in the HGPRT pathway, inosine monophosphate dehydrogenase (IMPDH) dehydrates 6-TIMP to 6-thioxanthosine monophosphate (6-TXMP), then guanosine monophosphate synthetase (GMPS) converts 6-TXMP into 6-thioguanine monophosphate (6-TGMP). Sequentially, nucleoside-phosphate kinase (NMPK) converts 6-TGMP to 6-thioguanine diphosphate (6-TGDP) and nucleoside-diphosphate kinase (NDPK) converts 6-TGDP to 6-TGTP, which is then reduced via a reductase to 6-thio-deoxyguanine triphosphate (6-TdGTP) (Bradford and Shih, 2011; Singh et al., 2017; Sheu et al., 2022). Recently, nudix hydrolase 15 (NUDT15) has been shown to interfere with the HGPRT pathway by dephosphorylating 6-TGTP to 6-TGMP, preventing 6-TdGTP production (Singh et al., 2017; He and Liu, 2019). **(3):** In the TPMT pathway, 6-MP and various intermediates are methylated with various outcomes. 6-MP is methylated to 6-methylmercaptopurine (6-MeMP), a therapeutically inactive metabolite that has been linked to hepatotoxicity (Dubinsky et al., 2000; Nygaard et al., 2004; van Asseldonk et al., 2012). 6-TIMP is methylated to 6-MeTIMP, a therapeutically active metabolite that can be further converted to 6-methylmercaptourine ribonucleotide (6-MeMPR), a therapeutically inactive metabolite which has also been linked to hepatotoxicity (Dubinsky et al., 2000; Shaye et al., 2007). 6-TGMP is methylated to 6-methylthioguanine monophosphate (6-MeTGMP), a therapeutically inactive metabolite that is not often discussed (Dubinsky et al., 2000; Karran and Attard, 2008; Zaza et al., 2010; Bradford and Shih, 2011; Singh et al., 2017; Sheu et al., 2022). The metabolic pathway of 6-TG is more direct and involves metabolism through three primary pathways, **(1):** the guanase/XO pathway, **(2):** the HGPRT pathway, and **(3):** the TPMT pathway.

(1): In the guanase/XO pathway, 6-TG is converted by guanase to form 6-thioxanthine (6-TX), and then oxidized by XO to form 6-TU (Bradford and Shih, 2011). (2): In the HGPRT pathway, 6-TG is converted by HGPRT directly to 6-TGMP (Aarbakke et al., 1997; Karran and Attard, 2008; Zaza et al., 2010; Bradford and Shih, 2011; Toksvang et al., 2022), which then is eventually metabolized to 6-TGTP and 6-TdGTP, by the various kinases that have been previously described above. **(3):** In the TPMT pathway 6-TG is methylated to 6-methylthioguanine (6-MeTG), a therapeutically inactive metabolite (Aarbakke et al., 1997; Karran and Attard, 2008; Toksvang et al., 2022). Understanding these three metabolic pathways is crucial for optimizing the clinical usage of 6-MP, as genetic variations that result in variability in the activity of enzymes involved in these pathways can lead to individual differences in drug response and off-target toxicity.

Figure 3. 6-MP intracellular metabolic pathway ►

Metabolic pathway of 6-MP and 6-TG upon transport into cell, labeled as the HGPRT pathway (Green), the TPMT pathway (Blue), and the XO pathway (Orange).

Abbreviations - 6-MP: 6-mercaptopurine; 6-MeMP: 6-methylmercaptopurine; TPMT: thiopurine methyltransferase; 6-TU: 6-thiouric acid; XO: xanthine oxidase; 6-TIMP: 6-thioinosine monophosphate; HGPRT: hypoxanthine guanine phosphoribosyl transferase; 6-MeTIMP: 6-methylthioinosine monophosphate; 6-MeMPR: 6-methylmercaptopurine ribonucleotide; 6-TXMP: 6-thioxanthine monophosphate; IMPDH: inosine monophosphate dehydrogenase; 6-TGMP: 6-thioguanine monophosphate; GMPS: guanosine monophosphate synthetase; 6-MeTGMP: 6-methylthioguanine monophosphate; 6-TGDP: 6-thioguanine diphosphate; 6-TGTP: 6-thioguanine triphosphate; NMPK: nucleoside-phosphate kinase; NDPK: nucleoside-diphosphate kinase; NUDT15: nudix hydrolase 15; 6-TdGTP: deoxy-6-thioguanine triphosphate; 6-TG: 6-thioguanine; 6-TX: 6-thioxanthine; 6-MeTG; 6-methylthioguanine.

Figure 3.

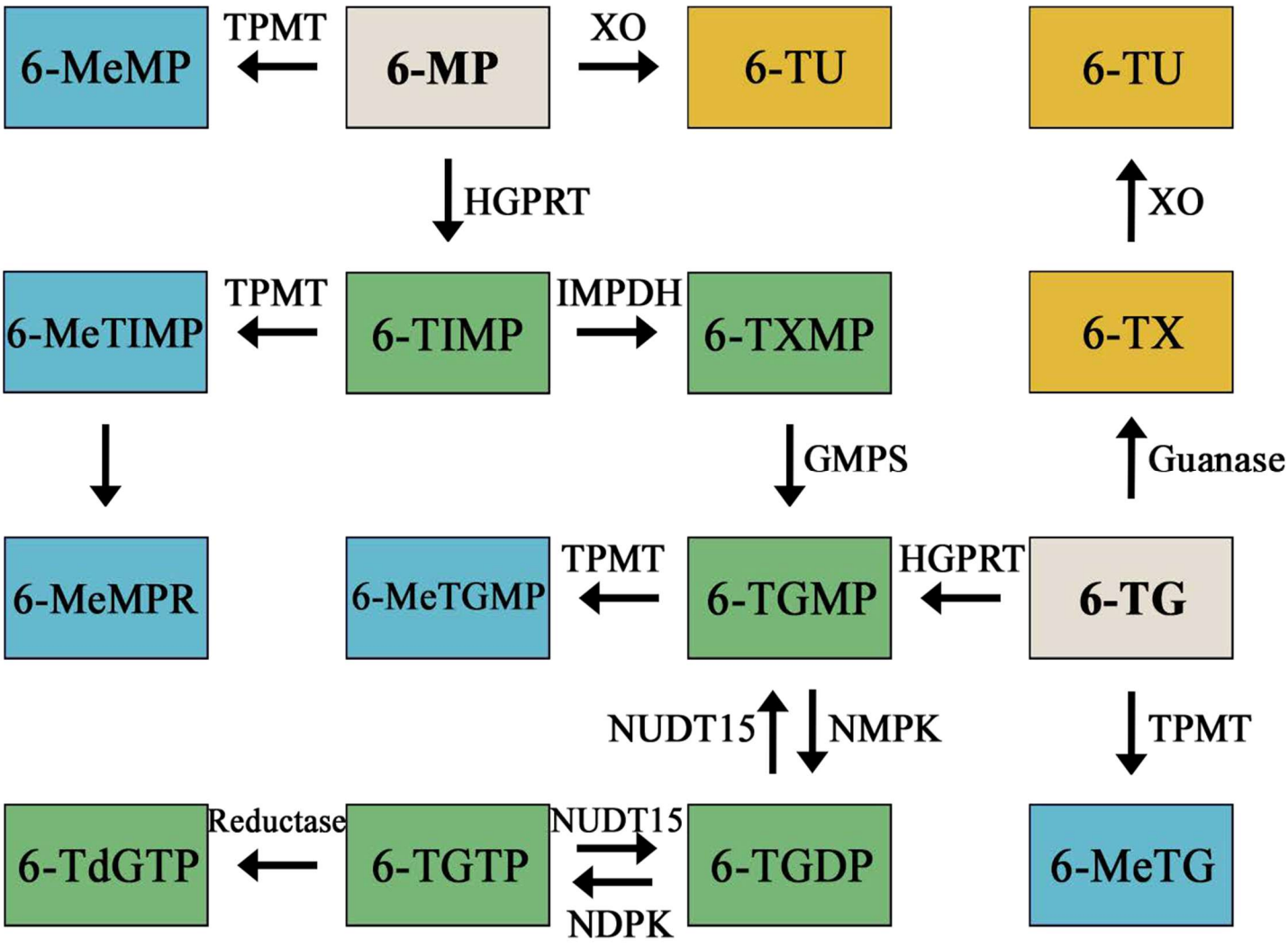
6-MeMP
TPMT
6-MP
XO
6-TU
6-TU
HGPRT
XO
6-MeTIMP
TPMT
6-TIMP
IMPDH
6-TXMP
6-TX
GMPS
Guanase
6-MeMPR
6-MeTGMP
TPMT
6-TGMP
HGPRT
6-TG
NUDT15
NMPK
TPMT
6-TdGTP
Reductase
6-TGTP
NUDT15
NDPK
6-TGDP
6-MeTG

1.2.d **Challenges associated with 6-MP usage**

Despite its success, the clinical usage of 6-MP comes with significant challenges. While most patients tolerate 6-MP well, intra-individual variability of 6-MP bioavailability between patients continues to complicate obtaining target therapeutic outcomes and minimizing off-target toxicities at standardized doses (Zimm et al., 1983; Lonnerholm et al., 1986; Larsen et al., 2020; Zou et al, 2023). Thus, careful dosing and monitoring is necessary to avoid severe side effects, including myelotoxicity, leukopenia, thrombocytopenia, and hepatotoxicity (Dubinsky et al., 2000; Gearry et al., 2004; van Asseldonk et al., 2012; Luber et al., 2019; Sousa et al., 2020). As a result, 6-MP therapy discontinuation due to low clinical efficacy or adverse events is commonly reported (Kontorinis et al., 2004; Nygaard et al., 2004; Bhatia et al., 2015), especially in pediatric cases (Kahn et al., 2023), despite this action being known to increase risk of symptom relapse with far lower survival rates (Bhatia et al., 2015; Gupta and Bhatia, 2017). Observed variability is primarily attributed to genetic variations in the enzymes involved in 6-MP metabolism such as TPMT and NUDT15 (Andersen et al., 1998; Lee et al., 2021; Khoo et al., 2022; Sheu et al., 2022). However, drug transporters like ENBT1 are under explored candidates. Overall, while 6-MP has proven to be a valuable treatment option for various leukemia's and autoimmune disorders. Its limitations emphasize the importance of personalized medicine approaches, such as pharmacogenomics testing to ensure the best possible outcomes.

1.3 Human and Murine SLC43A3-Encoded ENBT1

1.3.a Primary Structure

The gene *SLC43A3* encodes for hENBT1 and *slc43a3* encodes for mENBT1. hENBT1 and mENBT1 share a high degree of sequence similarity. Pairwise sequence alignment (Madeira et al., 2022) of hENBT1 and mENBT1 amino acid sequences, result in a percent identity of 73.4%, which relates to alignment of identical amino acids, and a percent similarity of 82.1%, which relates to alignment of identical or similar amino acids that share chemical properties (Figure 4). Suggesting that the two sequences are homologous, but do not have identical primary structure.

Figure 4. Human and murine ENBT1 pairwise sequence alignment ►

Pairwise global alignment via EMBOSS Needle of protein sequences hENBT1- 1476 bp, 491 aa (UniProt ID: Q8NBI5) and mENBT1- 1509 bp, 502 aa (UniProt ID: A2AVZ9). Software utilizes the Needleman-Wunsch algorithm to create the optimal global alignment of two sequences. The consensus symbols found between sequences denote where the sequence gapped, are identical, or are similar. A "-" indicates a gap in sequence alignment. A "|" (vertical bar) indicates a position with a fully conserved/identical residue. A "." (period) indicates conservation between groups of weakly similar properties (scores =<0.5 and >0). A ":" (colon) indicates conservation between groups of strongly similar properties (score >0.5). Similarities were scored utilizing the EBLOSUM62 substitution matrix (Madeira et al., 2022).

Figure 4.

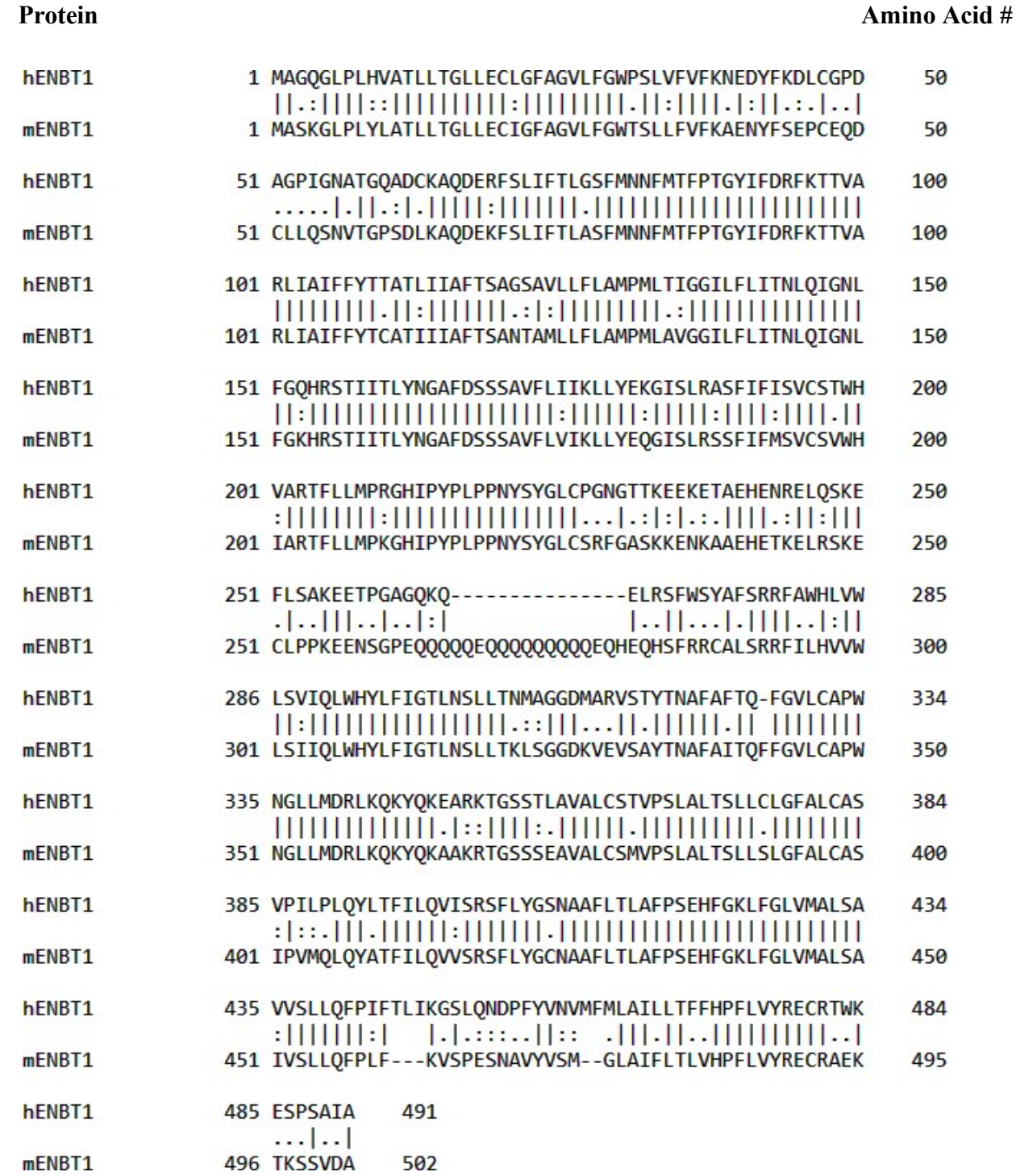
Protein
Amino Acid #
hENBT1 1 MAGQGLPLHVATLLTGLLECLGFAGVLFGWPSLVFVFKNEDYFKDLCGPD 50
mENBT1 1 MASKGLPLYLATLLTGLLECIGFAGVLFGWTSLLFVFKAENYFSEPCEQD 50
hENBT1 51 AGPIGNATGQADCKAQDERFSLIFTLGSFMNNFMTFPTGYIFDRFKTTVA 100
mENBT1 51 CLLQSNVTGPSDLKAQDEKFSLIFTLASFMNNFMTFPTGYIFDRFKTTVA 100
hENBT1 101 RLIAIFFYTTATLIIAFTSAGSAVLLFLAMPMLTIGGILFLITNLQIGNL 150
mENBT1 101 RLIAIFFYTCATIIIAFTSANTAMLLFLAMPMLAVGGILFLITNLQIGNL 150
hENBT1 151 FGQHRSTIITLYNGAFDSSSAVFLIIKLLYEKGISLRASFIFISVCSTWH 200
mENBT1 151 FGKHRSTIITLYNGAFDSSSAVFLVIKLLYEQGISLRSSFIFMSVCSVWH 200
hENBT1 201 VARTFLLMPRGHIPYPLPPNYSYGLCPGNGTTKEEKETAEHENRELQSKE 250
mENBT1 201 IARTFLLMPKGHIPYPLPPNYSYGLCSRFGASKKENKAAEHETKELRSKE 250
hENBT1 251 FLSAKEETPGAGQKQ---------------ELRSFWSYAFSRRFAWHLVW 285
mENBT1 251 CLPPKEENSGPEQQQQQEQQQQQQQQQEQHEQHSFRRCALSRRFILHVVW 300
hENBT1 286 LSVIQLWHYLFIGTLNSLLTNMAGGDMARVSTYTNAFAFTQ-FGVLCAPW 334
mENBT1 301 LSIIQLWHYLFIGTLNSLLTKLSGGDKVEVSAYTNAFAITQFFGVLCAPW 350
hENBT1 335 NGLLMDRLKQKYQKEARKTGSSTLAVALCSTVPSLALTSLLCLGFALCAS 384
mENBT1 351 NGLLMDRLKQKYQKAAKRTGSSSEAVALCSMVPSLALTSLLSLGFALCAS 400
hENBT1 385 VPILPLQYLTFILQVISRSFLYGSNAAFLTLAFPSEHFGKLFGLVMALSA 434
mENBT1 401 IPVMQLQYATFILQVVSRSFLYGCNAAFLTLAFPSEHFGKLFGLVMALSA 450
hENBT1 435 VVSLLQFPIFTLIKGSLQNDPFYVNVMFMLAILLTFFHPFLVYRECRTWK 484
mENBT1 451 IVSLLQFPLF---KVSPESNAVYVSM--GLAIFLTLVHPFLVYRECRAEK 495
hENBT1 485 ESPSAIA 491
mENBT1 496 TKSSVDA 502

1.3.b **Predicted Transmembrane Topology and Tertiary Structure**

Predicted transmembrane topology generated utilizing Protter (Omasits et al., 2014) suggests hENBT1 and mENBT1 share similar transmembrane topology, both displaying 12 transmembrane domains (TMD), prominent extracellular loops between TMD 1-2, and prominent intracellular loops between TMD 6 -7 (Figure 5). Relative to hENBT1, mENBT1 has a notably longer predicted extracellular loop between transmembrane domain 1 and 2 and intracellular loop between transmembrane domain 6 and 7 (Figure 5). These findings concur with predicted tertiary structure generated utilizing Alpha Fold (Jumper et al., 2021; Varadi et al., 2022), which suggest hENBT1 and mENBT1 share similar tertiary structure with the exception of an additional alpha helical structure in the mENBT1 extracellular loop between domains 1 and 2, and intracellular loop between domain 6 and 7 (Figure 6). hENBT1 and mENBT1 also share similar predicted topology as another SLC family member, *SLC43A1*/LAT3 (12 TMDs, prominent extracellular loop between TMD 1-2, and prominent intracellular loop between TMD 6-7) (Bodoy et al., 2013). However, the structures of LAT3 and LAT4 remain unsolved, making further predictions of interaction or binding sites difficult (Wang and Holst, 2015).

Another avenue to predict a substrate binding site, is to examine ENBT1 as a member of the major facilitator superfamily (MFS), which is a large group of transporters essential for the movement of small compounds across membranes. MFS members share broad structural similarities, such as 12 TMDs, that are divided into the N-domain (TMD1-TMD6) and the C-domain (TMD7-TMD12) (Yan N., 2015; Quistgaard et al., 2017; Sauve et al., 2023). These two domains can be further subdivided into four subdomains/bundles of three helices, that are alternatively inverted, or in other words organized in a zigzag pattern like the letter “N”, in which each ‘stroke’ is in an opposite orientation. These helices are often grouped as A-helices

(TMD1 and TMD4, TMD7 and TMD10), B-helices (TMD2 and TMD5, TMD8 and TMD11), and C-helices (TMD3 and TMD6, TDM9 and TMD12); each of the four bundles are comprised of an A-helix, B-helix, and C-helix. The A-helices, i.e., the first helix in each of the four bundles, are found in the center of MFS transporters, and form the central cavity which interacts with substrates (Yan N., 2015; Sauve et al., 2023). In fact, most residues identified for substrate binding in MFS members, are located in the A-helices (TMD1 and TMD4, TMD7 and TMD10). Of further interest, TMD1 and TMD7 are thought to be responsible for substrate interactions on the extracellular side, while TMD4 and TMD10 are responsible for substrate interactions on the intracellular side (Yan N., 2015). The B-helices (TMD2 and TMD5, TMD8 and TMD11), surround the central cavity and mediate interactions between the N-domain and the C-domain (Yan N., 2015; Quistgaard et al., 2017; Sauve et al., 2023). They (B-helices) also potentially contain residues that participate in substrate binding (Yan N., 2015). The C-helices (TMD3 and TMD6, TDM9 and TMD12) are the most distal helices from the central cavity and support transporter structural integrity (Yan N., 2015; Quistgaard et al., 2017). These described characteristics of MFS transporters are present in the predicted tertiary structures of hENBT1 and mENBT1 as seen in Figure.6.

Figure 5. hENBT1 and mENBT1 predicted topology ►

Predicted transmembrane topology of protein sequences hENBT1- 1476 bp, 491 aa (UniProt ID: Q8NBI5) and mENBT1- 1509 bp, 502 aa (UniProt ID: A2AVZ9), generated utilizing Protter version 1.0 (Omasits et al., 2014). Labelled is the N-terminus (left), C-terminus (right), extracellular region (top), intracellular region (bottom), 1-12 transmembrane domains (blue), and numbered every 10^{th} residue.

Figure 5.

hENBT1 predicted topology

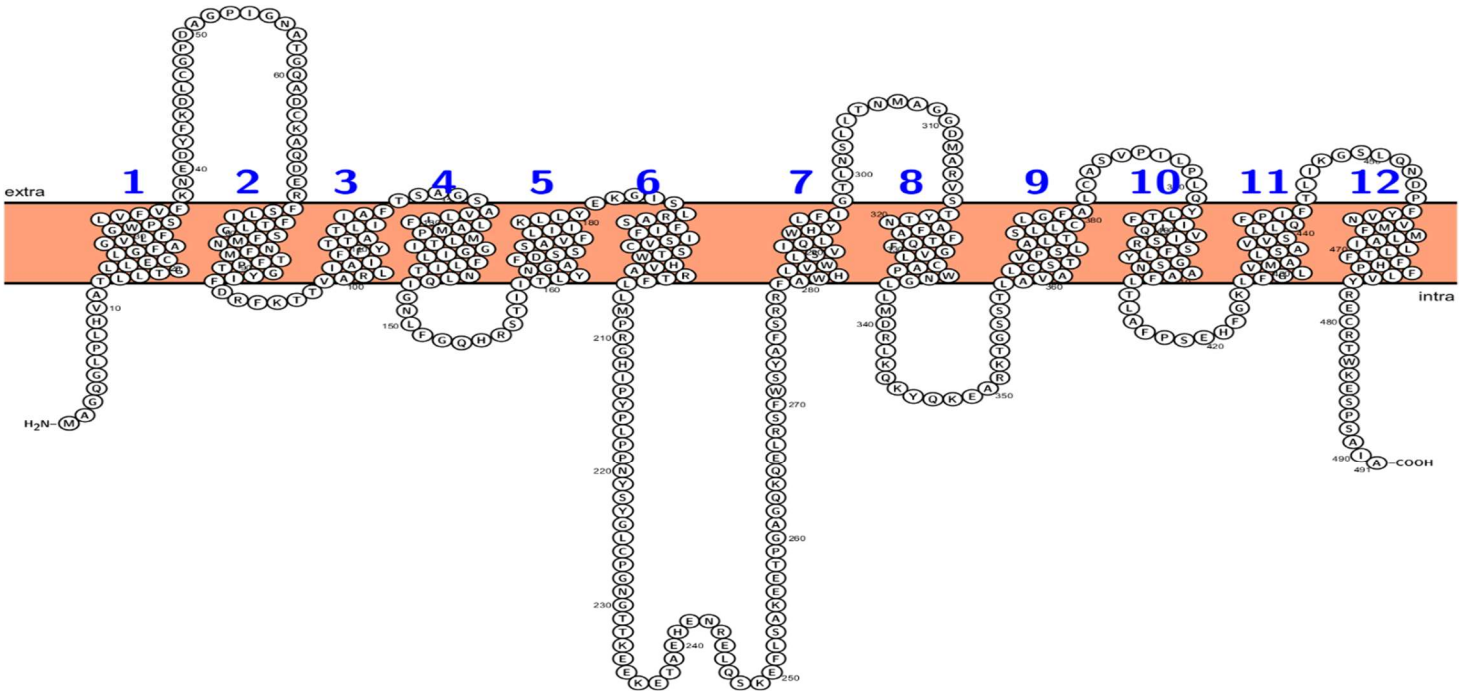

mENBT1 predicted topology

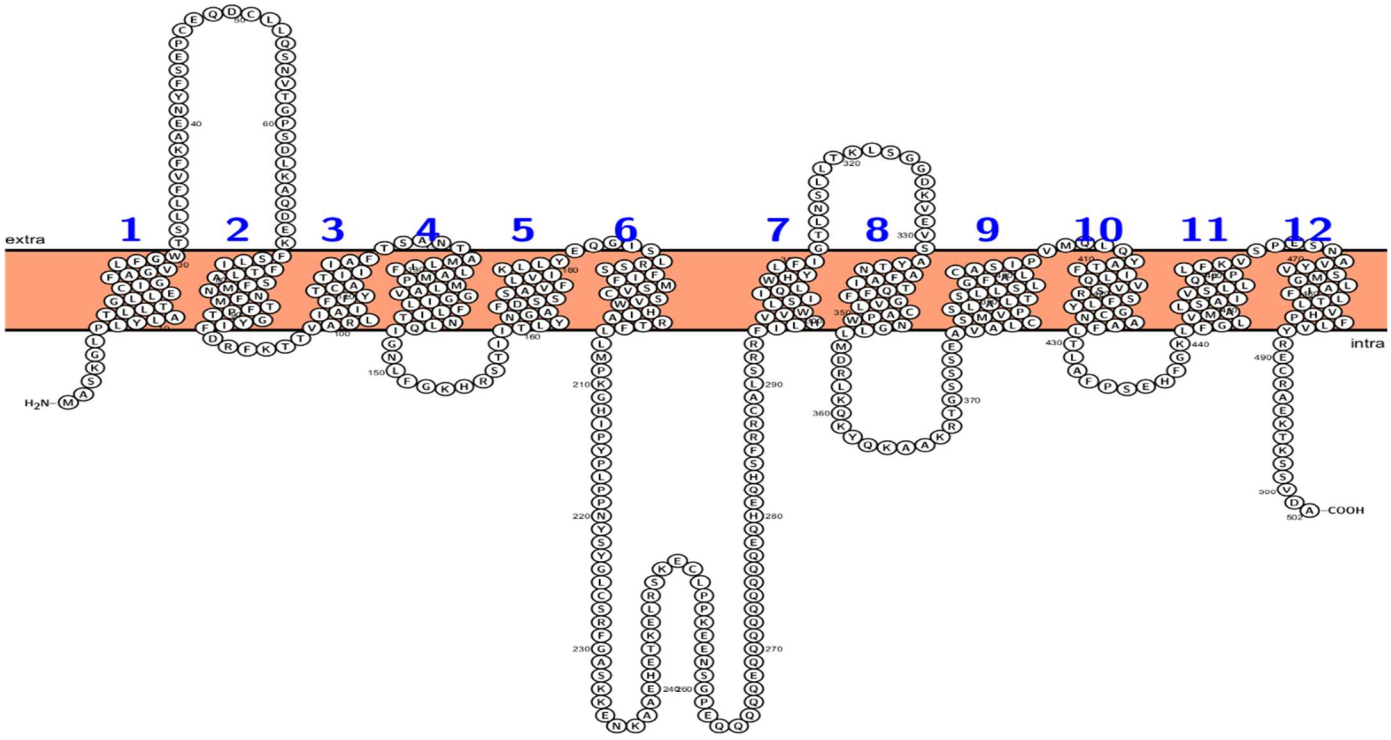

Figure 6. hENBT1 and mENBT1 Alpha fold tertiary structures ►

Predicted tertiary structures of protein sequences hENBT1- 1476 bp, 491 aa (UniProt ID: Q8NBI5) and mENBT1- 1509 bp, 502 aa (UniProt ID: A2AVZ9), generated utilizing Alpha Fold version 2022-11-01 (Jumper et al., 2021; Varadi et al., 2022). Structures coloured in red represent predicted A-helices (TMD1 and TMD4, TMD7 and TMD10), blue represent predicted B-helices (TMD2 and TMD5, TMD8 and TMD11), green represent predicted C-helices (TMD3 and TMD6, TDM9 and TMD12), and yellow regions represent extracellular/intracellular loops. Labelled are the A-helices (TMD1 and TMD4, TMD7 and TMD10), N-terminus (right), C-terminus (left), general extracellular region (above upper dashed line), and general intracellular region (below lower dashed line).

Figure 6.

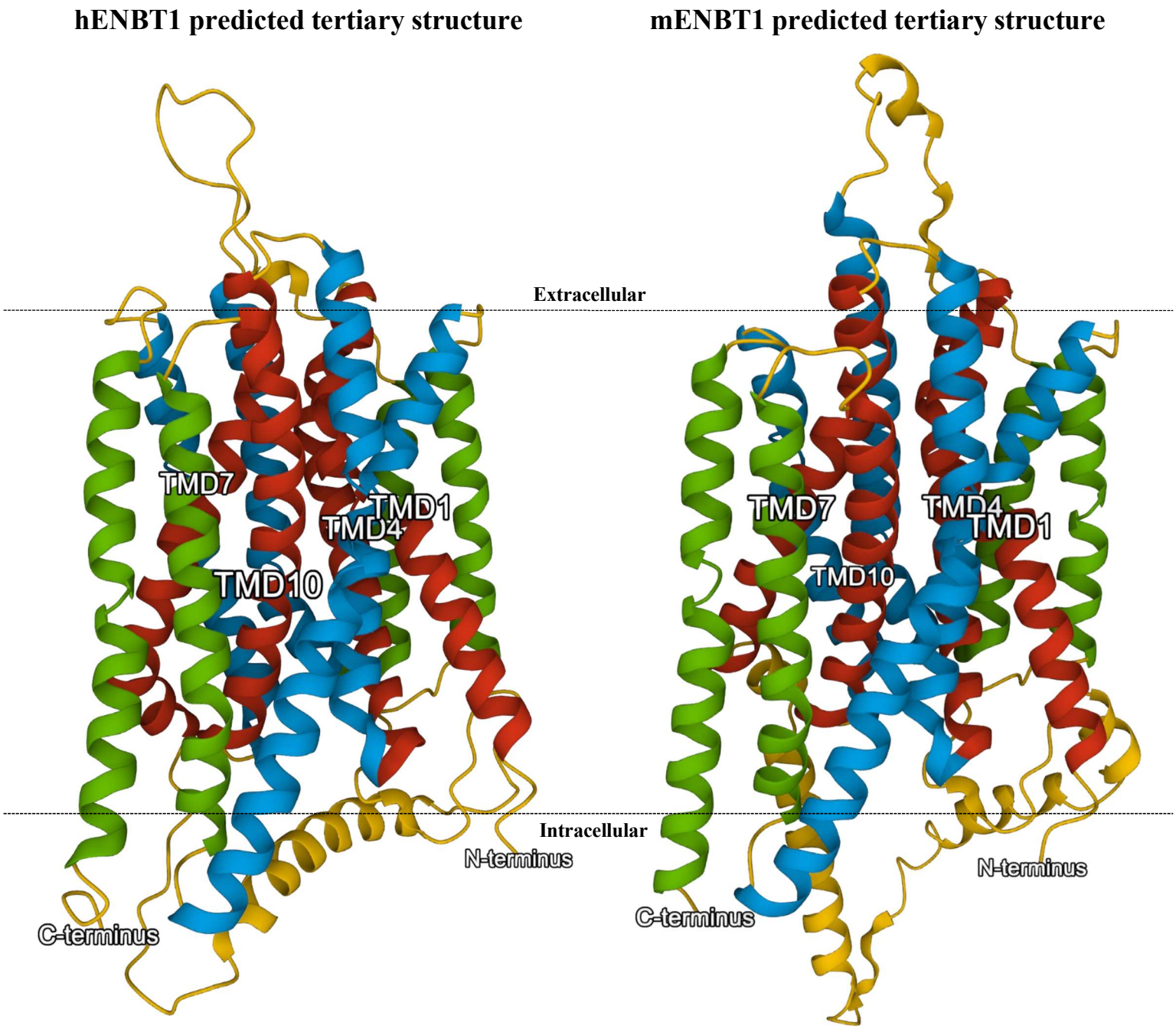
hENBT1 predicted tertiary structure
mENBT1 predicted tertiary structure
Extracellular
Intracellular
TMD7
TMD1
TMD4
TMD10
N-terminus
C-terminus
TMD7
TMD4
TMD1
TMD10
N-terminus
C-terminus

1.3.c **Polyglutamine Tract**

One of the most notable differences between hENBT1 and mENBT1, is the presence of a sequence of CAG codons/glutamine (Gln) residues, also known as a polyglutamine (polyQ) tract, in the aforementioned intracellular loops between transmembrane domain 6 and 7 (Figure 5) (Figure 6). PolyQ tracts are commonly observed in neurodegenerative diseases, such as Huntington's disease (HD), in which uninterrupted repeat lengths, ranging anywhere between 36 – 121 Gln residue repeats, are associated with misfolding and aggregation of the affected protein, leading to the formation of cytotoxic protein aggregates (Seidel et al., 2016; Jimenez-Sanchez et al., 2017). In comparison mENBT1 has an interrupted polyQ tract of 14 repeats, which is below the typical range of HD (>35 repeats), and thus is not expected to display the same polyQ gain of function characteristic of HD. However, the literature suggests that polyQ tracts stabilize protein interactions, and thus are site of high protein-protein interactions, which can lead to protein aggregation (Schafer et al., 2012).

CHAPTER 2.

Hypothesis and research aims

2.1 Introduction

The general hypothesis for the 6-MP/ENBT1 research project is that *SLC43A3*-encoded ENBT1 plays a major role in mediating the cellular-accumulation and subsequent cytotoxicity of 6-MP. One of our current interests is to investigate the relationship between *SLC43A3*-encoded ENBT1 and 6-MP absorption, and tissue biodistribution. To accomplish this, amongst other aims, we commissioned from Cyagen (Santa Clara, CA) a novel *slc43a3* full body knockout (KO) mouse to assess the effects of *slc43a3*-encoded ENBT1 expression has on the absorption and biodistribution of orally administered 6-MP.

Utilizing the *slc43a3* KO mouse model should provide greater insight on the impact ENBT1 has on the final destination of 6-MP/6-MP metabolites, compared to an in-vitro assessment in cell lines. However, a limitation of this model that impacts interpretations, is the lack of published data on the murine variant of *SLC43A3*-encoded ENBT1, herein by referred to as *slc43a3*-encoded mENBT1, compared to the human variant of *SLC43A3*-encoded ENBT1, herein by referred to as *SLC43A3*-encoded hENBT1. Our lab's extensive work with hENBT1 suggests that this transporter plays a major role in mediating the cellular-accumulation of purine nucleobases and purine nucleobase analogs such as 6-MP and sensitizing cells to 6-MP effects on cell viability (Ruel et al., 2019). However, there is no literature to date corresponding to mENBT1, especially in regard to the function of mENBT1 mediating the cellular-accumulation of 6-MP, and whether that function differs from hENBT1. Such information is necessary to determine if a *slc43a3* KO mouse is an appropriate model to investigate the relationship between *SLC43A3*-encoded ENBT1 expression levels and 6-MP absorption, tissue biodistribution, and accumulation of 6-MP and 6-MP metabolites.

2.2 General Hypothesis

With respect to the dogma that states; protein structure equals function (Biology 2e; https://openstax.org/books/biology-2e/pages/3-4-proteins/) (Clark et al., 2018), it is unknown whether the aforementioned differences in sequence and predicted structure between hENBT1 and mENBT1, will translate to functional differences in mediating the cellular-accumulation of 6-MP.

However, based on the preliminary *in silico* analysis discussed in section 1.3.a, my thesis hypothesis is that *SLC43A3*-encoded hENBT1 and *slc43a3*-encoded mENBT1 are functionally similar in mediating the cellular-accumulation of 6-MP. As a result, the *slc43a3* KO mouse is an appropriate model for investigating the role of ENBT1 in 6-MP absorption, tissue biodistribution, and accumulation of 6-MP and 6-MP metabolites.

2.3 Research Aims

2.3.a Aim 1. Elucidate the role of recombinant *slc43a3*-encoded mENBT1 in cellular accumulation of 6-MP/6-MP metabolites and their subsequent effect on cell viability utilizing ENBT1-deficient and recombinant mENBT1-overexpression models.

Transcript and protein expression level, 6-MP transport and inhibition kinetics, and the effect of 6-MP and other relevant compounds on cell viability, were assessed in innately ENBT1-deficient HEK293 cell lines (Ruel et al., 2019), stably transfected to overexpress recombinant *slc43a3*-encoded mENBT1 or a pcDNA3.1(-) empty vector control. Previous work by Ph.D. Candidate Nicholas M Ruel, was replicated in HEK293 cell lines stably transfected to

overexpress recombinant hENBT1, for direct side-by-side functional comparisons between hENBT1 and mENBT1 in my hands.

2.3.b **Aim 2. Examine the role of endogenous *slc43a3*-encoded mENBT1 in 6-MP cellular accumulation and subsequent effect on cell viability utilizing leukemia and hepatocyte-like cell lines.**

Transcript and protein expression level, 6-MP transport and inhibition kinetics, and the effect of 6-MP and other relevant compounds on cell viability were assessed in MOLT-4 and L1210 leukemia cell lines and FL83B hepatic cell line, with endogenous *slc43a3*-encoded mENBT1 expression and expression levels. Previous work was replicated in a human leukemia cell line, for direct side-by-side functional comparisons between hENBT1 and mENBT1 in my hands.

CHAPTER 3.

Materials and methods

3.1 **Material List**

[^{14}C]-6-MP (50 Ci/mmol), [^{3}H]-6-MP (0.3 Ci/mmol), [2,8-^{3}H]-adenine (20 Ci/mmol), and [^{3}H]-water (1 mCi/g) were purchased from Moravek Biochemicals (Brea, CA). Ecolite liquid scintillation cocktail were purchased from MP Biomedical (Irvine, CA). Adenine hydrochloride hydrate, 6-mercaptopurine monohydrate, 6-thioguanine, 3-(4,5-dimethylthiazol-2-yl)-2,5-diphenyltetrazolium bromide (MTT), dipyridamole, geneticin (G418 sulfate), Dulbecco's modified Eagle's medium (DMEM), fetal bovine serum (FBS), penicillin-streptomycin, D-glucose, 2-mercaptoethanol, and Immobilon®-P PVDF membrane were purchased from Sigma-Aldrich (St. Louis, MO). RPMI- 1640 medium and the ECL Prime western blotting system were purchased from Cytiva Life Sciences (Marlborough, MA). 6-Methylmercaptopurine, ultrapure agarose, oligo (dT)12–18 primer, HEPES, bicinchoninic acid (BCA) kit, lactate dehydrogenase (LDH) cytotoxicity assay kit, sodium pyruvate, horse serum, 0.05% trypsin/EDTA, Ham's F-12K (Kaighn's) Medium, PowerUp SYBR Green, HALT Protease Inhibitor Cocktail, ethylenediaminetetraacetic acid (EDTA), 200 kDa EZ-Run Protein Ladder, TRIzol Reagent, Taq DNA polymerase, and SuperScript III Reverse Transcriptase were purchased from Thermo Fisher Scientific (Waltham, MA). 6-Thiouric acid sodium salt dihydrate were purchased from Toronto Research Chemicals (Toronto, ON). All primers were purchased from Integrated DNA Technologies (Coralville, IA). The 100 bp DNA ladder were purchased from Truin Science (Edmonton, AB). RedSafe nucleic acid staining solution were purchased from iNtRON Biotechnology (Gyeonggi-do, Republic of Korea). The HEK293-WT, MOLT-4, L1210, and FL83B were purchased from ATCC (Manassas, VA). The primary antibodies used for immunoblotting were mouse monoclonal IgG_1 anti-β-actin (C4, sc-47778, Lot #B0719; Santa Cruz Biotechnology Inc., Texas), mouse monoclonal IgG_1 anti-MYC antibody (C-33, sc-42, Lot #3013479; Santa Cruz Biotechnology

Inc., Texas), rabbit polyclonal anti-hENBT1 (HPA030551, Lot #000001575; Sigma-Aldrich, St. Louis, MO), mouse monoclonal IgMκ anti-mENBT1 (E-10, sc-515451, Lot #H2319; Santa Cruz Biotechnology Inc., Texas), and mouse monoclonal IgM anti-mENBT1(CBMAB-S4924-CQ, Lot #CB2204LY29; Creative Biolabs., New York). Secondary antibodies were anti-mouse IgG horseradish perdoxidase (HRP)-linked antibody (#7076S, Lot #32; Cell |Signaling Technology; Massachusetts), anti-rabbit HRP-linked antibody (#7074S, Lot #27; Cell |Signaling Technology; Massachusetts), and mouse-IgGk BP-HRP (sc-516102, Lot #B0422; Santa Cruz Biotechnology Inc., Texas).

3.2 *SLC43A3* Plasmid Construct and Transfection

Oligonucleotides corresponding to the coding region of *SLC43A3* (NM_001278201) or *slc43a3* (NM_021398), with an N-terminal MYC-epitope tag, were prepared in the GeneArt Cloning pMA plasmid by Invitrogen. The MYC-SLC43A3 sequences (Figure 7. and Figure 8.) were ligated into the mammalian cloning vector pcDNA3.1 (-), after digestion with XbaI (5') and KpnI (3') restriction enzymes. The inserts were sequenced in both directions to confirm integrity, and then used to stably transfect wildtype HEK293 (HEK293-WT) cells, using the calcium phosphate method (Kingston et al., 2003). Cells expressing the transfected plasmid were selected based on their resistance to 600 µg/mL G418 sulfate, and expression of MYC-tag via dot blot. HEK293 cells stably transfected with the empty pcDNA3.1 vector were also tested to assess the impact of the transfection procedure and chronic G418 sulfate treatment, on the cell line.

Figure 7. ***SLC43A3*/hENBT1 cloned sequence and amino acid sequence**

MYC-*SLC43A3* Sequence (5'-XbaI---KpnI-3', 1533 bp)

CTAGAATGGAACAAAAACTCATCTCAGAAGAGGATCTGGGTGGCGGAGGGGGTGCGGGCCAGGGC
CTGCCCCTGCACGTGGCCACACTGCTGACTGGGCTGCTGGAATGCCTGGGCTTTGCTGGCGTCCTCT
TTGGCTGGCCTTCACTAGTGTTTGTCTTCAAGAATGAAGATTACTTTAAGGATCTGTGTGGACCAGA
TGCTGGGCCGATTGGCAATGCCACAGGGCAGGCTGACTGCAAAGCCCAGGATGAGAGGTTCTCACT
CATCTTCACCCTGGGGTCCTTCATGAACAACTTCATGACATTCCCCACTGGCTACATCTTTGACCGGT
TCAAGACCACCGTGGCACGCCTCATAGCCATATTTTTCTACACCACCGCCACACTCATCATAGCCTT
CACCTCTGCAGGCTCAGCCGTGCTGCTCTTCCTGGCCATGCCAATGCTCACCATTGGGGGAATCCTG
TTTCTCATCACCAACCTGCAGATTGGGAACCTATTTGGCCAACACCGTTCGACCATCATCACTCTGT
ACAATGGAGCATTTGACTCTTCCTCGGCAGTCTTCCTTATTATTAAGCTTCTTTATGAAAAAGGCATC
AGCCTCAGGGCCTCCTTCATCTTCATCTCTGTCTGCAGTACCTGGCATGTAGCACGCACTTTCCTCCT
GATGCCCCGGGGGCACATCCCATACCCACTGCCCCCCAACTACAGCTATGGCCTGTGCCCTGGGAAT
GGCACCACAAAGGAAGAGAAGGAAACAGCTGAGCATGAAAACAGGGAGCTACAGTCAAAGGAGTT
CCTTTCAGCGAAGGAAGAGACCCCAGGGGCAGGGCAGAAGCAGGAACTCCGCTCCTTCTGGAGCTA
CGCTTTCTCTCGGCGCTTTGCCTGGCACCTGGTGTGGCTGTCTGTGATACAGTTGTGGCACTACCTCT
TCATTGGCACTCTCAACTCCTTGCTGACCAACATGGCCGGTGGGGACATGGCACGAGTCAGCACCTA
CACAAATGCCTTTGCCTTCACTCAGTTCGGAGTGCTGTGTGCCCCCTGGAATGGCCTGCTCATGGAC
CGGCTTAAACAGAAGTACCAGAAGGAAGCAAGAAAGACAGGTTCCTCCACTTTGGCGGTGGCCCTC
TGCTCGACGGTGCCTTCGCTGGCCCTGACATCCCTGCTGTGCCTGGGCTTCGCCCTCTGTGCCTCAGT
CCCCATCCTCCCTCTCCAGTACCTCACCTTCATCCTGCAAGTGATCAGCCGCTCCTTCCTCTATGGGA
GCAACGCGGCCTTCCTCACCCTTGCTTTCCCTTCAGAGCACTTTGGCAAGCTCTTTGGGCTGGTGATG
GCCTTGTCGGCTGTGGTGTCTCTGCTCCAGTTCCCCATCTTCACCCTCATCAAAGGCTCCCTTCAGAA
TGACCCATTTTACGTGAATGTGATGTTCATGCTTGCCATTCTTCTGACATTCTTCCACCCCTTTCTGGT
ATATCGGGAATGCCGTACTTGGAAAGAAAGTCCCTCTGCAATTGCATAGGGTACC

Xbal restriction site - Start codon - MYC Tag + flexible linker - *SLC43A3* sequence - Kpnl restriction site

MYC-5xGly-hENBT1 Sequence (55.9 kDA)

MEQKLISEEDLGGGGGAGQGLPLHVATLLTGLLECLGFAGVLFGWPSLVFVFKNEDYFKDLCGPDAGPIG
NATGQADCKAQDERFSLIFTLGSFMNNFMTFPTGYIFDRFKTTVARLIAIFFYTTATLIIAFTSAGSAVLLFLA
MPMLTIGGILFLITNLQIGNLFGQHRSTIITLYNGAFDSSSAVFLIIKLLYEKGISLRASFIFISVCSTWHVARTF
LLMPRGHIPYPLPPNYSYGLCPGNGTTKEEKETAEHENRELQSKEFLSAKEETPGAGQKQELRSFWSYAFSR
RFAWHLVWLSVIQLWHYLFIGTLNSLLTNMAGGDMARVSTYTNAFAFTQFGVLCAPWNGLLMDRLKQK
YQKEARKTGSSTLAVALCSTVPSLALTSLLCLGFALCASVPILPLQYLTFILQVISRSFLYGSNAAFLTLAFPS
EHFGKLFGLVMALSAVVSLLQFPIFTLIKGSLQNDPFYVNVMFMLAILLTFFHPFLVYRECRTWKESPSAIA

MYC Tag + flexible linker - hENBT1 sequence

Figure 8. ***slc43a3*/mENBT1 cloned sequence and amino acid sequence**

MYC-*slc43a3* (5'-XbaI---KpnI-3', 1566 bp)

TCTAGAATGGAACAAAAACTCATCTCAGAAGAGGATCTGGGTGGCGGAGGGGGTGCAAGCAAGGG
CTTGCCCCTTTACTTGGCCACCTTGTTGACTGGACTCTTGGAATGCATCGGTTTTGCTGGTGTCCTCT
TTGGCTGGACTTCACTGTTGTTTGTGTTCAAAGCAGAAAACTACTTTTCAGAGCCCTGTGAACAGGA
CTGCTTGCTCCAGAGCAATGTAACAGGGCCTTCTGATTTAAAAGCGCAGGATGAGAAGTTCTCACTC
ATCTTTACCCTGGCATCCTTCATGAATAACTTCATGACCTTTCCCACTGGCTACATCTTTGACCGCTT
CAAGACTACTGTGGCCCGCCTGATAGCCATATTTTTCTACACCTGCGCCACGATCATCATTGCCTTC
ACCTCTGCAAACACTGCCATGCTGCTCTTCCTAGCCATGCCCATGCTCGCAGTGGGAGGAATCCTGT
TCCTTATCACCAACCTACAGATTGGGAACCTCTTTGGGAAACACCGTTCAACCATCATCACCCTCTA
CAATGGAGCATTTGACTCCTCCTCAGCAGTGTTCCTCGTCATTAAGCTGCTTTACGAGCAGGGCATC
AGCCTCAGGTCTTCCTTCATCTTCATGTCTGTCTGCAGTGTCTGGCACATTGCGCGTACTTTCCTTCT
GATGCCCAAGGGACATATCCCCTACCCACTGCCTCCCAACTACAGCTATGGCTTGTGCTCCAGGTTT
GGTGCTAGCAAGAAAGAGAATAAAGCAGCTGAACACGAAACCAAGGAGCTGCGGTCAAAGGAATG
TCTGCCACCCAAGGAAGAGAACTCTGGACCAGAACAGCAGCAGCAGCAGGAGCAGCAGCAGCAGC
AGCAGCAGCAGCAGGAGCAACACGAGCAACACTCTTTTCGACGCTGCGCGCTCTCTCGTCGATTCA
TCTTGCACGTGGTGTGGCTGTCTATCATACAGTTGTGGCATTACCTCTTCATTGGTACTCTCAACTCT
CTACTCACCAAGTTATCCGGTGGGGACAAAGTGGAAGTCAGTGCCTACACAAATGCCTTTGCCATC
ACCCAGTTCTTTGGCGTGCTGTGTGCCCCCTGGAATGGCTTACTCATGGACCGCCTTAAACAGAAGT
ATCAGAAGGCAGCCAAAAGGACAGGTTCCTCGTCTGAGGCTGTGGCTCTCTGCTCCATGGTGCCTTC
ACTGGCTCTGACGTCTCTGCTGTCCCTGGGCTTTGCCCTGTGTGCCTCCATTCCTGTCATGCAGCTAC
AGTACGCCACCTTCATCCTGCAAGTGGTCAGCCGCTCCTTCCTGTATGGATGCAATGCTGCCTTCCTC
ACGCTGGCATTTCCCTCAGAGCATTTTGGAAAGCTCTTTGGGCTGGTGATGGCCTTGTCAGCTATTG
TGTCTCTGCTACAGTTCCCCCTGTTCAAAGTCTCCCCTGAGAGCAACGCTGTGTATGTATCGATGGG
GCTTGCCATTTTCCTGACATTGGTCCATCCCTTCCTGGTGTACCGTGAGTGCCGTGCTGAGAAGACA
AAATCGTCTGTGGATGCCTAGGGTACC

XbaI restriction site - Start codon - MYC Tag + flexible linker - *slc43a3* sequence - KpnI restriction site

MYC-5xGly-mENBT1 (57.5 kDA)

MEQKLISEEDLGGGGGASKGLPLYLATLLTGLLECIGFAGVLFGWTSLLFVFKAENYFSEPCEQDCLLQSNV
TGPSDLKAQDEKFSLIFTLASFMNNFMTFPTGYIFDRFKTTVARLIAIFFYTCATIIIAFTSANTAMLLFLAMP
MLAVGGILFLITNLQIGNLFGKHRSTIITLYNGAFDSSSAVFLVIKLLYEQGISLRSSFIFMSVCSVWHIARTFL
LMPKGHIPYPLPPNYSYGLCSRFGASKKENKAAEHETKELRSKECLPPKEENSGPEQQQQQEQQQQQQQQ
QEQHEQHSFRRCALSRRFILHVVWLSIIQLWHYLFIGTLNSLLTKLSGGDKVEVSAYTNAFAITQFFGVLCA
PWNGLLMDRLKQKYQKAAKRTGSSSEAVALCSMVPSLALTSLLSLGFALCASIPVMQLQYATFILQVVSRS
FLYGCNAAFLTLAFPSEHFGKLFGLVMALSAIVSLLQFPLFKVSPESNAVYVSMGLAIFLTLVHPFLVYREC
RAEKTKSSVDA

MYC Tag + flexible linker - mENBT1 sequence

3.3 Cell Culture

Transfected-HEK293 cells were cultured in DMEM with 10% FBS, penicillin (100 U/mL), streptomycin (100 µg/mL), and sodium pyruvate (1 mM). G418 sulfate (300 µg/mL) was added to HEK293 cell media to maintain selection pressure on stable transfectants. FL83B mouse hepatocyte-like cells were cultured in Ham's F-12K (Kaighn's) Medium with 10% FBS, penicillin (100 U/mL), and streptomycin (100 µg/mL). Transfected-HEK293 and FL83B cells were harvested from flasks by exposure to 0.05% trypsin/EDTA for 5-10 minutes at 37°C in a humidified 5% CO_2 atmosphere, cell suspension was diluted with media containing serum and then centrifuged at 1000 x *g* for 5 minutes. L1210 cells were cultured in DMEM with 10% horse serum, penicillin (100 U/mL), and streptomycin (100 µg/mL). MOLT-4 cells were cultured in RPMI (Roswell Park Memorial Institute) 1640 medium supplemented with D-glucose (4500 mg/L), 10% FBS, penicillin (100 U/mL), streptomycin (100 µg/mL), sodium pyruvate (1 mM), and HEPES (10 mM). L1210 and MOLT-4 suspended cells were harvested from flasks and cell suspension was centrifuged at 1000 x *g* for 5 minutes.

3.4 Polymerase Chain Reaction

Cells from confluent 10-cm plates were suspended in 1 mL of TRIzol reagent and homogenized for total RNA extraction according to the manufacturer's protocol. Total RNA concentration and purity were determined using a Nanodrop 2000 spectrophotometer (Life Technologies Inc). For qualitative polymerase chain reaction (PCR), 1 µg of total RNA was reverse transcribed to complementary DNA (cDNA) using Oligo $(dT)_{12–18}$ primer and Superscript III. Target cDNA sequences were amplified using recombinant Taq DNA Polymerase and

primers designed for *SLC43A3*, *GAPDH*, *slc43a3*, and *gapdh* (Table 2.). Primer efficiency and melt curves were assessed prior to their use for gene expression analysis. The following conditions were used for amplification: 3 minutes at 95°C, followed by 40 cycles of 30 seconds at 95°C; 30 seconds at 56°C; and 60 seconds at 72°C, followed by extension for 10 minutes at 72°C in a BioRad T-100 Thermocycler. Semi-quantitative PCR (qPCR) was conducted using cDNA (~100 ng/well) prepared as described previously with the primer sets shown in (Table 2.), using Power Up SYBR Green fluorescence on a Roche Light Cycler 480 System (Cardiovascular Research Centre, Edmonton, Canada). qPCR conditions were: 2 minutes at 50°C (UDG activation); 2 minutes at 95°C (denaturation), followed by 45 cycles of 15 seconds at 95°C; and 60 seconds at 60°C for amplification, with a final melt curve analysis. Ct values were normalized to *GAPDH*/*gapdh* to obtain a ΔCt value, analyzed relative to expression in a calibrator cell using the ΔΔCt method, and converted into fold change using the 2^-ΔΔCt method (Livak and Schmittgen, 2001).

Table 2. PCR and qPCR primers

Gene	Sequence		Application
SLC43A3	Fwd	5'-GGAACTCCGCTCCTTCT-3'	PCR
	Rev	5'-GAAGTAGGACGTTCACTAGT-3'	
slc43a3	Fwd	5'-TTTACCCTGGCATCCTTCATG-3'	PCR
	Rev	5'-TAACGCGCATGAAAGGAAGA-3'	
GAPDH	Fwd	5'-ACATCATCCCTGCCTCTAC-3'	PCR
	Rev	5'-TAAACCGATGTCGTTGTCC-3'	
gapdh	Fwd	5'-ACATCATCCCTGCCTCTAC-3'	PCR
	Rev	5'-TAAACCGATGTCGTTGTCC-3'	
slc43a3	Fwd	5'-GAAACACCGTTCAACCATCATC-3'	qPCR
	Rev	5'-CTGATGCCCTGCTCGTAAA-3'	
abcc4	Fwd	5'-GCACTGAACAACAACAGAAAT-3'	qPCR
	Rev	5'-CGCAGTTAGACCTGCGTAAA-3'	
abcc5	Fwd	5'-CAGAGAATCAGCCTTGCTAGAG-3'	qPCR
	Rev	5'-CCGGATAGCACTGTTGAAGAT-3'	
tpmt	Fwd	5'-CCTTGATATGAAAGAGCACCCT-3'	qPCR
	Rev	5'-CCCACTTCTCTTTCCAGTCTTC-3'	
hgprt1	Fwd	5'-GATGATCTCTCAACTTTAACTGGAA-3'	qPCR
	Rev	5'-AGCTTGCAACCTTAACCATTT-3'	
xo	Fwd	5'-ACGGAGACAAGCACTAACAC-3'	qPCR
	Rev	5'-TGGTCTGACAGGCTTCATAAAT-3'	
impdh	Fwd	5'-AGAGTTCCAGGCCAATGAAG-3'	qPCR
	Rev	5'-CCAGAACATCACCCACAGTAT-3'	
gmps	Fwd	5'-GCACTTTACGGCCTGATCTAA-3'	qPCR
	Rev	5'-TCCCTCTTCCCTTAACTTCCT-3'	
nudt15	Fwd	5'-TTTGGAGCCGGCAGTTT-3'	qPCR
	Rev	5'-CAGCTTCTTCCCAGGTTTCT-3'	
gapdh	Fwd	5'-GGGTGTGAACCACGAGAAATA-3'	qPCR
	Rev	5'-GTCATGAGCCCTTCCACAAT-3'	

3.5 **Immunoblot**

Samples were extracted using radioimmunoprecipitation (RIPA) buffer (150 mM NaCl, 50 mM Tris, 1% NP-40, 0.5% sodium dodecyl sulfate (SDS) containing HALT™ Protease Inhibitor Cocktail + EDTA. Extracted protein concentrations were assessed using a BCA assay kit and accordingly diluted to 1.5 µg/µL protein and adjusted to 2% 2-mercaptoethanol for reducing conditions. 30 µg protein were resolved using sodium dodecyl sulfate-polyacrylamide gel electrophoresis (SDS-PAGE) on 12.5% acrylamide gels at 80 volts for 15 minutes, followed by 150 volts for 45 minutes, and semidry-transferred to Immobilon-P PVDF membranes at 25 volts for 30 minutes. Following the transfer, membranes were incubated with TBS-T (TBS-T; 150 mM NaCl, 50 mM Tris, pH 7.5, 1% Tween20) containing 3% bovine serum albumin (BSA) at room temperature for 30 minutes, to block nonspecific PVDF membrane binding. PVDF membranes were incubated for 16 hours at 4°C with anti-MYC, anti-hENBT1, anti-mENBT1, or anti-β-actin primary antibodies diluted in TBS-T containing 5% BSA, at 1:1000, 1:250, 1:500, and 1:1000, respectively. Membranes were washed several times in TBS-T, then incubated for 1 hour at room temperature with the relevant HRP-conjugated secondary antibody, anti-rabbit IgG-HRP or anti-mouse IgG-HRP diluted in TBS-T containing 5% BSA at 1:5000 or 1:3000, respectively. After further washing in TBS-T, membranes were treated with ECL Prime solution and visualized via chemiluminescence on an Amersham Imager 680 (GE Healthcare, Chicago, IL). Image J software was used to conduct densitometry analyses.

3.6 **Oil-Stop Centrifugation**

Harvested cells were suspended in nominally sodium-free N-methyl-D-glucamine (NMG) buffer (140 mM NMG, 5 mM KCl, 4.2 mM $KHCO_3$, 0.36 mM K_2HPO_4, 0.44 mM KH_2PO_4, 0.5 mM $MgCl_2$, 1.3 mM $CaCl_2$, 10 mM HEPES, pH 7.4), to minimize potential contribution of sodium-dependent concentrative nucleoside transporter-mediated uptake. Additionally, 10 μM DY was utilized to block potential equilibrative nucleoside transporter–mediated uptake, and incubated for 15 minutes at room temperature, protected from direct light. Cellular uptake was initiated at room temperature by adding 250 μL cell suspension to 250 μL [^{3}H]radiolabeled substrate (6-MP or adenine) layered over 21:4 silicone:mineral oil (200 μL) in 1.5 mL microcentrifuge tubes. The uptake reaction was terminated after specified times, by centrifugation of the cells through the oil layer at ~10,000g for 10 seconds. The aqueous layer was removed via a vacuum-powered aspirator, and the tube was washed with 1 mL of NMG buffer prior to removal of the oil layer. The resulting cell pellet was digested in 250 μL 1 M NaOH overnight (~16 hours), with 220 μL aliquots of digested cells assessed for radioactive content using standard liquid scintillation counting techniques in a Beckman Coulter LS6500 scintillation system (Brea, CA). In transfected-HEK293 cell lines, total uptake was defined as the uptake of [^{3}H]radiolabeled substrate in cells overexpressing recombinant *SLC43A3*-encoded hENBT1 or *slc43a3*-encoded mENBT1; non-mediated uptake was defined as the uptake of [^{3}H]radiolabeled substrate in HEK293-WT or pcDNA3.1(-) empty vector transfected-HEK293 cells that are ENBT1-deficient. In MOLT-4, L1210, and FL83B, total uptake was defined as the uptake of [^{3}H]6-MP in the absence of a competitive inhibitor, in assay; non-mediated uptake was defined as the uptake of [^{3}H]6-MP by cells in the presence of 5 mM competitive inhibitor (adenine), in assay. In all cases, total uptake is defined as a combination of ENBT1-mediated

uptake and background levels of transport, while non-mediated uptake is defined as background levels of transport. ENBT1-mediated uptake is defined as the difference between total uptake and non-mediated uptake components:

$$(\text{ENBT1 mediated uptake}) = (\text{Total uptake}) - (\text{Non ENBT1 mediated uptake})$$

Cell water volume (µL) was estimated by incubating cells with [^{3}H]H_2O for 3 minutes, centrifuging the cells through the oil layer at ~10,000g for 10 seconds, assessing 100 µL of the supernatant for radioactive content, and then processing as described above. Total cellular water volume was determined from the ratio of the decays per minute of the cell pellet, to the decays per minute of the supernatant, allowing for inter-experimental normalization via calculation of picomoles of substrate accumulated per microliter of cell-associated water.

3.7 **MTT Cell Viability**

Transfected-HEK293 cells were seeded into a 24-well plate at a density of 1.1*10^5 cells per well in complete culture medium. 1 hour following cell seeding onto plate, medium containing 6-MP (78 nM – 1.28 mM) was added and incubated for 48 hours at 37°C in a humidified 5% CO_2 atmosphere (compound-mediated response). Cells were treated with medium containing vehicle to determine baseline cell viability (100% cell viability); medium containing no cells was used to determine spontaneous MTT reduction (0% cell viability). Subsequently, media was removed and replaced with 150 µL of Dulbecco's phosphate buffered saline (DPBS - 137 mM NaCl, 2.7 mM KCl, 6.3 mM Na_2HPO4, 1.5 mM KH_2PO_4, 0.5 mM $MgCl_2$, 0.9 mM $CaCl_2$, pH 7.4) containing MTT (1 mg/mL) for 90 minutes at 37°C. The resultant formazan crystals in DPBS containing MTT, was solubilized in 500 µL of DMSO and transferred to a well plate in 200 µL duplicates.

L1210 and MOLT-4 cells were seeded into a 24-well plate at a density of 1.1*10^5 cells per well in complete culture medium. 1 hour following plate seeding, medium containing 6-MP (final concentration 78 nM – 1.28 mM), was added and incubated for 48 hours at 37°C in a humidified 5% CO_2 atmosphere. Suspended cells were then transferred to 1.5 mL microcentrifuge tubes and centrifuged for 10 minutes at 3000 rcf. Following centrifugation, media was removed and replaced with 150 µL of DPBS containing MTT (1 mg/mL) for 90 minutes at 37°C. Microcentrifuge tubes were centrifuged again for 15 minutes at 23,500 rcf, and then DPBS containing MTT was removed. The resultant formazan crystals were solubilized in 500 µL of DMSO and transferred to a 96-well plate in 200 µL duplicates. Absorbance was measured at 570 nM, in a SpectraMax® i3x Multi-Mode Detection Platform (Molecular Devices, San Jose, CA). % cell viability/% reduced MTT was calculated by dividing compound-mediated response by 100% cell viability:

$$\%\ reduced\ MTT = \frac{(\text{compound mediated response}) - (0\%\ \text{cell viability})}{(100\%\ \text{cell viability}) - (0\%\ \text{cell viability})}$$

In the case of a biphasic cell viability curve, only the first-phase EC_{50} value was utilized in analysis, as that EC_{50} value describes the population of cells that are actively proliferating and are therefore 6-MP sensitive. While the second-phase EC_{50} value describes the population of cells that are in a non-proliferative or quiescent state, and are therefore relatively insensitive to 6-MP after 48-hour treatment.

3.8 **LDH Release Assay**

Optimal cell density was determined beforehand by measuring signal to noise ratio of wells seeded at 0 cells/mL, 5*10^3 cells/well, 1*10^4 cells/well, and 2*10^4 cells/well. Transfected-

HEK293 cells were seeded into a 96-well plate at 2*10^4 cells per well in complete culture medium. L1210 and MOLT-4 cells were seeded into a 96-well plate at 1.5*10^4 cells per well in complete culture medium. 1 hour following plate seeding, medium containing 6-MP (final concentration 78 nM – 1.28 mM) was added to wells and incubated for 48 hours at 37°C in a humidified 5% CO_2 atmosphere (compound-mediated response); distilled H_2O was incubated as a control to determine background/spontaneous LDH activity in cells (0% cell death). Subsequently, supernatant was transferred to a 96-well plate, mixed with a reaction buffer and incubated for 30 minutes at 37°C in a humidified 5% CO_2 atmosphere; cell lysis buffer was used as a control to determine maximal LDH activity in cells (100% cell death). A reaction stop solution was added to wells prior to absorbance being measured at 490 nM and 680 nM, in a SpectraMax® i3x Multi-Mode Detection Platform (Molecular Devices, San Jose, CA). % cell death was calculated by dividing compound-mediated cell death by 100% cell death:

$$(\%\ cell\ death = \frac{(\text{compound mediated response}) - (0\%\ \text{cell death})}{(100\%\ \text{cell death}) - (0\%\ \text{cell death})})$$

3.9 **Data Analysis and Statistics**

Data was expressed as mean ± SD. Sample size was predetermined as n = 5 (five independent experiments with two to three internal replicates), which is the minimum needed to define statistical differences, based on the known historical variability inherent in these types of studies. In some circumstances, where higher variability was seen due to methodological issues (e.g., the rapid uptake profiles using the stably transfected cells), an additional one or two experiments were added to achieve statistical power. Nonlinear curves were fitted to data, and statistical analyses were done using GraphPad Prism 10 software. In all cases, if the p-value

determined from a statistical test was less than alpha = 0.05, the null hypothesis (no difference between data sets) was rejected and the alternative hypothesis (significant difference between data set) was favored; and vice versa when p-value was greater than alpha = 0.05. Significant differences between groups were assessed using either student's t-test or ordinary two-way analysis of variance (ANOVA) followed by a post hoc Šidák multiple comparison test. Best curve fits for specific data sets were determined by extra sum-of-squares F test. For influx and cell viability analyses, significant differences in K_m and EC_{50} values respectively, between hENBT1 and mENBT1 data sets, were determined by extra sum-of-squares F test. For inhibition analyses, the K_i values were determined from the IC_{50} values using the specified substrate concentration [S], based on the Cheng-Prusoff equation $K_i = IC_{50}/(1 + [S]/K_m)$ (Cheng and Prusoff, 1973) and K_m values both experimentally obtained by my hands and determined in previous studies (Ruel et al., 2019).

CHAPTER 4.

Interspecies Functional Comparison of Recombinant hENBT1 and mENBT1

4.1 **Introduction**

6-MP was first introduced in the therapy of leukemia and lymphoma in 1953 (Burchenal et al., 1953; Hall et al., 1953; Hill and Lajous, 1954; Toksvang et al., 2022), and is still used to this day in the treatment of ALL and IBD. Despite long history of clinical utilization, the mechanism in which 6-MP, a prodrug that requires intracellular metabolism to produce a therapeutic response, enters cells is not fully understood. This knowledge gap was evident by 1983, in which 6-MP bioavailability was observed to vary widely between patient populations upon administration of standardized doses (Zimm et al., 1983; Lonnerholm et al., 1986; Larsen et al., 2020; Zou et al, 2023). Concerns were compounded by severe side effects, including myelotoxicity, leukopenia, thrombocytopenia, & hepatotoxicity (Dubinsky et al., 2000; Gearry et al., 2004; van Asseldonk et al., 2012; Luber et al., 2019; Sousa et al., 2020). Potentially fatal adverse events are transient and subside upon 6-MP therapy discontinuation (Kontorinis et al., 2004; Nygaard et al., 2004). However, discontinuation is associated with higher relapse risk with lower survival rates (Bhatia et al., 2015; Gupta and Bhatia, 2017). Due to the prevalence of pediatric ALL cases, decreased 6-MP therapy adherence in adolescents, due to abundant incidents of adverse events is a known challenge (Kahn et al., 2023).

Relatively low affinity nucleoside transporters were initially cited as the mechanism for 6-MP intracellular accumulation (Baldwin et al., 2004; Zaza et al., 2010; Young et al., 2013), until Furukawa and colleagues, (2015) functionally characterized ENBT1 in stably transfected Madin-Darby canine kidney cells (MDCKII) and published that 6-MP significantly inhibited ENBT1-mediated [^{3}H]adenine uptake, which suggests 6-MP is a potential ENBT1 substrate. ENBT1 expression has been shown in human leukemia cells and hepatocytes, and thus was a promising 6-MP transporter candidate (Human Protein Atlas; https://www.proteinatlas.org/) (Uhlen et al.,

2015; Thul et al., 2017). To better investigate ENBT1 as a potential 6-MP flux transporter in a human model rather than canine, our laboratory stably transfected innately ENBT1-deficient HEK293 cell lines (Ruel et al., 2019), to overexpress recombinant *SLC43A3*-encoded hENBT1, *slc43a3*-encoded mENBT1, or a pcDNA3.1(-) empty vector control. These cell models were utilized to functionally characterize ENBT1-mediated adenine and 6-MP transport kinetics, inhibition kinetics, and 6-MP effects on cell viability, in cells models that express hENBT1, mENBT1, or neither transporter.

4.2 **Results**

4.2.a **Confirmation of HEK293 transfection with *SLC43A3* and *slc43a3***

HEK293-WT cell lines that are innately ENBT1-deficient (Ruel et al., 2019) were stably transfected with *SLC43A3*, *slc43a3* or a pcDNA3.1(-) empty vector, herein by referred to as HEK293-hSLC43A3, HEK293-mslc43a3, and HEK293-EV, respectively. Transfected cells were cultured and selected based on G418 sulfate resistance (600 μg/mL). Resulting HEK293-hSLC43A3 and HEK293-mslc43a3 clone colonies were further selected for MYC-ENBT1 expression via dot blot probing for MYC-tag. Circled HEK293-mslc43a3 C10 and E11 clones were selected for further experimentation based on exhibiting the highest MYC-mENBT1 expression levels (Figure 9.A). To confirm successful stable transfection, qualitative PCR and immunoblot were performed utilizing cDNA and cell lysates processed from HEK293-EV, HEK293-hSLC43A3, and HEK293-mslc43a3 cell lines. Assessment of PCR products exhibit that HEK293-EV cells express minimal levels of *SLC43A3* and undetectable levels of *slc43a3* transcript; HEK293-hSLC43A3 cells express *SLC43A3* and undetectable levels of *slc43a3* transcript; HEK293-mslc43a3 cells express *slc43a3* and undetectable levels of *SLC43A3*

transcript. *GAPDH* was utilized as a loading control (Figure 9.B). Assessment of immunoblot bands exhibit HEK293-EV cells express undetectable levels of hENBT1, mENBT1, and MYC; HEK293-hSLC43A3 cells express MYC-hENBT1; HEK293-mslc43a3 cells express MYC-mENBT1. β-actin was utilized as a loading control (Figure 9.C). Densitometry performed on MYC-hENBT1 and MYC-mENBT1 normalized to β-actin, on immunoblots intermittently run between July 2021 – January 2023, show normalized expression levels are not significantly different between HEK293-hSLC43A3 and HEK293-mslc43a3 cell lines (Unpaired student's t-test, $t_{16} = 0.2555$, $p = 0.8011$, $n = 9$) (Figure 9.D).

Figure 9. Transcript and protein expression of transfected-HEK293 ►

PCR products and protein expression was assessed in HEK293-EV, HEK293-hSLC43A3, and HEK293-mslc43a3 cell lines. **A:** Representative dot blot using protein from HEK293-mslc43a3 crude cell lysates, primary anti-MYC-tag antibodies, and HRP-conjugated anti-mouse secondary antibodies. Column #12: was a negative control. This dot blot was performed by Ph.D. Candidate Nicholas M Ruel. **B:** Representative PCR gel using cDNA synthesized from transfected-HEK293 total RNA and PCR primers to amplify products; *SLC43A3* (Expected Size: 400 bp), *slc43a3* (Expected Size: 400 bp), *GAPDH* (Expected Size: 356 bp). dH_2O blank was used as a negative control, *GAPDH* was used as a loading control. **C:** Representative immunoblot using 30 μg protein from transfected-HEK293 crude cell lysates, primary anti-hENBT1, anti-mENBT1, anti-MYC-tag, and anti-β-actin, and HRP-conjugated anti-rabbit and anti-mouse secondary antibodies; MYC-hENBT1 (Expected Size: 56.0 kDA), MYC-mENBT1 (Expected Size: 57.5 kDA), and β-actin (Expected Size: 42.0 kDa). β-actin was used as a loading control. **D:** Densitometry analysis performed on immunoblots comparing expression levels of MYC-hENBT1 and MYC-mENBT1, relative to β-actin loading control, in HEK293-hSLC43A3 and HEK293-mslc43a3 cell lines. MYC-tag expression was normalized to β-actin loading control:

$$\text{Normalized MYC ENBT1 Expression} = \frac{(\text{MYC ENBT1 band intensity AUC})}{(\beta\ \text{actin band intensity AUC})}$$

Robust regression and outlier removal (ROUT) method with ROUT coefficient Q = 1% was utilized to detect and remove outliers. Each numbered pair represent data points (#1 - #9) that were analyzed from the same blot. Data are shown as mean ± SD (n=9).

Figure 9.

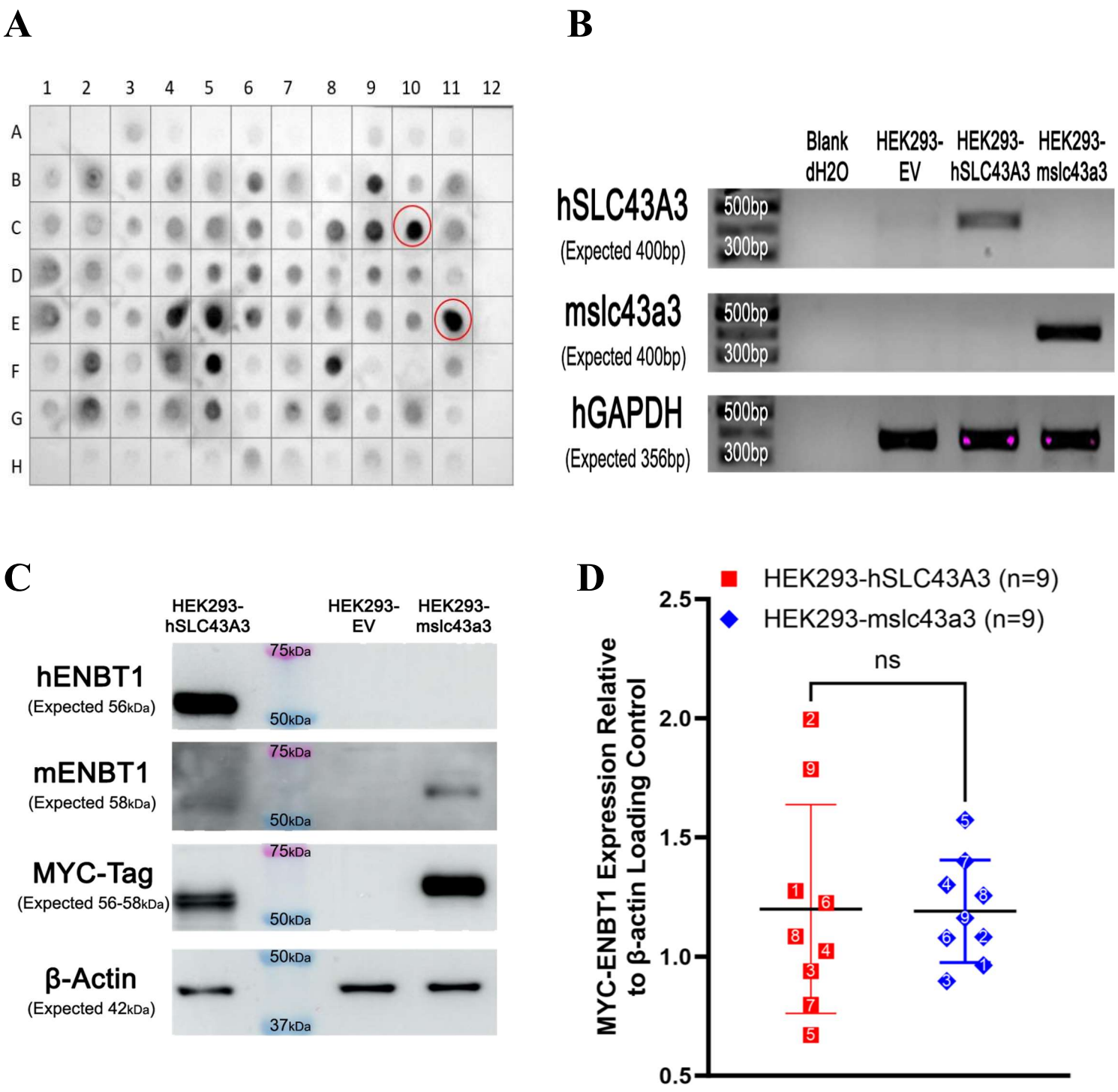
A
1 2 3 4 5 6 7 8 9 10 11 12
A
B
C
D
E
F
G
H
B
Blank dH2O
HEK293-EV
HEK293-hSLC43A3
HEK293-mslc43a3
hSLC43A3
(Expected 400bp)
mslc43a3
(Expected 400bp)
hGAPDH
(Expected 356bp)
500bp
300bp
C
HEK293-hSLC43A3
HEK293-EV
HEK293-mslc43a3
hENBT1
(Expected 56kDa)
mENBT1
(Expected 58kDa)
MYC-Tag
(Expected 56-58kDa)
β-Actin
(Expected 42kDa)
75kDa
50kDa
37kDa
D
HEK293-hSLC43A3 (n=9)
HEK293-mslc43a3 (n=9)
ns
MYC-ENBT1 Expression Relative to β-actin Loading Control
2.5
2.0
1.5
1.0
0.5

4.2.b **Functional characterization of recombinant mENBT1 in HEK293-mslc43a3 cells**

In the interest of assessing transport, determining a substrate incubation time or time point that captured the initial rate of transport, rather than at a steady-state/equilibrium state, was essential to better approximate transport kinetic parameters such as K_m and V_{max} (Michaelis et al., 2011). Functional assessment of the initial rate of mENBT1-mediated uptake was performed in HEK293-mslc43a3 clones (C10 and E11) and HEK293-WT cell lines. Total uptake was obtained in the HEK293-mslc43a3 clones (C10 and E11), by assessing the initial rate of transport of 30 μM [^{3}H]adenine at 2 second – 90 second time points, in the presence and absence of 10 μM decynium-22 (D22), an ENBT1 inhibitor which achieves 71% ± 6% inhibition of ENBT1 at 10 μM (Ruel et al., 2019). At the time, non-mediated uptake was obtained in the HEK293-WT cells, by assessing the initial rate of transport in the same conditions stated above. As described previously in section 3.6, ENBT1-mediated uptake was derived as the difference between total uptake, which contains ENBT1-mediated uptake and background transport components, and non-mediated uptake, which contains background transport components. HEK293-WT cells displayed minimal time-dependent/saturable and D22-insensitive uptake of [^{3}H]adenine, as seen by the linear fit (Figure 10.A). On the other hand, C10 and E11 HEK293-mslc43a3 clones exhibited time-dependent/saturable and D22-sensitive uptake of [^{3}H]adenine, plateauing at roughly 30 pmol/μL, with a rate constant (k-value) of 0.92 ± 0.73 sec^{-1} and 0.49 ± 0.05 sec^{-1} in the C10 and E11 clones, in absence of D22, respectively (Figure 10.B and 7.C).

Figure 10. Recombinant mENBT1 transport kinetics in HEK293-mslc43a3 ►

Initial rate of mENBT1-mediated uptake assessed in HEK293-WT and HEK293-mslc43a3 cell lines looking at [^{3}H]adenine in presence or absence of D22 at 2 second – 90 second time points. **A:** HEK293-WT (n=5) adenine time course showing non-mediated uptake of [^{3}H]adenine in presence or absence of 10 μM D22. **B:** HEK293-mslc43a3 E11 clone (n=5) and **C:** HEK293-mslc43a3 C10 clone (n=2); adenine time course showing ENBT1-mediated uptake of 30 μM [^{3}H]adenine in presence or absence of 10 μM D22. Data are shown as mean ± SD. k values were calculated by Graphpad Prism 10 software utilizing the following formula:

$$k = Ln(2)/t_{1/2}$$

This functional characterization work was performed by Ph.D. Candidate Nicholas M Ruel.

Figure 10.

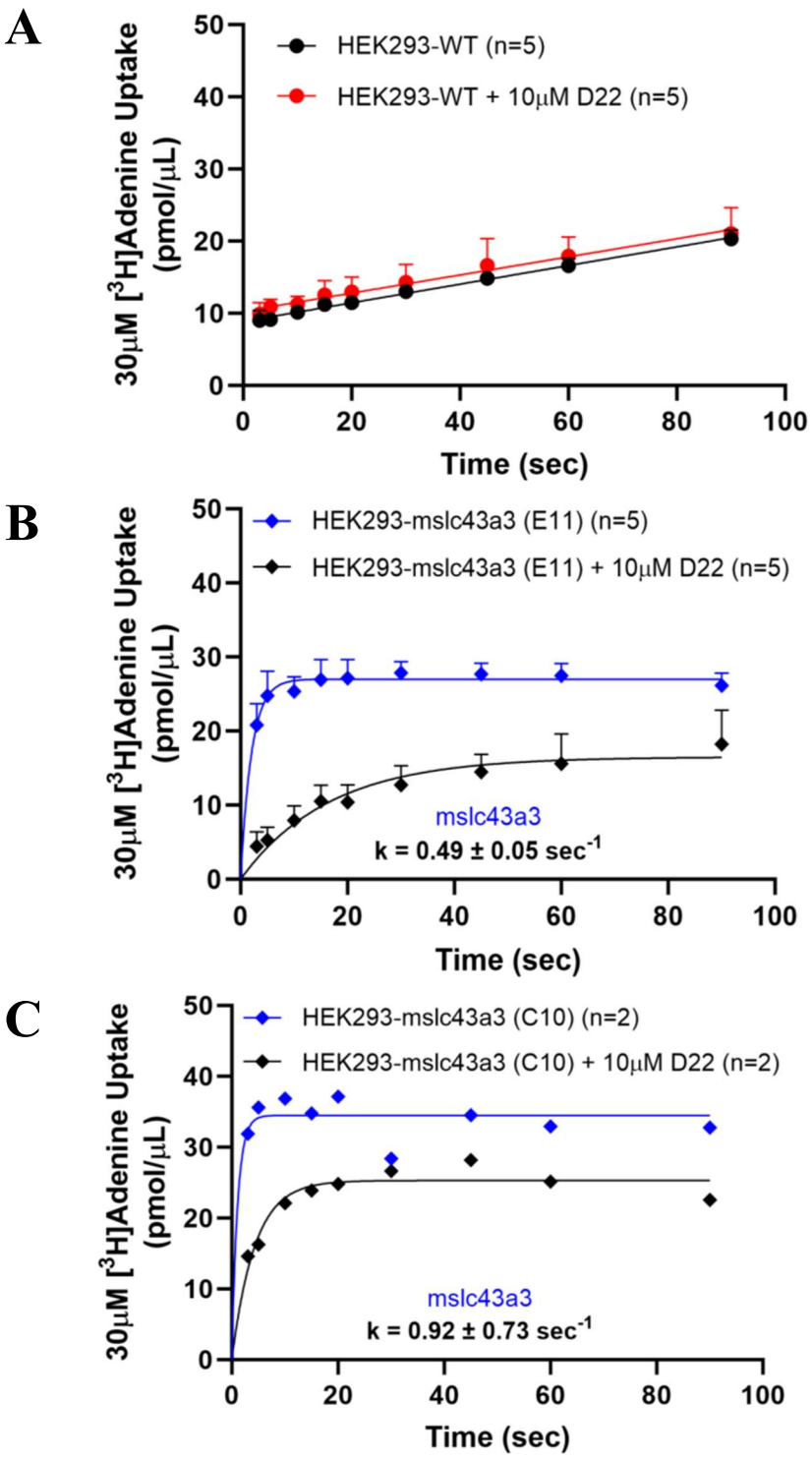
A
HEK293-WT (n=5)
HEK293-WT + 10μM D22 (n=5)
30μM [3H]Adenine Uptake (pmol/μL)
Time (sec)
B
HEK293-mslc43a3 (E11) (n=5)
HEK293-mslc43a3 (E11) + 10μM D22 (n=5)
mslc43a3
k = 0.49 ± 0.05 sec-1
C
HEK293-mslc43a3 (C10) (n=2)
HEK293-mslc43a3 (C10) + 10μM D22 (n=2)
mslc43a3
k = 0.92 ± 0.73 sec-1

4.2.c **Recombinant hENBT1 and mENBT1 transport kinetics in transfected-HEK293**

Functional comparison between hENBT1 and mENBT1 transport kinetics, of known substrates such as adenine and 6-MP, were made by assessing radiolabeled substrate influx in nominally sodium free conditions with NMG buffer, to eliminate potential sodium dependent transport (CNT2 and CNT3), and 15-minute cell incubation with 10 μM DY, to eliminate potential nucleoside transport (ENT1 and ENT2). Total uptake was obtained in the HEK293-hSLC43A3 and HEK293-mslc43a3 cells, by utilizing concentrations of [^{3}H]adenine ranging from 1 μM – 300 μM, or [^{3}H]6-MP ranging from 1 μM – 400 μM incubated in cells, at 2 second time points to capture initial rate of transport; due to not expressing ENBT1, non-mediated uptake was obtained in the HEK293-EV cells at the same conditions. As described previously in section 3.6, ENBT1-mediated uptake was derived as the difference between total uptake, which contains ENBT1-mediated uptake and background transport components, and non-mediated uptake, which contains background transport components.

Time course assays were replicated to confirm a suitable time point in HEK293-hSLC43A3 and HEK293-mslc43a3 cells using 1 μM [^{3}H]6-MP at 2 second – 30 second time points. As seen previously, HEK293-EV cells exhibited minimal time-dependent/saturable uptake of [^{3}H]6-MP, as seen by the linear fit (Figure 11.A). On the other hand, HEK293-hSLC43A3 and HEK293-mslc43a3 cells exhibited time-dependent/saturable uptake of [^{3}H]6-MP, plateauing at roughly 1 pmol/μL, with k-values of 1.03 ± 0.06 sec^{-1} and 1.10 ± 0.58 sec^{-1} in the HEK293-hSLC43A3 and HEK293-mslc43a3 cells, respectively (Figure 11.A). F-test analysis of k-values determined no significant difference between HEK293-hSLC43A3 and HEK293-mslc43a3 cells (Extra sum-of-squares F-test, $F_{1, 86}$ =0.006, p=0.938, n=5), suggesting that recombinant hENBT1 and mENBT1 transport [^{3}H]6-MP at similar rates (Figure 11.A). Obtained k-values suggested relatively rapid

uptake by ENBT1, thus 2 seconds was chosen again as the best estimation of initial rate with our current equipment. Subsequently, transport kinetics of the endogenous substrate adenine were assessed in HEK293-hSLC43A3 and HEK293-mslc43a3 cells, using 1 μM - 300 μM [^{3}H]adenine, at 2 second time points. [^{3}H]adenine uptake was found to be saturable with a K_m value of 93 ± 24 μM and a V_{max} value of 56 ± 6 μM/sec, and a K_m value of 86 ± 22 μM and a V_{max} value of 62 ± 6 μM/sec in the HEK293-hSLC43A3 and HEK293-mslc43a3 cells, respectively. F-test analysis of the K_m determined no significant difference between HEK293-hSLC43A3 and HEK293-mslc43a3 cells (Extra sum-of-squares F-test, $F_{1, 104}$ =0.048, p=0.8266, n=5), suggesting that hENBT1 and mENBT1 have similar [^{3}H]adenine affinities. F-test analysis of the V_{max} also determined no significant difference between HEK293-hSLC43A3 and HEK293-mslc43a3 cells (Extra sum-of-squares F-test, $F_{1, 104}$ =0.441, p=0.508, n=5) (Figure 11.B). This concurred with immunoblot densitometry (Figure 9.D) that MYC-hENBT1 and MYC-mENBT1 expression levels are similar and stable.

Similar assays were performed using the exogenous/xenobiotic substrate 6-MP, in HEK293-hSLC43A3 and HEK293-mslc43a3 cells, using 1 μM - 400 μM [^{3}H]6-MP, at 2 second time points. [^{3}H]6-MP uptake was found to be saturable with a K_m value of 269 ± 67 μM and a V_{max} value of 121 ± 16 μM/sec, and a K_m value of 253 ± 39 μM and a V_{max} value of 144 ± 12 μM/sec in the HEK293-hSLC43A3 and HEK293-mslc43a3 cells, respectively. F-test analysis of the K_m determined no significant difference between HEK293-hSLC43A3 and HEK293-mslc43a3 cells (Extra sum-of-squares F-test, $F_{1, 98}$ =0.049, p=0.825, n=6), suggesting that hENBT1 and mENBT1 have similar [^{3}H]6-MP affinities. F-test analysis of the V_{max} also determined no significant difference between HEK293-hSLC43A3 and HEK293-mslc43a3 cells (Extra sum-of-squares F-test, $F_{1, 98}$ =1.177, p=0.281, n=6); data point 8 were determined to be significantly different via 2-way ANOVA with post hoc Šidák multiple comparison test (Figure 11.C).

Figure 11. Recombinant hENBT1 and mENBT1 transport kinetics in transfected-HEK293 ►

Transport assays performed in HEK293-hSLC43A3, HEK293-mslc43a3, and HEK293-EV cells in sodium free conditions, and presence of 10 μM DY. HEK293-EV were utilized to determine non-mediated uptake/background levels of transport. **A:** HEK293-hSLC43A3 and HEK293-mslc43a3 6-MP time course assay showing initial rate and steady state of hENBT1 and mENBT1-mediated uptake of 1 μM [^{3}H]6-MP, at 2 second – 30 second time points (n=5). **B:** HEK293-hSLC43A3 and HEK293-mslc43a3 adenine K_m/V_{max} assay showing hENBT1 and mENBT1 transport kinetics of 1 μM - 300 μM [^{3}H]adenine, at 2 second time points (n=5). **C:** HEK293-hSLC43A3 and HEK293-mslc43a3 6-MP K_m/V_{max} assay showing hENBT1 and mENBT1 transport kinetics of 1 μM - 400 μM [^{3}H]6-MP, at 2 second time points (n=6). Data are shown as mean ± SD; * denotes a significant difference in initial rate of [^{3}H]6-MP uptake between HEK293-hSLC43A3 and HEK293-mslc43a3 at specified concentrations (2-way ANOVA with post hoc Šidák multiple comparison test, P=0.05).

Figure 11.

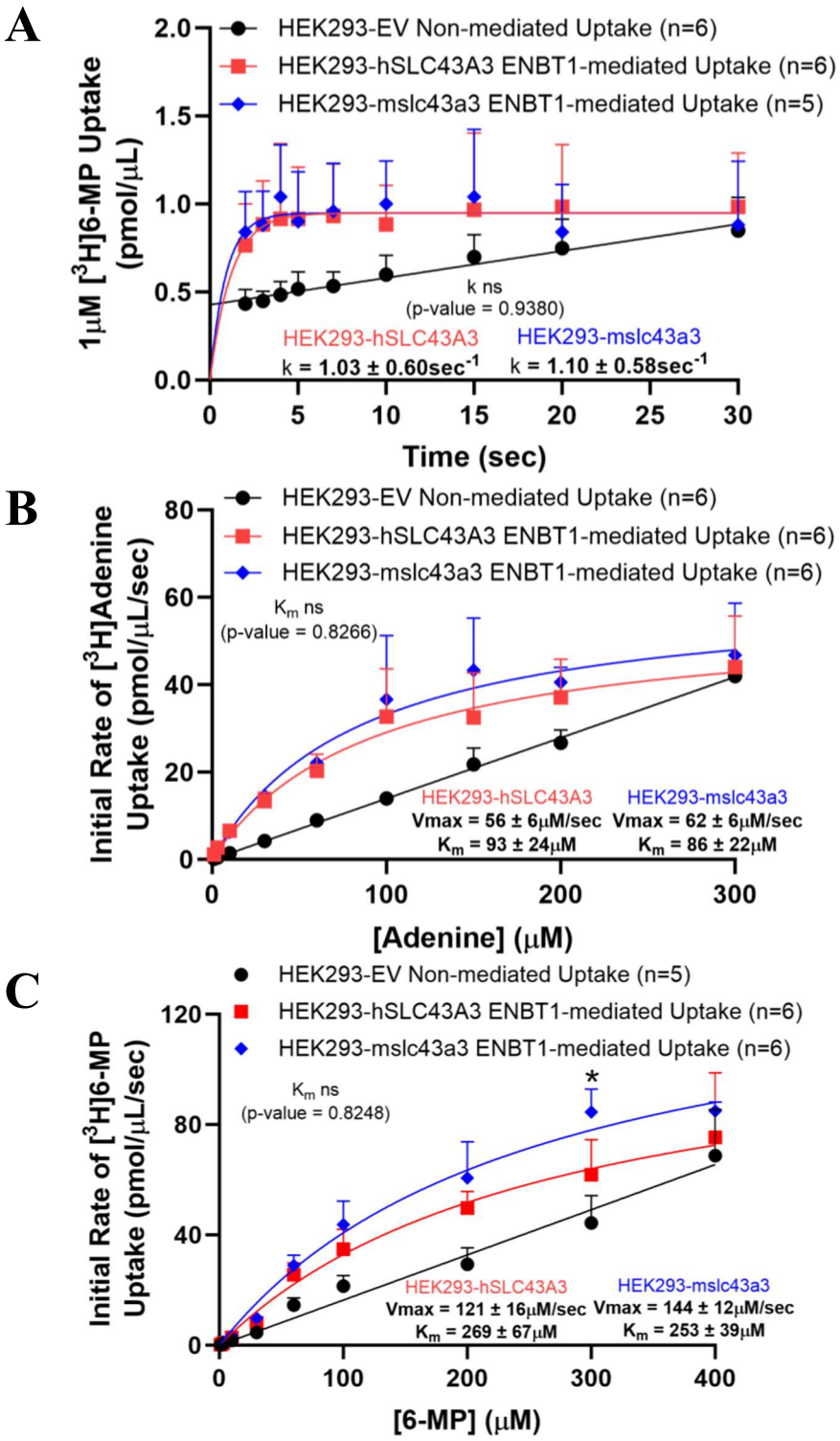
A
HEK293-EV Non-mediated Uptake (n=6)
HEK293-hSLC43A3 ENBT1-mediated Uptake (n=6)
HEK293-mslc43a3 ENBT1-mediated Uptake (n=5)
1μM [3H]6-MP Uptake (pmol/μL)
k ns
(p-value = 0.9380)
HEK293-hSLC43A3
k = 1.03 ± 0.60sec-1
HEK293-mslc43a3
k = 1.10 ± 0.58sec-1
Time (sec)
B
HEK293-EV Non-mediated Uptake (n=6)
HEK293-hSLC43A3 ENBT1-mediated Uptake (n=6)
HEK293-mslc43a3 ENBT1-mediated Uptake (n=6)
Km ns
(p-value = 0.8266)
Initial Rate of [3H]Adenine Uptake (pmol/μL/sec)
HEK293-hSLC43A3
Vmax = 56 ± 6μM/sec
Km = 93 ± 24μM
HEK293-mslc43a3
Vmax = 62 ± 6μM/sec
Km = 86 ± 22μM
[Adenine] (μM)
C
HEK293-EV Non-mediated Uptake (n=5)
HEK293-hSLC43A3 ENBT1-mediated Uptake (n=6)
HEK293-mslc43a3 ENBT1-mediated Uptake (n=6)
Km ns
(p-value = 0.8248)
*
Initial Rate of [3H]6-MP Uptake (pmol/μL/sec)
HEK293-hSLC43A3
Vmax = 121 ± 16μM/sec
Km = 269 ± 67μM
HEK293-mslc43a3
Vmax = 144 ± 12μM/sec
Km = 253 ± 39μM
[6-MP] (μM)

4.2.d **Recombinant hENBT1 and mENBT1 inhibition kinetics in transfected-HEK293**

In the interest of assessing inhibition kinetics of competitive inhibitors via an equation described by Cheng and Prusoff, (1973) and comparing to known transport kinetics, IC_{50} values were determined for substrates with known K_m values in the literature (adenine K_m: ~30 µM and 6-MP K_m: ~150 µM), and K_i values were calculated accordingly:

$$\text{Cheng Prusoff equation} = \left(K_i = \frac{IC50}{1+\frac{[S]}{Km}}\right)$$

Theoretically, in the case of a purely competitive inhibitor, the K_m value of a substrate, which denotes the affinity a substrate has for binding a transporter, should be similar to the K_i value, which denotes the affinity an inhibitor has for binding a transporter, when that substrate is used as an inhibitor. Thus, functional comparison was performed between hENBT1 and mENBT1 inhibition kinetics of previously identified inhibitors, such as adenine and 6-MP (Furukawa et al., 2015; Ruel et al., 2019), by assessing radiolabeled substrate influx in the same nominally sodium free, 10 µM DY conditions, 2 second time points, and presence or absence of an inhibitor. Adenine inhibition profiles on HEK293-hSLC43A3 and HEK293-mslc43a3 were performed by different individuals, and thus different concentrations of [^{14}C]6-MP were utilized; 100 µM was used for total (HEK293-hSLC43A3) and non-mediated (HEK293-EV) by Ph.D. candidate Nicholas M Ruel, while 150 µM was used for total (HEK293-mslc43a3) and non-mediated (HEK293-EV) by myself. Total uptake was obtained in HEK293-hSLC43A3 and HEK293-mslc43a3 cells with either 100 µM or 150 µM of [^{14}C]6-MP, and concentrations of adenine ranging from 300 nM – 1 mM; non-mediated uptake was obtained in the HEK293-EV cells at the same conditions. ENBT1-mediated uptake was calculated by subtracting non-mediated uptake from total uptake as previously described. 100% uptake control was obtained in HEK293,

HEK293-hSLC43A3 and HEK293-mslc43a3 cells with either 100 µM or 150 µM of [^{14}C]6-MP, in absence of adenine, instead an equal volume of solvent (NMG buffer) was added in assay. % of control [^{14}C]6-MP uptake was calculated by dividing ENBT1-mediated in presence of inhibitor by 100% uptake control:

$$\left(\%\ of\ control\ uptake = \frac{\text{(Total uptake)} - \text{(Non mediated uptake)}}{\text{(100\% uptake control)} - \text{(Non mediated uptake)}}\right)$$

Adenine exhibited concentration-dependent inhibition of ENBT1-mediated [^{14}C]6-MP uptake relative to the 100% uptake control, reaching near complete inhibition at 1 mM adenine. Analysis of IC_{50} values with student's t-test, determined no significant difference between HEK293-hSLC43A3 and HEK293-mslc43a3 cells (Unpaired student's t-test, $t_8 = 0.965$, $p = 0.363$, $n = 5$), suggesting that hENBT1 and mENBT1 bind adenine with similar affinities. Calculated K_i values were 25 ± 9 µM and 51 ± 13 µM in HEK293-hSLC43A3 and HEK293-mslc43a3 cells, respectively (Figure 12.A). Following up, 6-MP inhibition profile was performed on HEK293-hSLC43A3 and HEK293-mslc43a3 cells utilizing 30 µM [^{3}H]adenine. Total uptake was obtained in HEK293-hSLC43A3 and HEK293-mslc43a3 cells with 30 µM [^{3}H]adenine and concentrations of 6-MP ranging from 300 nM – 1 mM; non-mediated uptake was obtained in the HEK293-EV cells at the same conditions. 100% uptake control was obtained in HEK293, HEK293-hSLC43A3 and HEK293-mslc43a3 cells with 30 µM [^{3}H]adenine in absence of 6-MP, instead an equal volume of solvent (DMSO) was added in assay. All other conditions and analyses were as previously described. 6-MP also exhibited concentration-dependent inhibition of ENBT1-mediated [^{3}H]adenine uptake relative to the 100% uptake control, however, complete inhibition was not obtained at the highest 6-MP concentration (1 mM). Thus, inhibition curve was incomplete and IC_{50} was extrapolated. Analysis of IC_{50} values with student's t-test determined no significant difference between

HEK293-hSLC43A3 and HEK293-mslc43a3 cells (Unpaired student's t-test, $t_8 = 0.939$, $p = 0.375$, $n = 5$), suggesting that hENBT1 and mENBT1 bind 6-MP with similar affinities (Figure 12.B). Calculated K_i values were 5.9 ± 0.7 mM and 7.4 ± 1.3 mM in HEK293-hSLC43A3 and HEK293-mslc43a3 cells, respectively. These K_i values were several folds higher than expected K_m values for 6-MP. To further explore this discrepancy and determine whether adenine has a competitive advantage at the ENBT1 binding site, the same 6-MP inhibition profile was replicated utilizing 30 μM [^{3}H]adenine and pre-incubating cells with 6-MP or equal volumes of solvent (DMSO) for 10 mins prior to the assay. For example, cells utilized for the 1 mM 6-MP data point, were incubated with either 1 mM 6-MP or 1% DMSO for 10 minutes; considerations were made to ensure final in assay 6-MP concentrations were equal between conditions. However, pre-incubating cells with 6-MP did not affect concentration- dependent inhibition of ENBT1-mediated [^{3}H]adenine uptake, and calculated K_i values (Figure 12.C).

Figure 12. hENBT1 and mENBT1 inhibition kinetics in transfected-HEK293 ►

Transport assays performed in HEK293-hSLC43A3, HEK293-mslc43a3, and HEK293-EV cells in sodium free conditions and presence of 10 μM DY. HEK293-EV were utilized to determine non-mediated uptake. **A:** HEK293-hSLC43A3 and HEK293-mslc43a3 adenine inhibition profile showing hENBT1 and mENBT1 inhibition kinetics of 100 μM (HEK293-mslc43a3), or 150 μM (HEK293-hSLC43A3), of [^{14}C]6-MP in presence of 300 nM - 1 mM adenine, at 2 second time points (n=5). HEK293-hSLC43A3 work was performed by Ph.D. candidate Nicholas M Ruel. **B:** HEK293-hSLC43A3 and HEK293-mslc43a3 6-MP inhibition profile showing hENBT1 and mENBT1 inhibition kinetics of 30 μM [^{3}H]adenine, in presence of 300 nM - 1 mM 6-MP, at 2 second time points (n=5). **C:** HEK293-hSLC43A3 and HEK293-mslc43a3 6-MP inhibition profile showing hENBT1 and mENBT1 inhibition kinetics of 30 μM [^{3}H]adenine in presence of 3 μM - 1 mM 6-MP, at 2 second time points, with pre-incubation of cells with 3 μM - 1 mM 6-MP, or equal volumes of solvent (DMSO), 10 mins prior to [^{3}H]adenine introduction (n=5). Data are shown as mean ± SD.

Figure 12.

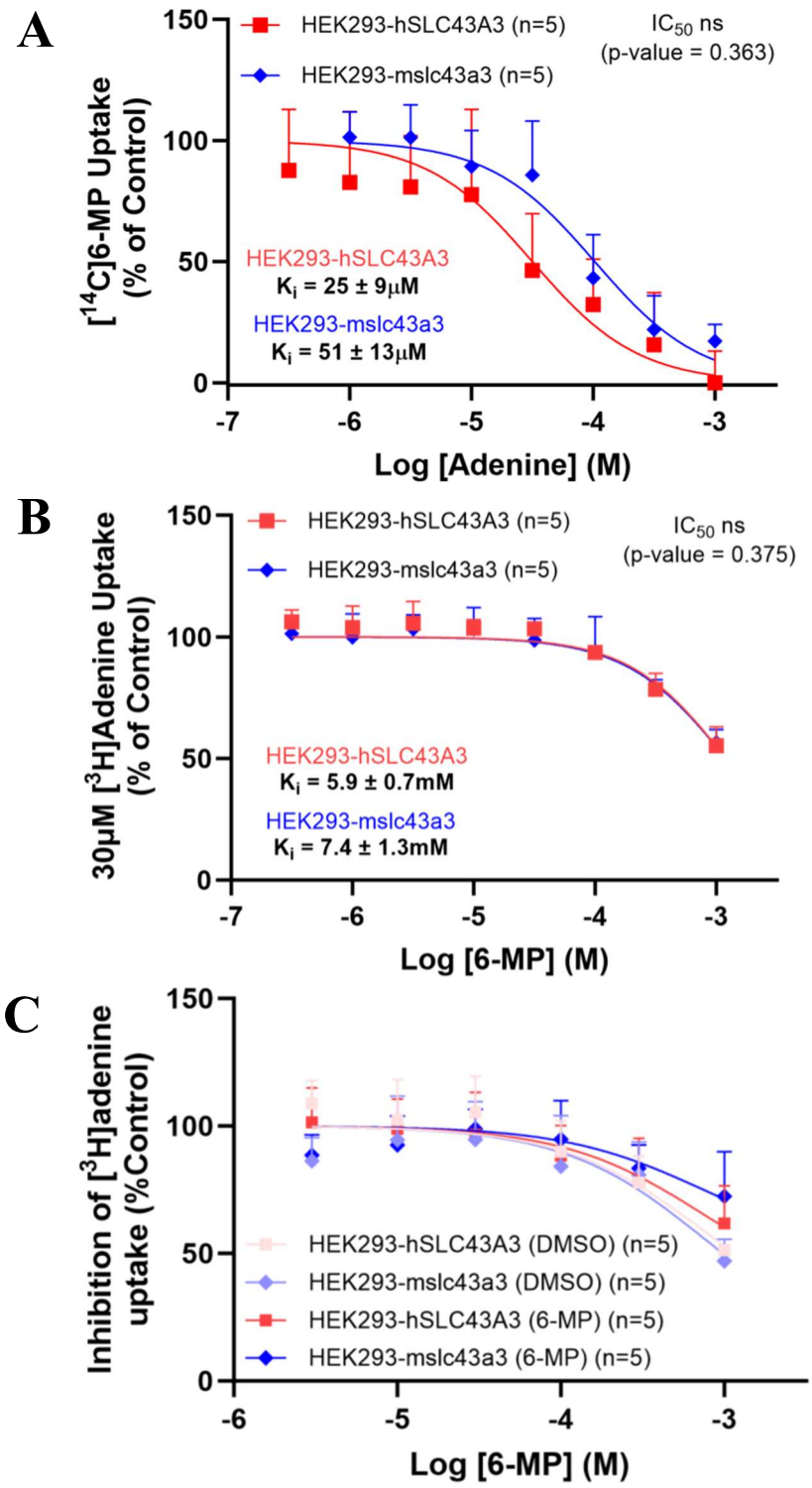
A
HEK293-hSLC43A3 (n=5)
HEK293-mslc43a3 (n=5)
IC50 ns
(p-value = 0.363)
[14C]6-MP Uptake
(% of Control)
HEK293-hSLC43A3
Ki = 25 ± 9μM
HEK293-mslc43a3
Ki = 51 ± 13μM
Log [Adenine] (M)
B
HEK293-hSLC43A3 (n=5)
HEK293-mslc43a3 (n=5)
IC50 ns
(p-value = 0.375)
30μM [3H]Adenine Uptake
(% of Control)
HEK293-hSLC43A3
Ki = 5.9 ± 0.7mM
HEK293-mslc43a3
Ki = 7.4 ± 1.3mM
Log [6-MP] (M)
C
Inhibition of [3H]adenine
uptake (%Control)
HEK293-hSLC43A3 (DMSO) (n=5)
HEK293-mslc43a3 (DMSO) (n=5)
HEK293-hSLC43A3 (6-MP) (n=5)
HEK293-mslc43a3 (6-MP) (n=5)
Log [6-MP] (M)

4.2.e **Effect of 6-MP/6-MP metabolites on cell viability in transfected-HEK293 cells**

Another indirect measure of ENBT1 function were assessed via 6-MP/6-MP metabolite cell viability assays in transfected-HEK293 cells. We hypothesized that if ENBT1 mediated the cellular accumulation of a compound that has cytotoxic properties, or is otherwise detrimental to cellular mitochondria function, HEK293-hSLC43A3 and HEK293-mslc43a3 cells which express hENBT1 and mENBT1, should upon treatment, exhibit higher sensitivity or a leftward shift in cell viability, relative to HEK293-EV cells which do not express either transporter. Compound-mediated response, 100% cell viability, 0% cell viability, and % reduced MTT were obtained and calculated as described previously in section 3.7. 6-MP exhibited a biphasic 6-MP cell viability curve with first-phase EC_{50} values of 18.8 ± 0.51 μM, 0.99 ± 0.09 μM, and 0.96 ± 0.28 μM for HEK293-EV, HEK293-hSLC43A3, and HEK293-mslc43a3 cells, respectively. F-test analysis of HEK293-hSLC43A3 and HEK293-mslc43a3 6-MP first-phase EC_{50} values (HEK293-EV excluded) determined no significant difference (Extra sum-of-squares F-test, $F_{1,255}$=1.427, p=0.233, n=8), suggesting that hENBT1 and mENBT1 mediate 6-MP effect on cell viability similarly (Figure 13.A). This assay was then replicated 1:1 with 80 nM – 1.28 mM 6-MeMP. 6-MeMP also exhibited a biphasic 6-MeMP cell viability curve with first-phase EC_{50} values of 45 ± 7 μM, 79 ± 2 μM, and 42 ± 6 μM for HEK293-EV, HEK293-hSLC43A3, and HEK293-mslc43a3 cells, respectively. No shift in cell viability or 6-MeMP first-phase EC_{50} values was observed between HEK293-EV cells and HEK293-hSLC43A3 and HEK293-mslc43a3 cells (Extra sum-of-squares F-test, $F_{2,444}$=0.904, p=0.406, n=8) (Figure 13.B). Further assays were performed on 6-TG, however, 6-TG had lower solubility in DMSO, thus DMSO % was triple that in previous assays at the same 80 nM – 1.28 mM concentration range. 6-TG exhibited a single-phase cell viability curve with EC_{50} values of 16 ± 4.3 μM, 3.4 ± 0.9 μM, and

3.4 ± 1.1 μM for HEK293-EV, HEK293-hSLC43A3, and HEK293-mslc43a3 cells, respectively. F-test analysis of HEK293-hSLC43A3 and HEK293-mslc43a3 6-TG EC_{50} values (HEK293-EV excluded) determined no significant difference (Extra sum-of-squares F-test, $F_{1,204}$=1.465, p=0.228, n=6), suggesting that hENBT1 and mENBT1 mediate 6-TG effect on cell viability similarly (Figure 13.C). This assay was then replicated 1:1 with 80 nM – 1.28 mM 6-TU. 6-TU exhibited an incomplete cell viability curve for HEK293-EV, HEK293-hSLC43A3, and HEK293-mslc43a3 cells (Figure 13.D). A drop in cell viability was observed in transfected-HEK293 cells at the highest 6-TU concentrations (640 μM and 1.28 mM). Therefore, DMSO effect on cell viability was performed mirroring DMSO % values in 6-TG and 6-TU cell viability assays, which ranged from 1/12500 (0.00008%) – 1/78 (1.28%). DMSO exhibited an incomplete cell viability curve that exhibited a drop in cell viability at the same DMSO % values as 6-TU (Figure 13.E). 6-MeMP, 6-TG, 6-TU, and DMSO cell viability curves were work performed by undergraduate student Hannah Dean, under my supervision for their PMCOL 301 and 302 projects.

Figure 13. 6-MP/6-MP metabolite cell viability in transfected-HEK293 ►

6-MP/6-MP metabolite cell viability curves in HEK293-hSLC43A3, HEK293-mslc43a3, and HEK293-EV cells plated in complete media, treated with 80 nM – 1.28 mM of various compounds, for 48 hours. **A:** Transfected-HEK293 cells 6-MP cell viability curve showing biphasic nature of 6-MP response, and a ~19-fold HEK293-hSLC43A3 and HEK293-mslc43a3 leftward curve shift, relative to HEK293-EV (n=7). **B:** Transfected-HEK293 cells 6-MeMP cell viability curve showing biphasic nature of 6-MeMP response, and no HEK293-hSLC43A3 and HEK293-mslc43a3 curve shift, relative to HEK293-EV (n=8). **C:** Transfected-HEK293 cells 6-TG cell viability curve showing single-phase nature of 6-TG response, and a ~7-fold HEK293-hSLC43A3 and HEK293-mslc43a3 leftward curve shift, relative to HEK293-EV (n=7). **D:** Transfected-HEK293 cells 6-TU cell viability curve showing incomplete 6-TU response, and no HEK293-hSLC43A3 and HEK293-mslc43a3 curve shift, relative to HEK293-EV (n5). **E:** Transfected-HEK293 cells DMSO cell viability curve showing incomplete DMSO response, and no HEK293-hSLC43A3 and HEK293-mslc43a3 curve shift, relative to HEK293-EV (n=5). Figures **B**, **C**, **D**, and **E** were performed by undergraduate student Hannah Dean, under my supervision for their PMCOL 301 and 302 projects. Data are shown as mean ± SD.

Figure 13.

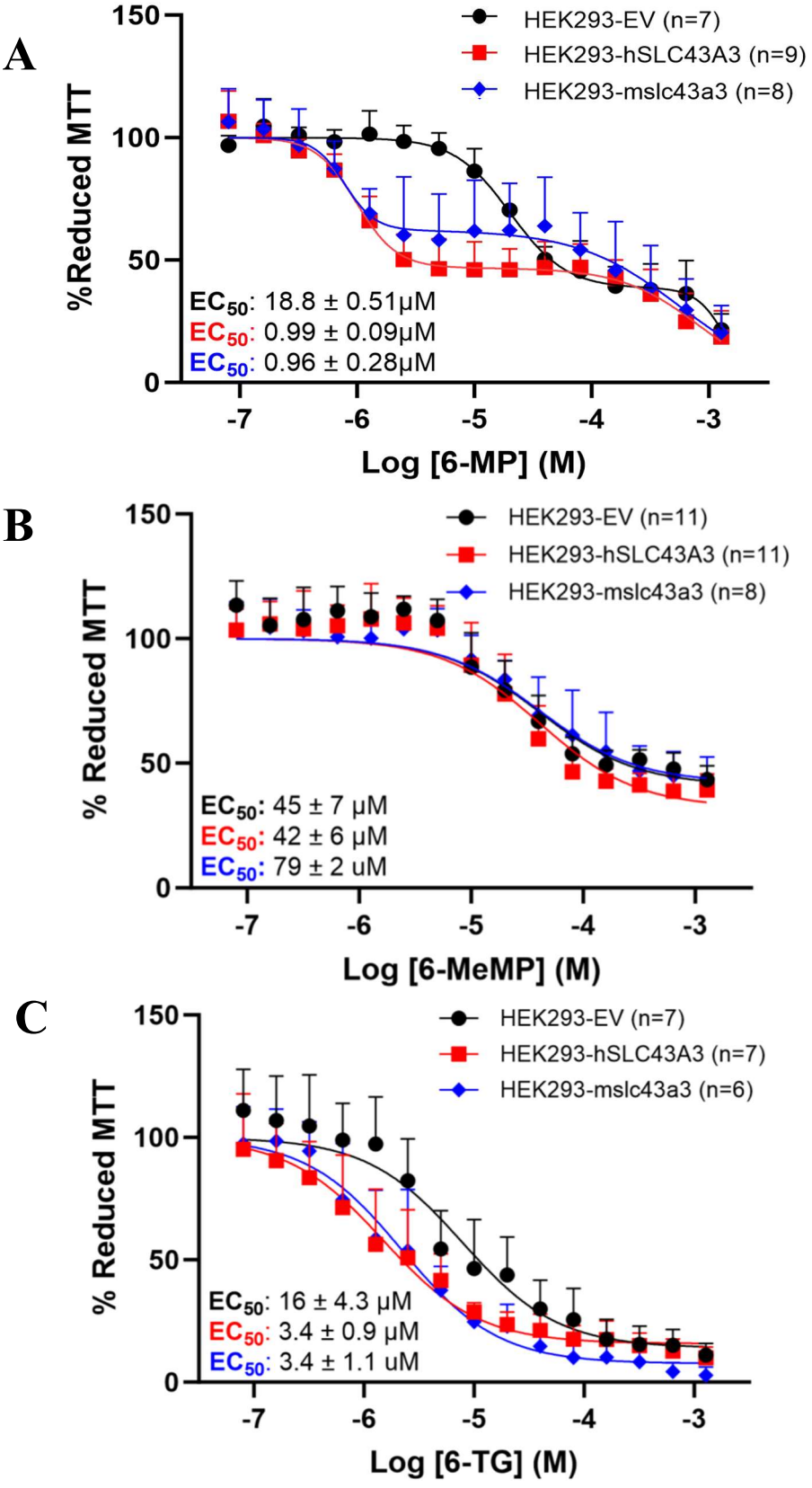
A
HEK293-EV (n=7)
HEK293-hSLC43A3 (n=9)
HEK293-mslc43a3 (n=8)
%Reduced MTT
EC50: 18.8 ± 0.51μM
EC50: 0.99 ± 0.09μM
EC50: 0.96 ± 0.28μM
Log [6-MP] (M)
B
HEK293-EV (n=11)
HEK293-hSLC43A3 (n=11)
HEK293-mslc43a3 (n=8)
% Reduced MTT
EC50: 45 ± 7 μM
EC50: 42 ± 6 μM
EC50: 79 ± 2 uM
Log [6-MeMP] (M)
C
HEK293-EV (n=7)
HEK293-hSLC43A3 (n=7)
HEK293-mslc43a3 (n=6)
% Reduced MTT
EC50: 16 ± 4.3 μM
EC50: 3.4 ± 0.9 μM
EC50: 3.4 ± 1.1 uM
Log [6-TG] (M)

Figure 13

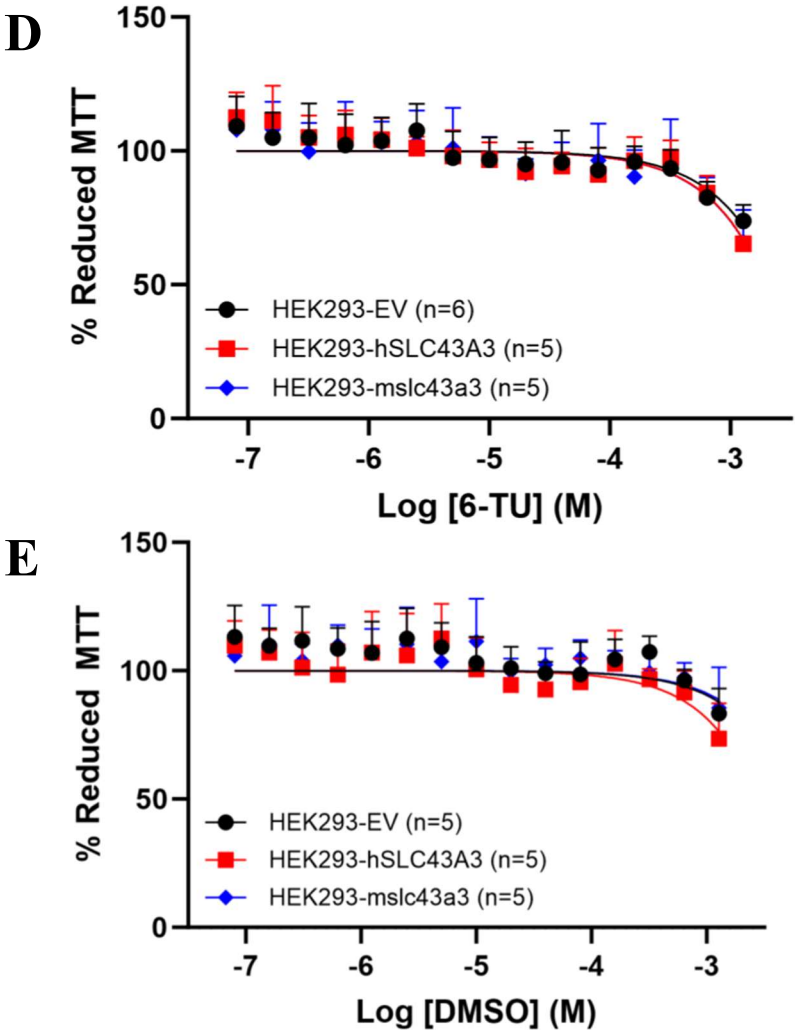
D
150
100
50
0
% Reduced MTT
HEK293-EV (n=6)
HEK293-hSLC43A3 (n=5)
HEK293-mslc43a3 (n=5)
-7
-6
-5
-4
-3
Log [6-TU] (M)
E
150
100
50
0
% Reduced MTT
HEK293-EV (n=5)
HEK293-hSLC43A3 (n=5)
HEK293-mslc43a3 (n=5)
-7
-6
-5
-4
-3
Log [DMSO] (M)

4.3 Discussion

4.3.a **Transfected-HEK293 PCR and immunoblot**

4.3.a.i *SLC43A3* expression detected in HEK293-EV cells

SLC43A3 transcript expression has been detected previously by PCR in HEK293-WT and HEK293-EV cell lines at faint band intensities (Figure 9.B). However, *SLC43A3* transcript expression does not necessarily translate to hENBT1 protein expression (Figure 9.C), as HEK293-WT (Figure 10.A) and HEK293-EV (Figure 9.C and Figure 11.A) cell lines do not express functional hENBT1 with measurable ENBT1-mediated nucleobase flux capacity (Ruel et al., 2019).

4.3.a.ii Anti-hENBT1 primary antibody cannot detect mENBT1

The species reactivity of the anti-hENBT1 (HPA030551) primary antibody has repeatedly shown to not cross react with murine ENBT1 (Figure 9.C). Likely because the anti-hENBT1 antibody epitope site is found on the intracellular loop between TMD 6-7, in a region that is disrupted by a polyQ tract in mENBT1 (Figure 14.). Several commercially available mENBT1 antibodies from suppliers such as Abcam, Santa Cruz, Sigma Aldrich, and Creative Biolabs have been tested utilizing transfected-HEK293 crude cell lysates, to limited success, despite these suppliers advertising appropriate species reactivity and epitope sequences. These antibodies were primarily rejected due to lack of mENBT1 specificity, which manifested as either observing bands in the HEK293-EV cell line (Abcam, Santa Cruz, and Creative Biolabs), or observing no bands in the HEK293-mslc43a3 cell line (Sigma Aldrich). Figure 9.C mENBT1 was probed with anti-mENBT1 antibody from Creative Biolabs, however, these results were not replicable, potentially due to antibody degradation. This was likely due to improper storage

procedures that were initially stated by the supplier, but were later changed without notifying us, sometime after purchase. The suppliers were contacted for a free sample to confirm whether the antibody can detect mENBT1 but degraded due to improper storage, before our lab purchased another vial. However, an agreement was not reached with Creative Biolabs and further work with the antibody was halted.

Figure 14. Anti-hENBT1 antibody antigen sequence alignment ►

Pairwise alignment via EMBOSS Needle of protein sequences hENBT1- 1476 bp, 491 aa (UniProt ID: Q8NBI5) and mENBT1- 1509 bp, 502 aa (UniProt ID: A2AVZ9). Software utilizes the Needleman-Wunsch algorithm to create the optimal global alignment of two sequences. The consensus symbols found between sequences denote where the sequence gapped, are identical, or are similar. A "-" indicates a gap in sequence alignment. A "|" (vertical bar) indicates a position with a fully conserved/identical residue. A "." (period) indicates conservation between groups of weakly similar properties (scores =<0.5 and >0). A ":" (colon) indicates conservation between groups of strongly similar properties (score >0.5). Similarities were scored utilizing the EBLOSUM62 substitution matrix (Madeira et al., 2022). Anti-hENBT1 antibody (HPA030551) antigen sequence was obtained from supplier's (Sigma Aldrich) product page.

Figure 14.

Anti-hENBT1 antibody (HPA030551) antigen sequence:

SFIFISVCSTWHVARTFLLMPRGHIPYPLPPNYSYGLCPGNGTTKEEKETAEHENRELQSKEFLSAKEETPGAGQKQELRSFWSYAFSR

```
hENBT1          151 FGQHRSTIITLYNGAFDSSSAVFLIIKLLYEKGISLRASFIFISVCSTWH    200
                    ||:|||||||||||||||||||:||||||:||||||:||||:||||.||
mENBT1          151 FGKHRSTIITLYNGAFDSSSAVFLVIKLLYEQGISLRSSFIFMSVCSVWH    200

hENBT1          201 VARTFLLMPRGHIPYPLPPNYSYGLCPGNGTTKEEKETAEHENRELQSKE    250
                    :||||||||:||||||||||||||||...|.:|:|.:.||||.:||:|||
mENBT1          201 IARTFLLMPKGHIPYPLPPNYSYGLCSRFGASKKENKAAEHETKELRSKE    250

hENBT1          251 FLSAKEETPGAGQKQ---------------ELRSFWSYAFSRRFAWHLVW    285
                    .|..|||..|..|:|                |..||...|.||||..|:||
mENBT1          251 CLPPKEENSGPEQQQQQEQQQQQQQQQEQHEQHSFRRCALSRRFILHVVW    300
```

4.3.a.iii mENBT1 expression detected in HEK293-hSLC43A3 cells

mENBT1 expression seen in HEK293-hSLC43A3 cells is potentially due to cross-reaction with the mENBT1 antibody, this is supported by densitometry analysis confirming bands observed in HEK293-hSLC43A3 and HEK293-mslc43a3 cells are different molecular weights, 56.8 kDa and 61.8 kDa, respectively. Calculated molecular weights mostly line up with predicted protein molecular weights for MYC-hENBT1 and MYC-mENBT1, 55.9 kDa (Figure 7.) and 57.5 kDa (Figure 8.), respectively. Deviations in observed and predicted molecular weights may be explained by post-translational modifications, such as glycosylation, which on average add 2.5-4 kDa per N-glycosylation site. hENBT1 and mENBT1 are predicted to have several N-glycosylation sites (Figure 15.). However, NetNGlyc - 1.0 (Gupta and Brunak, 2002) does not consider intracellular or extracellular localization of asparagine (asn) residues. Cross referencing predicted N-glycosylation sites with predicted transmembrane topology (Figure 5.), reveal hENBT1 and mENBT1 each have a valid N-glycosylation site at asn55, but mENBT1 (+++) showed higher prediction confidence than hENBT1 (+), due to differing adjacent residues. Another potential explanation for the deviation, may be due to presence of the polyQ tract in mENBT1 driving protein-protein interactions intracellularly (Schafer et al., 2012). However, this hypothesis has not been properly tested, nor has a target peptide been identified.

Figure 15. hENBT1 and mENBT1 predicted N-linked glycosylation sites ►

Predicted N-linked glycosylation sites of protein sequences hENBT1- 1476 bp, 491 aa (UniProt ID: Q8NBI5) and mENBT1- 1509 bp, 502 aa (UniProt ID: A2AVZ9), generated utilizing NetNGlyc - 1.0 (Gupta and Brunak, 2002). Shown is protein sequence with predicted N-glycation sites with potential scores crossing 0.5 threshold. Potentials are scored by nine separate neural networks and average. Jury agreement indicates the number of neural networks that support a prediction. Results are categorized according to potential and jury agreement scores: "+" - Potential < 0.5, "++" - Potential < 0.5 and Jury agreement (9/9) or Potential<0.75, and "+++" - Potential < 0.75 and Jury agreement.

Figure 15.

hENBT1 predicted N-glycosylation sites

```
AGQGLPLHVATLLTGLLECLGFAGVLFGWPSLVFVFKNEDYFKDLCGPDAGPIGNATGQADCKAQDERFSLIFTLGSFMN      80
NFMTFPTGYIFDRFKTTVARLIAIFFYTTATLIIAFTSAGSAVLLFLAMPMLTIGGILFLITNLQIGNLFGQHRSTIITL     160
YNGAFDSSSAVFLIIKLLYEKGISLRASFIFISVCSTWHVARTFLLMPRGHIPYPLPPNYSYGLCPGNGTTKEEKETAEH     240
ENRELQSKEFLSAKEETPGAGQKQELRSFWSYAFSRRFAWHLVWLSVIQLWHYLFIGTLNSLLTNMAGGDMARVSTYTNA     320
FAFTQFGVLCAPWNGLLMDRLKQKYQKEARKTGSSTLAVALCSTVPSLALTSLLCLGFALCASVPILPLQYLTFILQVIS     400
RSFLYGSNAAFLTLAFPSEHFGKLFGLVMALSAVVSLLQFPIFTLIKGSLQNDPFYVNVMFMLAILLTFFHPFLVYRECR     480
TWKESPSAIA
```

Position	Potential	Jury agreement	N-Glyc result
55 NATG	0.6807	(7/9)	+
219 NYSY	0.6518	(9/9)	++
228 NGTT	0.5626	(8/9)	+

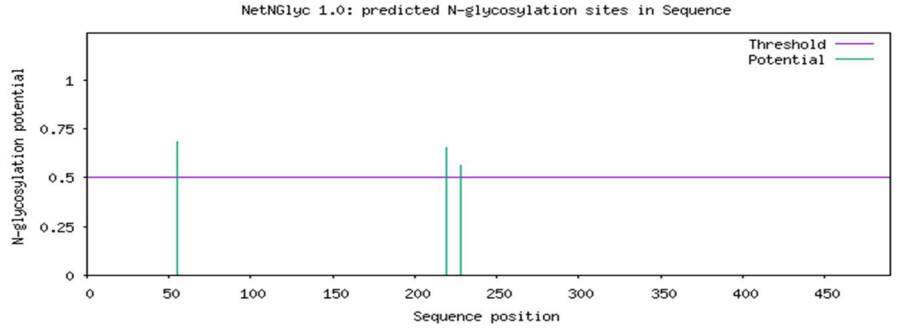

mENBT1 predicted N-glycosylation sites

```
ASKGLPLYLATLLTGLLECIGFAGVLFGWTSLLFVFKAENYFSEPCEQDCLLQSNVTGPSDLKAQDEKFSLIFTLASFMN      80
NFMTFPTGYIFDRFKTTVARLIAIFFYTCATIIIAFTSANTAMLLFLAMPMLAVGGILFLITNLQIGNLFGKHRSTIITL     160
YNGAFDSSSAVFLVIKLLYEQGISLRSSFIFMSVCSVWHIARTFLLMPKGHIPYPLPPNYSYGLCSRFGASKKENKAAEH     240
ETKELRSKECLPPKEENSGPEQQQQQEQQQQQQQQQQEQHEQHSFRRCALSRRFILHVVWLSIIQLWHYLFIGTLNSLLTK     320
LSGGDKVEVSAYTNAFAITQFFGVLCAPWNGLLMDRLKQKYQKAAKRTGSSSEAVALCSMVPSLALTSLLSLGFALCASI     400
PVMQLQYATFILQVVSRSFLYGCNAAFLTLAFPSEHFGKLFGLVMALSAIVSLLQFPLFKVSPESNAVYVSMGLAIFLTL     480
VHPFLVYRECRAEKTKSSVDA
```

Position	Potential	Jury agreement	N-Glyc result
55 NVTG	0.7833	(9/9)	+++
219 NYSY	0.6498	(9/9)	++

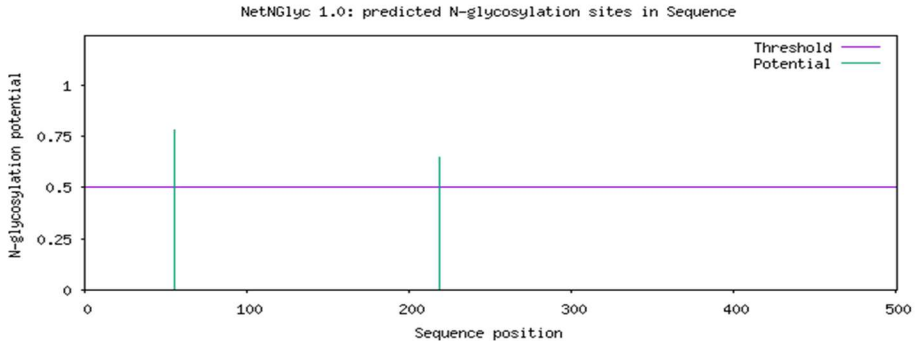

4.3.a.iv hENBT1 and mENBT1 relative expression levels

Densitometry performed on MYC-hENBT1 and MYC-mENBT1 normalized to β-actin on immunoblots intermittently run between July 2021 – January 2023 (Figure 9.D), show mean MYC-ENBT1 expression levels between HEK293-hSLC43A3 and HEK293-mslc43a3 cells are not significantly different (Unpaired student's t-test, $t_{16} = 0.2555$, $p = 0.8011$, $n = 9$). Variability was observed in MYC-ENBT1 expression levels in HEK293-hSLC43A3 and HEK293-mslc43a3 cells; the largest of which was seen in blots #2 and #5. Normalizing total cell protein mass (μg protein/μL cell suspension) for further experiments utilizing these cell lines may be warranted to minimize effects of differing expression levels.

4.3.b **Functional characterization of recombinant mENBT1 in HEK293-mslc43a3 cells**

4.3.b.i HEK293-WT cells exhibit minimal time-dependent/saturable and D22-insensitive [^{3}H]adenine uptake

Minimal time-dependent/saturable and D22-insensitive uptake of [^{3}H]adenine as seen by a linear fit (Figure 10.A), concurs with previously seen transport kinetic data suggesting HEK293-WT cells do not have measurable ENBT1-mediated nucleobase flux capacity (Ruel et al., 2019). [^{3}H] signal increases overtime, despite HEK293-WT cells lacking ENBT1 expression, potentially due to extracellular trapping of [^{3}H]adenine in the extracellular spaces between cells, in addition to low affinity binding of substrate to cell membrane receptors/ transporters, which pellets alongside cells and contributes to measured disintegrations per minute (DPM) values. Alternatively, although our NMG buffer is set to pH 7.4, CNT3 may be mediating the slow rate of [^{3}H]adenine uptake in a low affinity and proton-dependent manner (Smith et al., 2005; Elwi et al., 2006), as CNT3 has been found to be functional at pH levels as

high as 8.5 in sodium free conditions (Smith et al., 2005). In a typical transport assay this background signal is classified as a part of non-mediated uptake and is therefore accounted for when calculating ENBT1-mediated uptake.

4.3.b.ii 2 second time point captures the latter half of initial rate

ENBT1-mediated uptake has been shown to be very rapid (Figure 11.A), thus a 2 second time point often only captures the latter half of initial rate, which complicates obtaining true ENBT1 transport kinetics. Particularly so in the transfected-HEK293 cells that overexpress recombinant ENBT1 (Figure 10.B, and Figure 10.C). However, methodological limitations complicate consistently obtaining time points lower than 2 seconds. For instance, with our lab's equipment, it is not physically possible to consistently, inject cells into a centrifuge tube containing the aqueous radiolabeled-substrate, cap off the centrifuge tube, and shut the centrifuge lid to start the centrifuge, all in under 2 seconds. Therefore, despite the limitation, a 2 second time point is utilized as the best estimation of initial rate for room temperature transport assays involving recombinant ENBT1.

4.3.b.iii Rationale for selecting the HEK293-mslc43a3 C10 clone

The E11 clone was initially chosen for continued experimentation based on initial data of mENBT1-mediated adenine uptake in the E11 and C10 clones (Figure 10.B and Figure 10.C). However, due to early complications brought on by the COVID-19 pandemic, such as on-campus work restrictions, periodic lab lockdowns, and supply chain issues for tissue culture related products, the lab's E11 clone frozen stocks were lost. As a result, the C10 clone was utilized instead for further experimentation as the next best available HEK293-mslc43a3 clone.

4.3.c **Recombinant hENBT1 & mENBT1 transport kinetics in transfected-HEK293 cells**

4.3.c.i HEK293-EV cells exhibit minimal time-dependent/saturable 6-MP and adenine uptake

Minimal time-dependent/saturable uptake of [^{3}H]6-MP and [^{3}H]adenine, as seen by a linear fit (Figure 11.A, Figure 11.B, and Figure 11.C), concurs with previously seen expression profiles suggesting HEK293-EV cells do not express functional ENBT1 (Figure 9.B and Figure 9.C). Much like HEK293-WT cells, [^{3}H] signal increases overtime, despite HEK293-EV cells lacking ENBT1 expression for similar stated potential causes.

4.3.c.ii Rationale for selection of 1 μM 6-MP

1 μM [^{3}H]6-MP was utilized because 1 μM is reported to be around the mean therapeutic maximal 6-MP plasma concentration (C_{max}) observed in adolescent patients undergoing 6-MP therapy; 0.89 ± 0.51 μM (Zimm et al., 1983) and 0.68 ± 0.42 μM (Lonnerholm et al., 1986), presented as mean ± SD or 1.08 μM (Larsen et al., 2020), presented as a median. Rapid uptake of 1 μM 6-MP supports the therapeutic relevance of ENBT1 as the candidate mechanism for 6-MP uptake into cells at therapeutic concentrations (Figure 11.A). However, this assessment was only performed in human embryonic kidney cells with recombinant ENBT1 and overexpression, rather than therapeutically relevant leukemia cells. Further experiments should be replicated in human leukemia cell lines to minimize confounding variables of recombinant ENBT1.

4.3.c.iii Differing published and obtained adenine K_m values in transfected-HEK293 cells

Observed ENBT1 adenine K_m values in HEK293-hSLC43A3 and HEK293-mslc43a3 cells (Figure 11.B), were 2-fold higher than published adenine K_m values (Table 3.). Previous K_m value was obtained by Ph.D. candidate Nicholas M Ruel, whom performed K_m /V_{max} transport assays utilizing various adenine concentrations at various time points to extrapolate a 0.5 second time point, and calculate adenine K_m. Our current K_m /V_{max} transport assay method is relatively less rigorous, and utilizes a time point that is inadequate to capture true ENBT1 initial rate, however, it is sufficient considering available equipment, time, and resource costs of assays.

Additionally, these differing adenine K_m values highlight the necessity of critically evaluating assay time points when interpreting apparent K_m values. As described previously in section 1.1.e, Furukawa and colleagues, (2015) obtained an apparent ENBT1 guanine K_m value of 1.70 μM, utilizing a 40 second time point. Our lab has not performed a guanine time course and confirmed an appropriate time point, due to guanine solubility issues. However, based on ENBT1 interaction with other nucleobase substrates, 40 seconds is unlikely to be an appropriate estimation of initial rate. Due to problematic time point selection, Furukawa and colleagues, (2015) were potentially observing the transporter system at steady state equilibrium, at which point the enzyme GDA and XO, which metabolize guanine and downstream xanthine, would be the rate limiting factor(s) that disrupt guanine equilibrium and drive guanine influx. Meaning observed K_m values are likely the enzyme kinetics of GDA and XO, rather than transport kinetics of ENBT1.

4.3.c.iv Differing $V_{max\text{-}adenine}$ and $V_{max\text{-}6\text{-}MP}$ values in transfected-HEK293 cells

HEK293-hSLC43A3 (56 ± 6 μM/sec) and HEK293-mslc43a3 (62 ± 6 μM/sec) $V_{max\text{-}adenine}$ values were not significantly different (Figure 11.B) (Extra sum-of-squares F-test, $F_{1,104}$=0.441, p=0.5082, n=6). Additionally, HEK293-hSLC43A3 (121 ± 16 μM/sec) and HEK293-mslc43a3 (144 ± 12 μM/sec) $V_{max\text{-}6\text{-}MP}$ values were not significantly different (Figure 11.C) (Extra sum-of-squares F-test, $F_{1,98}$=1.177, p=0.281, n=6).

However, $V_{max\text{-}6\text{-}MP}$ and $V_{max\text{-}adenine}$ values were assessed and found to be significantly different. Statistical analysis was performed with ($V_{max\text{-}adenine:hSLC43A3}$, $V_{max\text{-}6\text{-}MP:hSLC43A3}$; Extra sum-of-squares F-test, $F_{1,101}$=16.32, p<0.001, n=6), and ($V_{max\text{-}adenine:mslc43a3}$, $V_{max\text{-}6\text{-}MP:mslc43a3}$; Extra sum-of-squares F-test, $F_{1,101}$=34.27, p<0.001, n=6) (Figure 11.B and Figure 11.C).

V_{max} refers to the maximum velocity of a transporter system, at full saturation with substrate, and is affected by transporter expression levels, and speed of conformation changes between inward and outward facing conformations. Assuming on average equal transporter expression levels (Figure 9.A), differing V_{max} values suggest adenine and 6-MP have differing rates of ENBT1-substrate complex decomposition (K_{off}) (Corzo J., 2016; Vauguelin G., 2016). Adenine exhibits higher affinity for ENBT1 relative to 6-MP, and high affinity interactions are characterized by K_{off} (strong complex stability). Adenine having a longer time for substrate complex decomposition than 6-MP, would mean decreased concentration necessary to fully saturate ENBT1- mediated adenine transport and therefore result in $V_{max\text{-}adenine} < V_{max\text{-}6\text{-}MP}$.

4.3.d **Recombinant hENBT1 & mENBT1 inhibition kinetics in transfected-HEK293 cells**

4.3.d.i Shifted adenine inhibition profile in transfected-HEK293 cells

Adenine inhibition profile were performed by two individuals, using different [^{3}H]6-MP concentrations. The HEK293-hSLC43A3 data set was performed by Ph.D. candidate Nicholas M Ruel, using 100 µM [^{3}H]6-MP and the HEK293-mslc43a3 data set was performed by myself, using 150 µM [^{3}H]6-MP. Adenine inhibition profile appears shifted due to differing experimental design and handling, as greater adenine concentrations are necessary to sufficiently inhibit the accumulation of 150 µM [^{3}H]6-MP relative to 100 µM [^{3}H]6-MP (Figure 12.A).

4.3.d.ii Calculated and expected adenine K_i values

Obtained adenine IC_{50} values were not significantly different between HEK293-hSLC43A3 (162 ± 82 µM) and HEK293-mslc43a3 (78 ± 28 µM) cell lines (Unpaired student's t-test, $t_8 = 0.965$, $p = 0.363$, $n = 5$), suggesting hENBT1 and mENBT1 have similar inhibition kinetics (Figure 12.B). Calculated K_i values were similar to expected K_m values for adenine (Table 3), suggesting adenine has a purely competitive relationship with [^{3}H]6-MP at the ENBT1 substrate binding site.

4.3.d.iii Incomplete 6-MP inhibition curve in transfected-HEK293 cells

6-MP concentrations used in assay were inadequate to capture a full 6-MP inhibition curve. Inhibition curves were extrapolated by GraphPad prism 10 to obtain theoretical IC_{50} values, however, this process can lead to potentially inaccurate IC_{50} values. Increasing assay 6-MP concentrations above 1 mM to capture a complete inhibition curve was not possible as high DMSO solvent percentages (>1%) has been found to interfere with ENBT1 function (NM. Ruel, personal communication, August 17, 2023).

4.3.d.iv Calculated 6-MP K_i values versus expected 6-MP K_m values

Calculated K_i values were over 30-folder higher than expected 6-MP K_m values (Table 3), suggesting 6-MP does not have a purely competitive relationship with [^{3}H]adenine at the ENBT1 substrate binding site. To investigate whether adenine had a competitive advantage at the ENBT1 binding site, relative to 6-MP, transfected-HEK293 cells were pre-incubated with 3 μM – 1 mM 6-MP, for 10 minutes prior to the assay. However, 6-MP pre-incubation was found to have no effect on concentration dependent inhibition of ENBT1-mediated [^{3}H]adenine uptake (Figure 12.C). This may again be due to differing rates of ENBT1-substrate complex decomposition (K_{off}) between adenine and 6-MP. If adenine were to have a lower K_{off} (strong complex stability) compared to 6-MP, based on their affinity (K_m), then adenine would remain bound in a ENBT1-adenine complex for longer periods of time. On the other hand, 6-MP would dissociate from the ENBT1-6-MP complex faster, and provide more frequent opportunities for adenine to bind instead. Thus, increasing 6-MP IC_{50}, and potentially explaining lack of a significant 6-MP pre-incubation effect.

Table 3. ENBT1 K_m and calculated K_i values ►

Table of published ENBT1 substrate K_m values (Ruel et al., 2019), experimentally obtained ENBT1 substrate K_m values (Figure 11.B and Figure 11.C), and ENBT1 inhibitor K_i values calculated using the Cheng-Prusoff equation (Figure 12.A and Figure 12.B), for human and murine ENBT1. There are currently no known published mENBT1 substrate K_m values and thus have been labeled as N/A. Data are shown as mean ± SEM.

Table 3.

Adenine	**hENBT1**	**mENBT1**
Published K_m values	37 ± 26 μM	N/A
Obtained K_m values	93 ± 24 μM	86 ± 22 μM
Calculated K_i values	25 ± 9 μM	51 ± 13 μM

6-MP	**hENBT1**	**mENBT1**
Published K_m values	163 ± 126 μM	N/A
Obtained K_m values	269 ± 67 μM	253 ± 39 μM
Calculated K_i values	5.9 ± 0.7 mM	7.4 ± 1.3 mM

4.3.e **6-MP/6-MP metabolite cell viability in transfected-HEK293**

4.3.e.i Leftward 6-MP cell viability curve shift in HEK293 cells transfected with *SLC43A3*

Relative to HEK293-EV cells, *SLC43A3* or *slc43a3* transfected cells exhibited enhanced 6-MP mediated reduction in cell viability (Figure 13.A). HEK293-hSLC43A3 (EC_{50}: 0.99 ± 0.09 μM) and HEK293-mslc43a3 (EC_{50}: 0.96 ± 0.28 μM) cells were over 19-fold more sensitive to 6-MP, relative to HEK293-EV (EC_{50}: 18.8 ± 0.51 μM) cells. Obtained HEK293-hSLC43A3 and HEK293-mslc43a3 6-MP first-phase EC_{50} values were not significantly different (Extra sum-of-squares F-test, $F_{1,255}$=1.427, p=0.233, n=8), suggesting recombinant hENBT1 and mENBT1 mediate 6-MP effect on cell viability similarly. Overall, based on the rationale stated in section 4.2.e, these results (Figure 13.A) provide further indirect evidence that recombinant hENBT1 and mENBT1 mediate the cellular accumulation of 6-MP.

4.3.e.ii No 6-MeMP cell viability curve shift in HEK293 cells transfected with *SLC43A3*

Relative to HEK293-EV cells, *SLC43A3* or *slc43a3* transfected cells exhibited no change in 6-MeMP mediated reduction in cell viability (Figure 13.B). HEK293-hSLC43A3 (EC_{50}: 42 ± 6 μM), HEK293-mslc43a3 (EC_{50}: 79 ± 2 μM), and HEK293-EV (EC_{50}: 45 ± 7 μM) cells 6-MeMP first-phase EC_{50} values were not significantly different (Extra sum-of-squares F-test, $F_{2,444}$=0.904, p=0.406, n=8). Overall, 6-MeMP has been shown to decrease transfected-HEK293 cell viability >10 μM and is known to be an ENBT1 inhibitor (Ruel et al., 2019). However, these results (Figure 13.B) suggest that recombinant hENBT1 and mENBT1 do not mediate the cellular accumulation of 6-MeMP.

4.3.e.iii Leftward 6-TG cell viability curve shift in HEK293 cells transfected with *SLC43A3*

Relative to HEK293-EV cells, *SLC43A3* or *slc43a3* transfected cells exhibited enhanced 6-TG mediated reduction in cell viability (Figure 13.C). HEK293-hSLC43A3 (EC_{50}: 3.4 ± 0.9 μM) and HEK293-mslc43a3 (EC_{50}: 3.4 ± 1.1 μM) cells were over 4-fold more sensitive to 6-TG relative to HEK293-EV (EC_{50}: 16 ± 4.3 μM) cells. Obtained HEK293-hSLC43A3 and HEK293-mslc43a3 6-TG EC_{50} values were not significantly different (Extra sum-of-squares F-test, $F_{1,204}$=1.465, p=0.238, n=6), suggesting recombinant hENBT1 and mENBT1 mediate 6-TG effect on cell viability similarly. Overall, these results (Figure 13.C) provide indirect evidence that recombinant hENBT1 and mENBT1 mediate the cellular accumulation of 6-TG.

4.3.e.iv Discrepancy between 6-MP and 6-TG cell viability curves

6-MP is thought to decrease cell viability via DNA MMR-dependent apoptosis, inhibiting de-novo purine synthesis, depleting intracellular AMP, ADP, and ATP, and Rac1 inactivation. On the other hand, 6-TG metabolism is limited due to entering the metabolic pathway at a different point; therefore 6-TG is thought to primarily decrease cell viability via DNA MMR-dependent apoptosis and Rac1 inactivation. However, despite lacking multiple cytotoxic pathways, 6-TG exhibited a single-phase cell viability curve and achieved 0% reduced MTT/cell viability (Figure 13.C) at lower concentrations relative to 6-MP, which exhibits a biphasic cell viability curve (Figure 13.A). This may be because 6-TG is known to have a more direct metabolism to the therapeutically active 6-TGN metabolite than 6-MP (Lancaster et al., 1998). Thus, at equal concentrations 6-TG yields higher levels of 6-TGN than 6-MP. These data may also suggest DNA MMR-dependent apoptosis and Rac1 inactivation contribute more to decreasing cell viability compared to inhibiting de-novo purine synthesis and depleting

intracellular AMP, ADP, and ATP. However, it should also be noted that 6-MP EC_{50} value is slightly lower than 6-TG.

4.3.e.v Incomplete 6-TU cell viability curve in transfected-HEK293 cells

HEK293-EV, HEK293-hSLC43A3, and HEK293-mslc43a3 cells all exhibited an incomplete 6-TU cell viability curve (Figure 13.D). Based on literature, 6-TU was not expected to affect cell viability (Chan et al., 1990), however, decreased viability was observed at the highest 2 6-TU concentrations (640 μM and 1.28 mM). As follow-up, DMSO effect on cell viability was assessed, and resulted in the same incomplete cell viability curve (Figure 13.E), with decreased viability observed at the highest 2 DMSO percentages (0.64% and 1.28% DMSO). Similarities between 6-TU and DMSO cell viability curves suggest decreased viability was DMSO-mediated rather than 6-TU-mediated (Figure 13.D and Figure 13.E). Based on these data alone, it is not clear whether ENBT1 mediates the cellular accumulation of 6-TU.

4.4 **Limitations**

Data from HEK293 cells transfected with *SLC43A3* or *slc43a3,* thus far suggest that hENBT1 and mENBT1 are functionally similar in mediating the cellular accumulation of 6-MP and mediating 6-MP/6-MP metabolite effect on cell viability. However, it is worth noting that these experiments assessed recombinant hENBT1 and mENBT1. Although it varies on the system being looked at, differences between recombinant and native/endogenous proteins are often documented (Kenakin, T., 1997; Reichel, C., 2011). For instance, **(1):** Recombinant proteins are often not native to the organism they are made in, such as the expression of *slc43a3* in a human HEK293 cell line. Thus, species specific post-translational modifications, chaperone assisted protein folding, or trafficking and degradation signaling may impact recombinant protein

function. **(2):** Recombinant proteins tend to be over expressed at non-physiologically relevant levels. For instance, HEK293-hSLC43A3 cells express 180-fold higher hENBT1 than human leukemia cells (Figure 16.B). Over expressed proteins cannot only aggregate and directly become cytotoxic; over expression can also affect the cell by overloading cellular mechanisms related to protein translation, folding, post-translational modifications, trafficking, and degradation. Dubbed the protein burden/cost effect, overexpression can indirectly affect mechanisms such as protein turnover and cell proliferation. Therefore, impacting function of both recombinant protein and function of other endogenous proteins (Moriya, H., 2015; Eguchi et al., 2018; Saeki et al., 2020).

CHAPTER 5.

Interspecies Functional Comparison of Endogenous hENBT1 and mENBT1

5.1 Introduction

To address limitations associated with investigating the function of recombinant ENBT1, three cell lines with endogenous ENBT1 expression were subsequently assessed. **(1):** MOLT-4 is a human T lymphoblast cell line isolated by Minowada et al, (1972) derived from the peripheral blood of an adolescent male with T-cell acute lymphoblastic leukemia. Since their establishment, the MOLT-4 cell line has been widely used in the literature as a model for research in leukemia and immunology, as both an *in vitro* cell line and more recently inoculated into mice as an *in vivo* xenograft model. Due to their origin, they are a valuable tool to study the biology of human leukemia cells and investigate the mechanisms of action and efficacy of chemotherapeutic agents. **(2):** L1210 is a mouse lymphoblast cell line first described by Law et al, (1949) it was initially isolated from mice that spontaneously developed leukemia after exposure to the carcinogen methylcholanthrene. They were one of the first widely used murine transplantable solid tumor models utilized for early screening of anti-cancer agents, due to ease of *in vitro* propagation, and inoculation in mice as an *in vivo* rapidly growing xenograft model. Many early chemotherapeutic agents such as MTX and 6-MP were evaluated using L1210 cells and have remained a staple in cancer research since. **(3):** FL83B is a hepatic cell line isolated from a normal fetal mouse liver by Waymouth C in 1969 and later characterized by Breslow et al, (1973). Since their establishment, FL83B cells saw use as an *in vitro* hepatocyte model for studying liver biology, drug metabolism, and viral infections as the cells retained many characteristics of normal hepatocytes. In recent years they have been used extensively to investigate mechanisms underlying liver diseases, such as viral hepatitis and alcohol-induced liver injury, and were initially selected for this project to investigate 6-MP-associated induced liver injury in a non-tumorigenic mouse hepatic cell line.

5.2 **Results**

5.2.a **Endogenous ENBT1 expression profile in leukemia and hepatic cell lines**

SLC43A3/hENBT1 and *slc43a3*/mENBT1 expression levels were assessed via qualitative PCR and immunoblot assay, utilizing cDNA and cell lysates processed from MOLT-4, L1210, and FL83B cell lines. Assessment of PCR products show that relative to HEK293-EV *SLC43A3* expression levels, MOLT-4 cells express 4.8-fold more *SLC43A3* and undetectable levels of *slc43a3* transcript; L1210 cells express *slc43a3* transcript and undetectable levels of *SLC43A3* transcript, and FL83B cells express undetectable levels of *SLC43A3* and *slc43a3* transcript expression. *GAPDH* and *gapdh* were utilized as a loading control where appropriate (Figure 16.A). To investigate whether mouse liver expresses *slc43a3* transcript, whole liver was dissected from wildtype C57BL/6 mice that were 8-10 weeks old and processed via qualitative PCR. Unlike FL83B hepatic cell lines, *slc43a3* transcript was detected in mouse whole liver (Figure 16.A). Assessment of immunoblot bands reflect that relative to HEK293-hSLC43A3 ENBT1 expression levels, MOLT-4 cells express over 14.3-fold less hENBT1 (an exact fold is uncertain as band is being overshadowed/masked by HEK293-hSLC43A3 expression levels) and L1210 and FL83B cells express undetectable levels of hENBT1. β-actin was utilized as a loading control (Figure 16.B).

Figure 16. Transcript and protein expression of leukemia and hepatic cells ►

PCR products and protein expression was assessed in MOLT-4, L1210, and FL83B cell lines. **A:** Representative PCR gel using cDNA synthesized from total RNA and PCR primers to amplify products; *SLC43A3* (Expected Size: 400 bp), *slc43a3* (Expected Size: 400 bp), *GAPDH* (Expected Size: 356 bp), *gapdh* (Expected Size: 463 bp). dH_2O blank was used as a negative control, *GAPDH* was used as a loading control for MOLT-4 cells, and *gapdh* was used as a loading control for L1210 and FL83B cells. **B:** Representative immunoblot using 30 µg protein from crude cell lysates, primary anti-hENBT1, and anti-β-actin, and HRP-conjugated anti-rabbit and anti-mouse secondary antibodies; hENBT1 (Expected Size: 55.0 kDA), mENBT1 (Expected Size: 56.5 kDA), and β-actin (Expected Size: 42.0 kDa). hENBT1 blot was cut to visualize endogenous hENBT1 levels due to recombinant hENBT1 overshadowing other bands. β-actin was used as a loading control.

Figure 16.

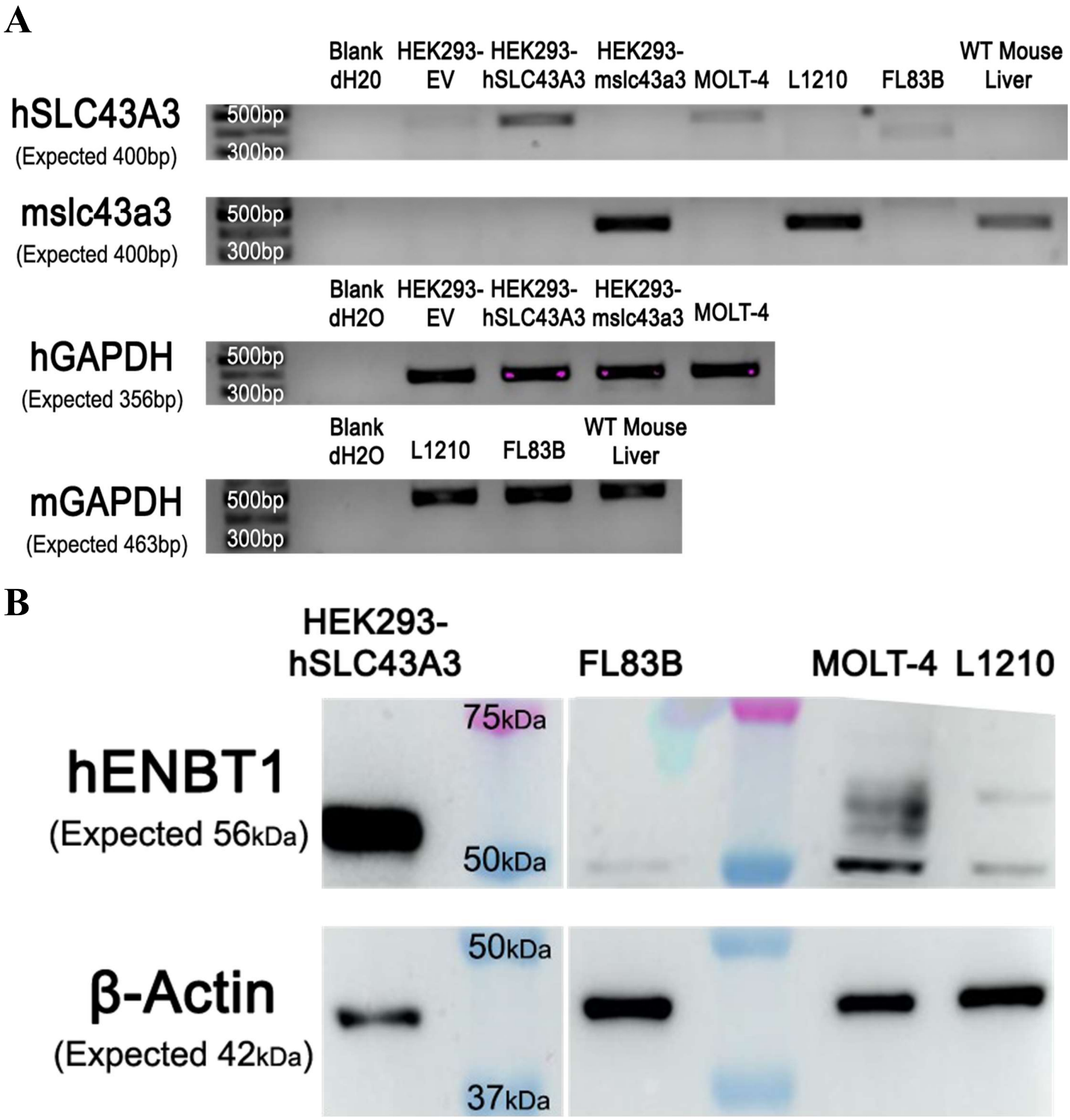
A
Blank dH20
HEK293-EV
HEK293-hSLC43A3
HEK293-mslc43a3
MOLT-4
L1210
FL83B
WT Mouse Liver
hSLC43A3
(Expected 400bp)
500bp
300bp
mslc43a3
(Expected 400bp)
500bp
300bp
Blank dH2O
HEK293-EV
HEK293-hSLC43A3
HEK293-mslc43a3
MOLT-4
hGAPDH
(Expected 356bp)
500bp
300bp
Blank dH2O
L1210
FL83B
WT Mouse Liver
mGAPDH
(Expected 463bp)
500bp
300bp
B
HEK293-hSLC43A3
FL83B
MOLT-4
L1210
hENBT1
(Expected 56kDa)
75kDa
50kDa
β-Actin
(Expected 42kDa)
50kDa
37kDa

5.2.b **Endogenous hENBT1 and mENBT1 transport kinetics in leukemia and hepatic cell lines**

Functional comparison between endogenous hENBT1 and mENBT1 6-MP transport kinetics were made by assessing radiolabeled substrate influx in nominally sodium free conditions with NMG buffer, to eliminate potential sodium dependent transport (CNT2 and CNT3), and 15-minute cell incubation with 10 μM DY, to eliminate potential nucleoside transport (ENT1 and ENT2). Total uptake was obtained in MOLT-4, L1210, and FL83B cells with concentrations of [^{3}H]6-MP, ranging from 1 μM – 400 μM; non-mediated uptake was obtained in MOLT-4, L1210, and FL83B cells at the same conditions, with the addition of 5 mM adenine as a competitive inhibitor, based on adenine inhibition profile performed in transfected-HEK293 cells (Figure 12.A**)**. ENBT1-mediated uptake was calculated by subtracting non-mediated uptake from total uptake as described previously. Time course assays were performed to determine a suitable time point in MOLT-4 and L1210 cells, using 30 μM [^{3}H]6-MP, at 2 second – 30 second time points. MOLT-4 and L1210 cells exhibited time-dependent/saturable uptake of [^{3}H]6-MP, seen by the curve plateauing at roughly 30 pmol/μL, and with a k-value of 0.34 ± 0.09 sec^{-1} and 0.22 ± 0.05 sec^{-1} in the MOLT-4 and L1210 cells, respectively (Figure 17.A). The k-value suggests rapid, but relatively slower rate of ENBT1-mediated uptake, relative to the transfected-HEK293 cells. 2 seconds was again chosen as the best estimation of initial rate. F-test analysis of the k-values determined no significant difference between MOLT-4 and L1210 cells (Extra sum-of-squares F-test, $F_{1,\ 86}$ =1.089, p=0.299, n=5), suggesting that endogenous hENBT1 and mENBT1 transport [^{3}H]6-MP at similar rates (Figure 17.A). Separate time course assay was performed in FL83B cells, using 1 μM [^{3}H]6-MP, at 2 second – 30 second time points. FL83B cells did not exhibit time-dependent/saturable uptake of [^{3}H]6-MP (Figure 17.B). To rule out potential that 1 μM [^{3}H]6-MP is too low of a concentration for assessing

endogenous ENBT1-mediated 6-MP uptake, the time course assay was repeated using 100 μM [^{3}H]6-MP. However, FL83B cells again did not exhibit time-dependent/saturable uptake of [^{3}H]6-MP (Figure 17.C). Subsequently, transport kinetics of the exogenous/xenobiotic substrate 6-MP were assessed in MOLT-4 and L1210 cells, using 1 μM - 300 μM [^{3}H]6-MP, at 2 second time points. [^{3}H]6-MP uptake was found to be saturable with a K_m value of 115 ± 68 μM and a V_{max} value of 39 ± 9 μM/sec, and a K_m value of 272 ± 91 μM and a V_{max} value of 81 ± 15 μM/sec in the MOLT-4 and L1210 cells, respectively. F-test analysis of the K_m determined no significant difference between MOLT-4 and L1210 cells (Extra sum-of-squares F-test, $F_{1,87}$ = 1.662, p=0.201, n=5), suggesting that endogenous hENBT1 and mENBT1 have similar [^{3}H]6-MP affinities (Figure 17.D). F-test analysis of the V_{max} determined a significant difference between MOLT-4 and L1210 cells (Extra sum-of-squares F-test, $F_{1,87}$ = 4.660, p=0.034, n=5) (Figure 17.D).

Figure 17. Endogenous hENBT1 and mENBT1 transport kinetics in leukemia and hepatic cells ►

Transport assays performed in MOLT-4, L1210 and FL83B cells in sodium free conditions, in presence of 10 μM DY. Presence of 5 mM adenine in assay was utilized to determine non-mediated uptake. **A:** MOLT-4 and L1210 6-MP time course assay showing initial rate, and steady state of endogenous hENBT1 and mENBT1-mediated uptake of 30 μM [^{3}H]6-MP, at 2 second – 30 second time points (n=5). This work was performed by undergraduate student Aaron L Sayler. **B:** FL83B 6-MP time course assay showing lack of endogenous mENBT1-mediated uptake of 1 μM [^{3}H]6-MP, at 2 second – 30 second time points (n=5). **C:** FL83B 6-MP time course assay showing lack of endogenous mENBT1-mediated uptake of 100 μM [^{3}H]6-MP, at 2 second – 30 second time points (n=6). **D:** MOLT-4 and L1210 6-MP K_m/V_{max} assay showing endogenous hENBT1 and mENBT1 transport kinetics of 1 μM - 300 μM [^{3}H]6-MP, at 2 second time points (n=5). L1210 work was performed by undergraduate student Aaron L Sayler and MOLT-4 work was performed by Ph.D. candidate Nicholas M Ruel. Robust regression and outlier removal (ROUT) method with ROUT coefficient Q = 1% was utilized to detect and remove outliers. Data are shown as mean ± SD.

Figure 17.

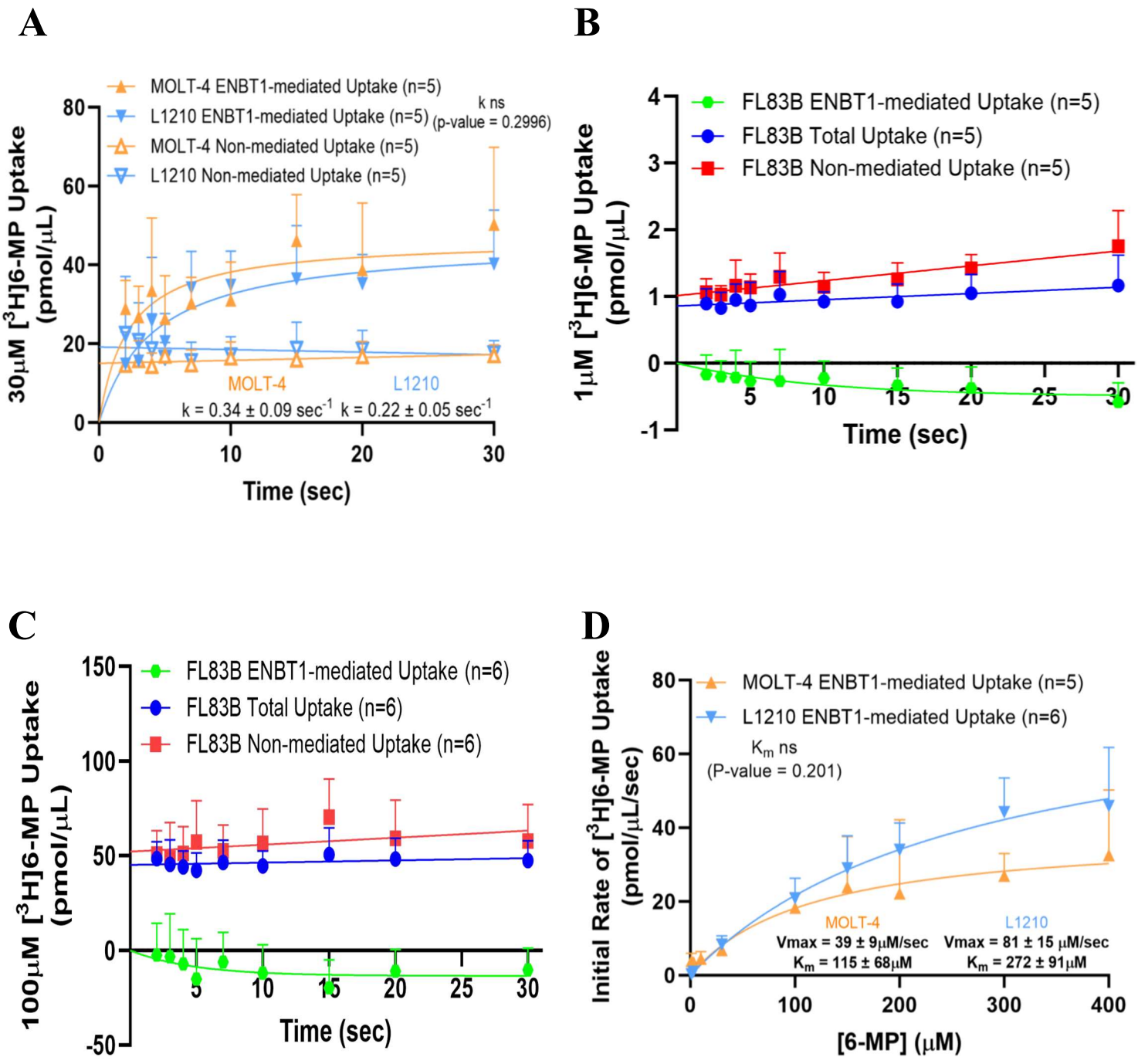
A
MOLT-4 ENBT1-mediated Uptake (n=5)
L1210 ENBT1-mediated Uptake (n=5)
MOLT-4 Non-mediated Uptake (n=5)
L1210 Non-mediated Uptake (n=5)
k ns
(p-value = 0.2996)
30μM [3H]6-MP Uptake (pmol/μL)
MOLT-4
L1210
k = 0.34 ± 0.09 sec-1
k = 0.22 ± 0.05 sec-1
Time (sec)
B
FL83B ENBT1-mediated Uptake (n=5)
FL83B Total Uptake (n=5)
FL83B Non-mediated Uptake (n=5)
1μM [3H]6-MP Uptake (pmol/μL)
Time (sec)
C
FL83B ENBT1-mediated Uptake (n=6)
FL83B Total Uptake (n=6)
FL83B Non-mediated Uptake (n=6)
100μM [3H]6-MP Uptake (pmol/μL)
Time (sec)
D
MOLT-4 ENBT1-mediated Uptake (n=5)
L1210 ENBT1-mediated Uptake (n=6)
Km ns
(P-value = 0.201)
Initial Rate of [3H]6-MP Uptake (pmol/μL/sec)
MOLT-4
Vmax = 39 ± 9μM/sec
Km = 115 ± 68μM
L1210
Vmax = 81 ± 15 μM/sec
Km = 272 ± 91μM
[6-MP] (μM)

5.2.c **MOLT-4, L1210, and FL83B 6-MP cell viability and cell death curves**

Indirect measures of ENBT1 function were assessed again via 6-MP cell viability assays in MOLT-4, L1210, and FL83B cells. Under the same hypothesis that if ENBT1 mediated the cellular accumulation of 6-MP, MOLT-4 and L1210 cells should exhibit sensitivity to 6-MP, with EC_{50} values comparable to those observed in HEK293-hSLC43A3 and HEK293-mslc43a3 cells. On the other hand, FL83B cells which do not appear to express functional mENBT1, should exhibit resistance to 6-MP with EC_{50} values, comparable to those observed in HEK293-EV cells. Compound-mediated response, 100% cell viability, 0% cell viability, and % reduced MTT were obtained and calculated as described previously in section 3.7. MOLT-4 and L1210 cells exhibited a biphasic 6-MP cell viability curve with first-phase EC_{50} values of 0.7 ± 0.2 μM and 0.6 ± 0.2 μM for MOLT-4 and L1210 cells, respectively. F-test analysis of MOLT-4 and L1210 first-phase EC_{50} values determined no significant difference (Extra sum-of-squares F-test, $F_{1, 133} = 1.950$, p=0.165, n=5) (Figure 18.A).

To evaluate the effect of 10 μM DY, which is present in all transport assays, 6-MP cell viability assays were replicated in MOLT-4 cells, in presence or absence of 10 μM DY. MOLT-4 cells exhibited a biphasic 6-MP cell viability curve with first-phase EC_{50} values of 0.3 ± 0.1 μM and 0.5 ± 0.1 μM for MOLT-4 cells co-treated with 6-MP and DY (6-MP DY+) and just 6-MP (6-MP DY-), respectively. MOLT-4 cells were also treated with DY and matching DMSO percentages, as in 6-MP experimental groups, as a solvent control (DMSO DY+). F-test analysis of 6-MP DY+ and 6-MP DY- first-phase EC_{50} values determined a significant difference (Extra sum-of-squares F-test, $F_{1, 166} = 6.911$, p=0.009, n=6) (Figure 18.B). In FL83B cells with the same conditions as Figure 18.A, 6-MP exhibited an incomplete cell viability curve with an extrapolated EC_{50} value of 2.0 ± 0.2 mM (Figure 18.C).

Subsequently, 6-MP-mediated cell death was assessed in MOLT-4 and L1210 cells, based on the LDH release assay. Compound-mediated response, 100% cell death, 0% cell death, and % cell death were obtained and calculated as described previously in Section 3.8. MOLT-4 cells exhibited a relatively robust 6-MP cell death response of approximately 20% cell death after 48-hour incubation with 80 μM 6-MP. On the other hand, L1210 cells exhibited a relatively blunted cell death response of approximately 5% cell death after 48-hour incubation with 80 μM 6-MP.

Figure 18. 6-MP cell viability in leukemia and hepatic cells ►

6-MP cell viability and cell death curves in MOLT-4, L1210, and FL83B cells plated in complete media, treated with 80 nM – 1.28 mM of 6-MP, for 48 hours. **A:** MOLT and L1210 cells 6-MP cell viability curve showing biphasic nature of 6-MP response (n=5). **B:** Biphasic MOLT-4 6-MP cell viability curve, in presence or absence of 10 μM DY, showing significant difference in 6-MP response, between 10 μM DY treated and untreated cells (n=6). **C:** FL83B cell 6-MP cell viability curve showing incomplete 6-MP response (n=8). **D:** MOLT and L1210 cells 6-MP cell death curve showing varying 6-MP responses (n=5). Data are shown as mean ± SD.

Figure 18.

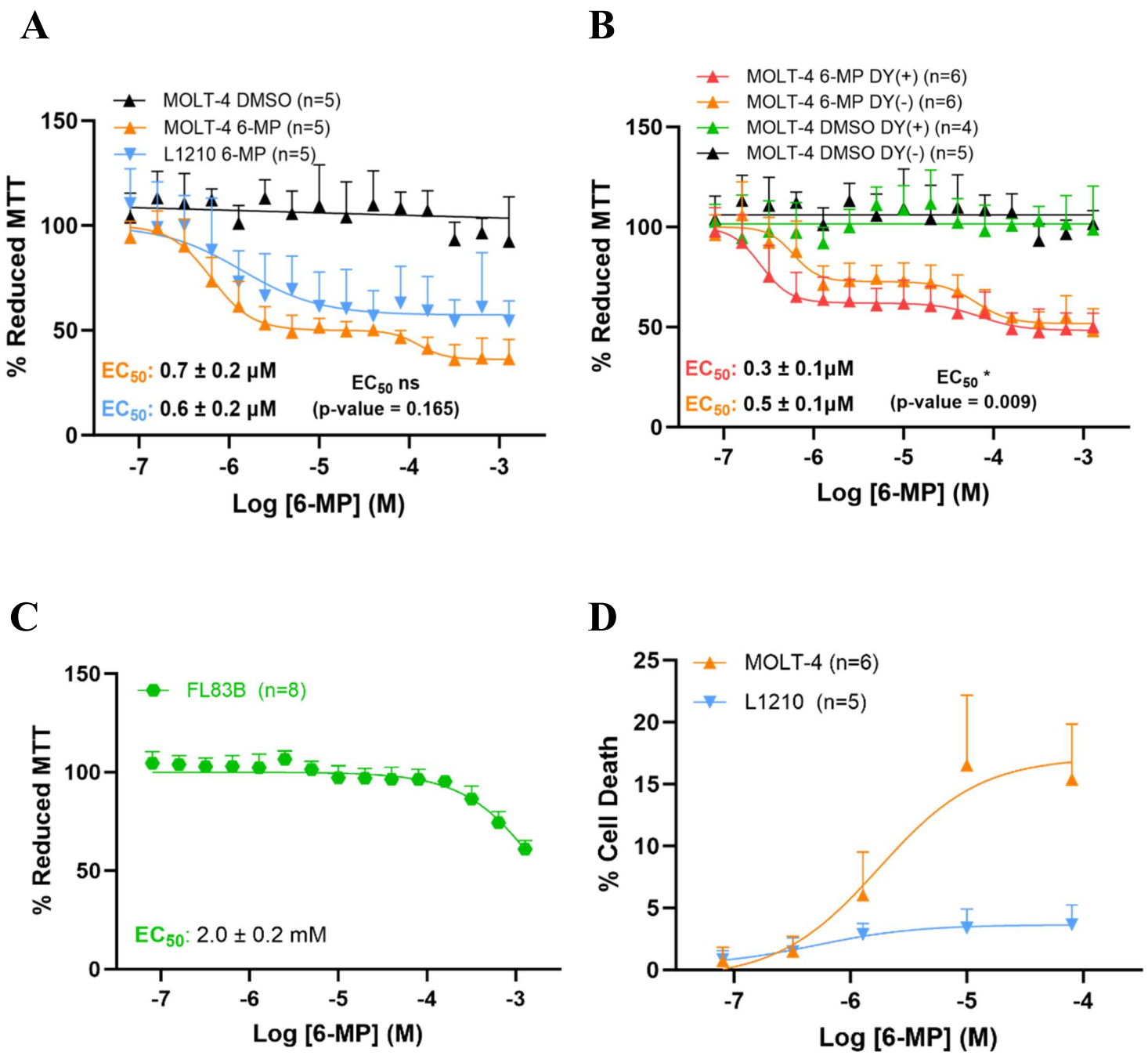
A
MOLT-4 DMSO (n=5)
MOLT-4 6-MP (n=5)
L1210 6-MP (n=5)
% Reduced MTT
150
100
50
0
-7
-6
-5
-4
-3
Log [6-MP] (M)
EC50: 0.7 ± 0.2 µM
EC50: 0.6 ± 0.2 µM
EC50 ns
(p-value = 0.165)
B
MOLT-4 6-MP DY(+) (n=6)
MOLT-4 6-MP DY(-) (n=6)
MOLT-4 DMSO DY(+) (n=4)
MOLT-4 DMSO DY(-) (n=5)
% Reduced MTT
Log [6-MP] (M)
EC50: 0.3 ± 0.1µM
EC50: 0.5 ± 0.1µM
EC50 *
(p-value = 0.009)
C
FL83B (n=8)
% Reduced MTT
EC50: 2.0 ± 0.2 mM
Log [6-MP] (M)
D
MOLT-4 (n=6)
L1210 (n=5)
% Cell Death
25
20
15
10
5
0
Log [6-MP] (M)

5.2.d **qPCR gene expression profile of FL83B and L1210 cells**

Previously, FL83B cells have been shown to be more 6-MP resistant than HEK293-EV cells (Figure 13.A and Figure 18.C). Suggesting FL83B 6-MP resistance cannot be explained by mENBT1 expression levels alone. Thus, transcript levels of murine drug efflux genes, such as *abcc4* and *abcc5,* and murine 6-MP metabolism genes such as *tpmt*, *hgprt1*, *xo*, *impdh*, *gmps*, and *nudt15,* were assessed in L1210 and FL83B cells. qPCR was performed on cDNA synthesized from L1210 and FL83B cell total RNA and qPCR primers, to amplify products and obtain Ct values. *gapdh* was utilized as the housekeeping gene. Analysis was performed using the L1210 cells as the calibrator to determine fold change. Results demonstrated that relative to L1210 cells, FL83B cells express approximately 15,000-fold less *slc43a3*, 54-fold more *abcc4*, 2.4-fold more *abcc5*, 1.2-fold less *tpmt*, 16-fold less *hgprt1*, 9.5-fold more *xo,* 2.6-fold less *impdh,* 3.8-fold less *gmps, and* 8.9-fold less *nudt15*.

Figure 19. qPCR 2^-ΔΔCt analysis of L1210 and FL83B cells ►

Transcript level fold change relative to L1210 calibrator, of relevant murine 6-MP transporter genes such as *slc43a3*, *abcc4,* and *abcc5*, and murine 6-MP metabolism genes such as *tpmt*, *hgprt1*, *xo*, *impdh*, *gmps*, and *nudt15* were assessed in L1210 and FL83B cells. qPCR was performed on cDNA synthesized from L1210 and FL83B cell total RNA and qPCR primers, to amplify products, and obtain Ct values (n=6). Fold change > 1 is linear, i.e. 2.0 fold change equals 2-fold increase in transcript expression, relative to L1210. However, fold change < 1 is exponential, i.e. 0.2 fold change equals 5-fold decrease in transcript expression, relative to L1210; 0.1 fold change equals 10-fold decrease.

Figure 19.

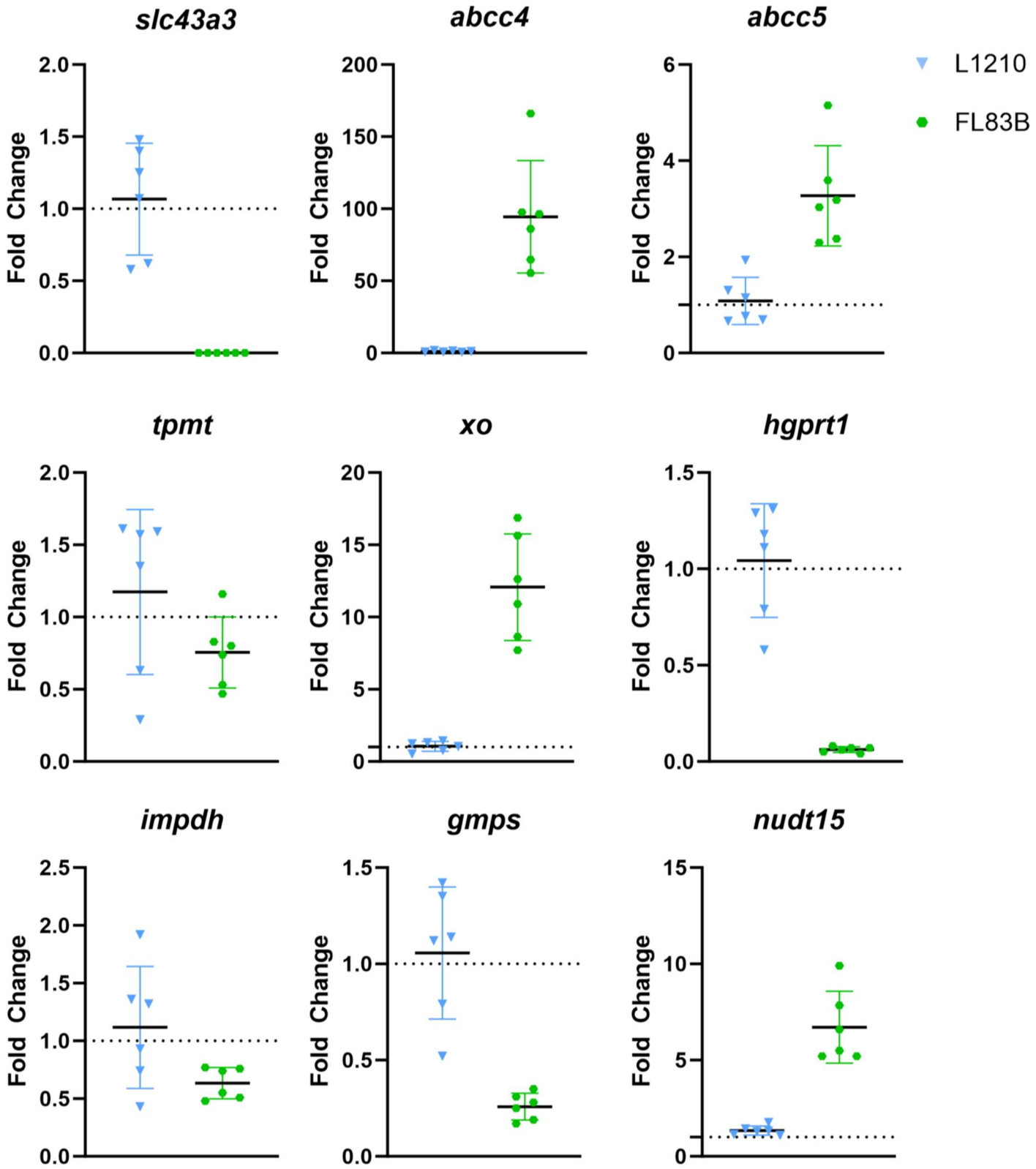
slc43a3
abcc4
abcc5
tpmt
xo
hgprt1
impdh
gmps
nudt15
Fold Change
L1210
FL83B

5.3 **Discussion**

5.3.a **Leukemia and hepatic cell line PCR and immunoblot**

5.3.a.i Endogenous *SLC43A3* and *slc43a3* expression detected in leukemia cells

Endogenous *SLC43A3* and *slc43a3* transcript expression was detected in leukemia cell lines via PCR (Figure 16.A). These finding concur with literature that hypothesizes ENBT1 plays a major role in purine salvage pathways, by mediating the accumulation of extracellular nucleotide precursors in cooperation with salvage enzymes (Furukawa et al., 2015), and therefore would be beneficial for the growth and survival of highly proliferative and resource intensive leukemia cell lines, such as MOLT-4 and L1210 cells. Furthermore, endogenous ENBT1 expression in leukemia cells, increase the therapeutic relevance of ENBT1 as the candidate transporter of 6-MP.

5.3.a.ii No *slc43a3* expression detected in FL83B hepatic cells

slc43a3 transcript expression was not detected in FL83B mouse hepatic cell lines via PCR, suggesting that FL83B are ENBT1-deficient much like HEK293-WT cells. This finding was unexpected, as ENBT1 has been found to be highly expressed in the sinusoidal membrane of human hepatocytes (Furukawa et al., 2015). On the other hand, a band was detected in FL83B and potentially L1210 cells using the *SLC43A3* primer set (Table 2. And Figure 16.A). However, this band is smaller than the expected product size for *SLC43A3* (400 bp), and is therefore likely non-specific binding and amplification of murine genes that were overlooked when designing the *SLC43A3* primer set, for use in human samples. It was uncertain whether mouse hepatocytes generally do not express *slc43a3,* or if this was a trait unique to FL83B hepatic cell lines. Thus, whole liver dissected from an 8–10-week-old wildtype C57BL/6 mouse, was assessed and

slc43a3 transcript expression was detected. Hepatocytes account for only around 52% of cells in mouse liver; the remainder is comprised of endothelial cells (22%), Kupffer cells (18%), and hepatic stellate/Ito cells (8%) (Baratta et al., 2009). Therefore, it is certain *slc43a3* transcript is expressed in mouse liver. However, it is still uncertain whether expression is localized to hepatocytes, or in other cells that comprise mouse liver.

5.1.a.i Endogenous hENBT1 expression detected in human leukemia cells

Endogenous hENBT1 expression was detected in MOLT-4 human leukemia cells via immunoblot (Figure 16.B). However, Figure 16.B does not properly convey differing levels of recombinant (HEK293-hSLC43A3), and endogenous (MOLT-4) hENBT1 expression in cells. Recombinant hENBT1 is over-expressed in HEK293-hSLC43A3 cells and when imaged on the same blot as endogenous hENBT1 in MOLT-4 cells, recombinant hENBT1 band intensity overshadows endogenous hENBT1 band intensity, to the degree that endogenous hENBT1 is not detectable at reasonable exposure times (Figure 20). Thus, presented immunoblot is two separate visualizations of the same blot, plus or minus HEK293-hSLC43A3. Attempt at densitometry of the full blot showed HEK293-hSLC43A3 cells express 180-fold more hENBT1 than MOLT-4 cells. Additionally of note, an antibody does not exist to consistently detect endogenous mENBT1, thus L1210, FL83B, and whole WT-mouse liver mENBT1 expression levels are unknown.

Figure 20. Full hENBT1 immunoblot

Full representative immunoblots using 30 μg protein from HEK293-EV, HEK293-hSLC43A3, HEK293-mslc43a3, FL83B, MOLT-4, and L1210 crude cell lysates. Anti-hENBT1 and anti-β-actin primary antibodies; HRP-conjugated anti-rabbit and anti-mouse secondary antibodies. MYC-hENBT1 (Expected Size: 56.0 kDA), and β-actin (Expected Size: 42.0 kDa). β-actin was used as a loading control.

Figure 20.

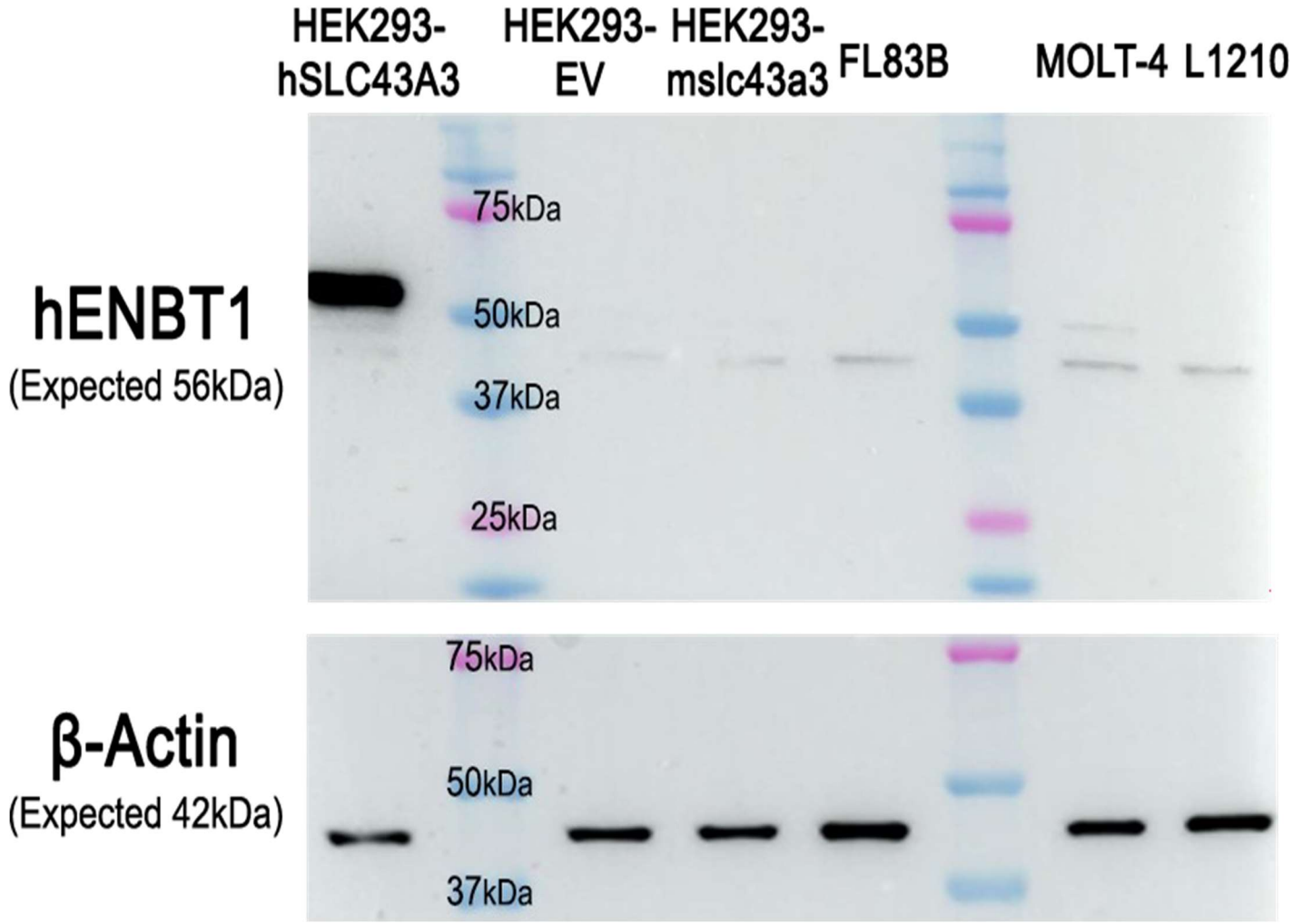
HEK293-hSLC43A3
HEK293-EV
HEK293-mslc43a3
FL83B
MOLT-4
L1210
hENBT1
(Expected 56kDa)
75kDa
50kDa
37kDa
25kDa
β-Actin
(Expected 42kDa)
75kDa
50kDa
37kDa

5.1.b **Endogenous hENBT1 and mENBT1 transport kinetics in leukemia and hepatic cell lines**

5.1.b.i 2 second time point partially captures initial rate in leukemia cells

The rate constant obtained in leukemia cells, suggest rapid but relatively slower rate of transport by ENBT1 (Figure 17.A) compared to the transfected-HEK293 cells (Figure 11.A). This is indicative of differing expression levels between cell lines with endogenous and recombinant ENBT1 expression (Figure 16.B). Due to lower ENBT1 expression levels in leukemia cells, a 2 second time point more holistically captures initial rate of [^{3}H]6-MP uptake, and thus is more appropriate. Therefore, 6-MP K_m values obtained in leukemia cells is likely more accurate than 6-MP K_m values obtained in transfected-HEK293 cells.

5.1.b.ii FL83B cells exhibit minimal time-dependent/saturable 6-MP uptake

FL83B cells did not exhibit time-dependent/saturable uptake of 1 μM [^{3}H]6-MP, instead results display 'negative' ENBT1-mediated uptake (Figure 17.B). To rule out the potential that 1 μM [^{3}H]6-MP, is not sufficient to assess endogenous ENBT1-mediated 6-MP uptake, time course assay was replicated using 100 μM [^{3}H]6-MP. However, results displayed similar 'negative' ENBT1-mediated uptake (Figure 17.C). Negative ENBT1-mediated uptake is a consequence of how ENBT1-mediated uptake is calculated and is in itself a misnomer, as it's not physically possible. This error occurs when non-mediated uptake is higher than total uptake as in Figure 17.B and Figure 17.C. These data initially suggest utilizing 5 mM adenine as a competitive inhibitor of ENBT1-mediated [^{3}H]6-MP uptake, increases [^{3}H]6-MP uptake. An effect like this implies incomplete inhibition of ENBT1, and has not been observed in MOLT-4 and L1210 cells (Figure 17.A). However, FL83B cells do not express *slc43a3* based on PCR (Figure 16.A) and qPCR data (Figure 19. A), respectively. Therefore, observed adenine effect is not ENBT1 mediated and may instead be an artifact due to high background and low

signal, based on how similar total uptake and non-mediated uptake are in value. Overall, results suggest FL83B cells have minimal, if any functional mENBT1 expression (Figure 17.C and Figure 17.C).

5.1.c **6-MP cell viability and cell death in leukemia and hepatic cell lines**

5.1.c.i Leftward 6-MP cell viability curve shift in MOLT-4 cells treated with 1 μM DY

Obtained 6-MP DY- (0.5 ± 0.1 μM) and 6-MP DY+ (0.3 ± 0.1 μM) first-phase EC_{50} values were significantly different (Extra sum-of-squares F-test, $F_{1, 166}$ =6.911, p=0.009, n=6) (Figure 18.B). These results demonstrate that treating cells with 10 μM DY increased MOLT-4 sensitivity to 6-MP. DY is a relatively potent inhibitor that at 10 μM inhibits ENT1 and ENT2 function but not ENBT1. Therefore, observed DY effect is likely ENT1 and ENT2-mediated, rather than ENBT1-mediated.

This ENT1 and ENT2-mediated mechanism is potentially linked to the role ENT1 and ENT2 play in exogenous nucleoside salvage (Griffiths et al., 1997; Yao et al., 1997; Crawford et al., 1998; Lin and Buolamwini, 2007; Paproski et al., 2008). **(1):** inhibiting ENT1/ENT2-mediated nucleoside salvage, depletes intracellular precursors necessary for nucleotide biosynthesis. This will lead to a decrease in the supply of endogenous nucleotides necessary for RNA and DNA synthesis. On the other hand, ENBT1 is undeterred in mediating the accumulation of 6-MP, which is then intracellularly converted to 6-TGN, an antimetabolite that competes with endogenous nucleotides to interfere with DNA synthesis. With a decrease in endogenous nucleotide supply and therefore competition between endogenous and fraudulent nucleotides, more 6-TGN will be falsely incorporated during DNA synthesis. Leading to an increase in

DNA MMR-dependent apoptosis and a leftward 6-MP cell viability curve shift. Alternatively, **(2):** depletion of intracellular precursors necessary for nucleotide biosynthesis, reduces 6-MP competition for enzymes that are involved in both purine salvage pathways and 6- MP metabolic pathways. The most important enzyme involved in both is HGPRT which is involved in metabolizing guanine into guanine monophosphate (GMP), hypoxanthine into inosine monophosphate (IMP), and 6-MP into 6-TIMP; which ultimately leads to the synthesis of deoxyguanosine triphosphate (dGTP), deoxyadenosine triphosphate (dATP), and 6-TdGTP (Bradford and Shih, 2011; Singh et al., 2017; Sheu et al., 2022). With a decrease in endogenous nucleoside/nucleobase supply, and therefore competition between endogenous and xenobiotic substrates, more 6-MP will ultimately be converted to 6-TGN. Leading to an increase in DNA MMR-dependent apoptosis, and a leftward 6-MP cell viability curve shift. Either explanation is non-exclusive and could both contribute, perhaps even synergistically, to the observed DY effect. A DY-like effect on 6-MP effect on cell viability was also observed in a HEK293-ENT1KO cell line which only expresses endogenous levels of ENT2, further suggesting ENT1 involvement (N. Shahid, personal communication, November 3, 2023).

5.1.c.ii FL83B 6-MP resistance

Obtained FL83B 6-MP EC_{50} values suggest substantial 6-MP resistance (Figure 18.C) relative to other previously assessed cells. Compared to previously presented 6-MP EC_{50} values (Table 4.), FL83B cells are >100-fold more resistant than HEK293-EV cells (Figure 13.A), >2,000-fold more resistant than HEK293-mslc43a3 cells (Figure 13.A), and >3,300-fold more resistant than L1210 cells (Figure 18.A). HEK293-EV and FL83B cells have been shown to not express *SLC43A3* or *slc43a3* therefore, FL83B elevated 6-MP resistance cannot be explained by

SLC43A3/hENBT1 or *slc43a3*/mENBT1 expression alone. Specific targets of interest for investigation include 6-MP efflux pumps such as *abcc4*/MRP4, and 6-MP metabolic enzymes such as *tpmt*/TPMT, *xo*/XO, *hgprt1*/HGPRT, *impdh*/IMPDH, *gmps*/GMPS, and *nudt15*/NUDT1

Table 4. 6-MP EC_{50} values ►

Table of experimentally obtained 6-MP first phase EC_{50} values in various human and murine cell lines. HEK293-EV, HEK293-hSLC43A3, and HEK293-mslc43a3 EC_{50} values (Figure 13.A), MOLT-4 and L1210 EC_{50} values (Figure 18.A), and FL83B EC_{50} values (Figure 18.C). Note EC_{50} values are presented as μM units, with the exception of FL83B presented as mM units. Data are shown as mean ± SEM.

Table 4.

Cell Line	**Obtained 6-MP EC_{50}**
HEK293-EV	19 ± 0.5 μM
HEK293-hSLC43A3	1.0 ± 0.1 μM
HEK293-mslc43a3	1.0 ± 0.3 μM
MOLT-4	0.7 ± 0.2 μM
L1210	0.6 ± 0.2 μM
FL83B	2.0 ± 0.2 mM

5.1.c.iii Discrepancy between MOLT-4 and L1210 6-MP cell death curves

48-hour incubation treatment of cells with 6-MP induced higher levels of cell death in MOLT-4 (<20% cell death) cells compared to L1210 (<5% cell death) cells (Figure 18.D). The MOLT-4 data concurs with Fernandez-Ramos and colleagues, (2017), who observed approximately 30% cell death after 48-hour incubation with 50 μM 6-MP in Jurkat T cells. On the other hand, L1210 cells exhibited a relatively blunted cell death. As previously described in section 1.2B, 6-TGN incorporation into DNA ultimately induces DNA MMR- dependent apoptosis. A mechanism for the discrepancy between leukemia cells may be that the L1210 cells assessed in the assay have a DNA repair-deficiency. This is not without precedence as L1210 cells have been previously described to spontaneously develop DNA repair- deficiencies (Vilpo et al., 1995) that would confer resistance to antimetabolite drugs such as 6- MP.

5.1.d **L1210, HEK293-mslc43a3, and FL83B qPCR gene expression profile**

5.1.d.i Rationale for selecting L1210 as the calibrator cell

qPCR data is commonly presented as ΔΔCt or 2^-ΔΔCt (fold change) values (Livak and Schmittgen, 2001), which are analyzed utilizing Ct values in a calibrator cell/group, that Ct values from all other cells/groups are made relative to. Ideally, a calibrator cell/group should have a before/after relationship with the cells/groups being analyzed (eg. untreated sample as the calibrator for treated samples). However, that was not an option for the current question of whether differences in transcript expression between L1210 and FL83B cells can explain observed differences in 6-MP EC_{50} values. As this particular investigation pertained to endogenous *slc43a3*/ENBT1, the L1210 cell line was chosen as the calibrator cell over FL83B cells due to expressing *slc43a3* (Figure 16.A).

5.1.d.ii Differing expression levels potentially explain elevated 6-MP resistance

qPCR results demonstrated that relative to L1210 cells, FL83B cells express approximately 15,000-fold less *slc43a3* (reduced 6-MP influx capacity), 54-fold more *abcc4* (elevated 6-MP efflux capacity), 2.4-fold more *abcc5* (elevated 6-MP efflux capacity), 1.2-fold less *tpmt* (elevated 6-MP activation), 16-fold less *hgprt1* (reduced 6-MP activation), 9.5-fold more *xo* (elevated 6-MP inactivation), 2.6-fold less *impdh* (reduced 6-MP activation), 3.8-fold less *gmps* (reduced 6-MP activation), and 8.9-fold less *nudt15* (reduced 6-MP inactivation). With the exception of decreased *tpmt* expression, FL83B gene expression profile concurs with observed substantial 6-MP resistance. Although mRNA transcript expression does not necessarily equal protein expression (Fortelny et al., 2017), this gene expression profile suggest FL83B elevated resistance to 6-MP is multifaceted, and not solely due to near zero expression of mENBT1.

5.2 **Limitations**

Data from MOLT-4 and L1210 cells suggest that endogenous hENBT1 and mENBT1 are functionally similar in mediating the uptake of 6-MP (Figure 17.A and Figure 17.D), and mediating 6-MP/6-MP metabolite effect on cell viability (Figure 18.A). However, current challenges are with the FL83B hepatic cell line, due to those cells not expressing *slc43a3* transcript and functional ENBT1. This put into question whether hepatocytes in general do not express *slc43a3*/ENBT1, or if this is a characteristic unique to the FL83B hepatic cell line. Additionally, an appropriate mENBT1 specific antibody has not yet been experimentally verified in our lab. This is essential to assess endogenous mENBT1 expression, as unlike recombinant mENBT1, endogenous mENBT1 does not have a MYC-tag that can be probed as a proxy in immunoblots. Quantifying protein expression, in addition to currently obtained transcript expression, is desirable because transcript expression levels do not

necessarily translate to protein expression levels (Fortelny et al., 2017). Assessing *SLC43A3*/ ENBT1 expression and function in additional hepatic cell lines such as THLE-3 (human), Hepa-RG (human), or AML12 (mouse) cells or isolated primary mouse hepatocytes, would aid in elucidating whether hepatocyte's express ENBT1.

CHAPTER 6.

Summary and Discussion

6.1 **Summary**

Data presented in Chapter 4. *Interspecies Functional Comparison of Recombinant hENBT1 and mENBT1* display **(1):** Successful stable transfection of recombinant *SLC43A3* in HEK293-hSLC43A3 and *slc43a3* in HEK293-mslc43a3 cells (Figure 9.A, Figure 9.B, Figure 9.C, Figure 9.D, Figure 10.B, and Figure 10.C). **(2):** HEK293-WT and HEK293-EV cells do not express detectable levels of recombinant *SLC43A3*/ENBT1 (Figure 9.B and Figure 9.C), and do not exhibit measurable ENBT1-mediated nucleobase flux capacity (Figure 10.A and Figure 11.A,). **(3):** Recombinant hENBT1 and mENBT1 have similar [^{3}H]adenine and [^{3}H]6-MP transport kinetics (k values and K_m values) (Figure 11.A, Figure 11.B, and Figure 11.C). **(4):** Recombinant hENBT1 and mENBT1 have similar adenine and 6-MP inhibition kinetics (IC_{50} values and matching adenine K_m/K_i values) (Figure 12.A and Figure 12.B). **(5):** Recombinant hENBT1 and mENBT1 are functionally similar in mediating 6-MP (Figure 13.A) and 6-TG (Figure 13.C) effect on cell viability.

In relation to Research Aim 1: these results have aided in elucidating the role of recombinant *slc43a3*/mENBT1 as a mediator of adenine and 6-MP cellular accumulation and of 6-MP and 6-TG effect on cell viability. Additionally, direct interspecies functional comparison between recombinant *SLC43A3*/hENBT1 and *slc43a3*/mENBT1 concludes recombinant human and murine SLC43A3-encoded ENBT1 are functionally similar in mediating the cellular accumulation of 6-MP and subsequent effect on cell viability.

Data presented in Chapter 5. *Interspecies Functional Comparison of Endogenous hENBT1 and mENBT1* display **(1):** MOLT-4 and L1210 leukemia cells endogenously express *SLC43A3*/hENBT1 and *slc43a3*/mENBT1, respectively (Figure 16.A and Figure 16.B). **(2):** Endogenous hENBT1 and mENBT1 have similar 6-MP transport kinetics in leukemia cells (k values, K_m values) **(3):** Endogenous hENBT1 and mENBT1 are functionally similar in mediating 6-MP effect on cell viability, in leukemia cells (Figure 18.A). MOLT-4 6-MP cell viability matched (Figure 18.A) with 6-MP cell death (Figure 18.D), however there was a discrepancy in L1210 cells. Suggesting L1210 cells may have differing intercellular mechanisms from MOLT-4 cells, that lead to 6-MP being more of a cytostatic agent rather than a cytotoxic agent. **(4):** Co-treating MOLT-4 cells with 6-MP and DY, increased sensitivity to 6-MP (Figure 18.B). Suggesting indirectly that ENTs can affect cell sensitively to 6-MP. **(5):** Relative to L1210 cell transcript expression levels, FL83B cells express 15,000-fold less *slc43a3*, 54.2-fold more *abcc4*, 2.4-fold more *abcc5*, 1.2-fold less *tpmt*, 16-fold less *hgprt1*, 9.5-fold more *xo,* 2.6-fold less *impdh,* 3.8-fold less *gmps, and* 8.9-fold less *nudt15*; potentially explaining substantial 6-MP resistance observed in FL83B cells.

In relation to Research Aim 2: these results have also aided in elucidating the role of endogenous *slc43a3*/mENBT1, in leukemia cells, as a mediator of 6-MP cellular accumulation and of 6-MP effect on cell viability. Unfortunately, FL83B hepatic cell lines do not endogenously express *slc43a3*/mENBT1. Thus, the role of ENBT1 in hepatocytes and any association with 6-MP associated hepatotoxicity is currently unknown. Finally, direct interspecies functional comparison between endogenous *SLC43A3*/hENBT1 and *slc43a3*/mENBT1 in leukemia cells, concludes endogenous human and murine SLC43A3- encoded ENBT1 are functionally similar in mediating the cellular accumulation of 6-MP and subsequent effect on cell viability.

6.2 **Closing Remarks**

This thesis project was primarily focused on functionally characterizing *slc43a3*/mENBT1. As summarized in Section 6.1, recombinant and endogenous *slc43a3*/mENBT1 have been shown to be the primary mechanism that mediates the cellular accumulation of 6-MP and subsequent effect on cell viability. An additional overarching aim was to perform an interspecies functional comparison on recombinant and endogenous, human and murine *SLC43A3*-encoded ENBT1. Overall, results suggest recombinantly and endogenously expressed human and murine *SLC43A3*-encoded ENBT1 are functionally similar in mediating the cellular accumulation of 6-MP and subsequent effect on cell viability. Therefore, a *slc43a3* KO mouse is an appropriate model to explore the role of ENBT1 in 6-MP/6-MP metabolite absorption, cellular accumulation, and tissue biodistribution.

Reference List:

Aarbakke, J., Janka-Schaub, G., & Elion, G. B. (1997). Thiopurine biology and pharmacology. *Trends Pharmacol Sci*, *18*(1), 3-7. https://doi.org/10.1016/s0165-6147(96)01007-3

Andersen, J. B., Szumlanski, C., Weinshilboum, R. M., & Schmiegelow, K. (1998). Pharmacokinetics, dose adjustments, and 6-mercaptopurine/methotrexate drug interactions in two patients with thiopurine methyltransferase deficiency. *Acta Paediatr*, *87*(1), 108-111. https://doi.org/10.1080/08035259850158001

Aymerich, I., Duflot, S., Fernandez-Veledo, S., Guillen-Gomez, E., Huber-Ruano, I., Casado, F. J., & Pastor-Anglada, M. (2005). The concentrative nucleoside transporter family (SLC28): new roles beyond salvage? *Biochem Soc Trans*, *33*(Pt 1), 216-219. https://doi.org/10.1042/BST0330216

Babu, E., Kanai, Y., Chairoungdua, A., Kim, D. K., Iribe, Y., Tangtrongsup, S., Jutabha, P., Li, Y., Ahmed, N., Sakamoto, S., Anzai, N., Nagamori, S., & Endou, H. (2003). Identification of a novel system L amino acid transporter structurally distinct from heterodimeric amino acid transporters. *J Biol Chem*, *278*(44), 43838-43845. https://doi.org/10.1074/jbc.M305221200

Baldwin, S. A., Beal, P. R., Yao, S. Y., King, A. E., Cass, C. E., & Young, J. D. (2004). The equilibrative nucleoside transporter family, SLC29. *Pflugers Arch*, *447*(5), 735-743. https://doi.org/10.1007/s00424-003-1103-2

Ball, D. W., Hill, J. W., Scott, R. J., & Open Textbook, L. (2011). *The basics of general, organic, and biological chemistry*. Saylor Academy

Baratta, J. L., Ngo, A., Lopez, B., Kasabwalla, N., Longmuir, K. J., & Robertson, R. T. (2009). Cellular organization of normal mouse liver: a histological, quantitative immunocytochemical, and fine structural analysis. *Histochem Cell Biol*, *131*(6), 713-726. https://doi.org/10.1007/s00418-009-0577-1

Becerra, E., Berumen, L., Soto-Ontiveros, V., & Garcia-Alcocer, G. (2022). Specific MRP4 Inhibitor Ceefourin-1 Enhances Apoptosis Induced by 6-Mercaptopurine in Jurkat Leukemic Cells, but Not in Normal Lymphoblast Cell Line CRL-1991. *Medicina (Kaunas)*, *58*(6). https://doi.org/10.3390/medicina58060695

Bodoy, S., Fotiadis, D., Stoeger, C., Kanai, Y., & Palacin, M. (2013). The small SLC43 family: facilitator system l amino acid transporters and the orphan EEG1. *Mol Aspects Med*, *34*(2-3), 638-645. https://doi.org/10.1016/j.mam.2012.12.006

Bodoy, S., Martin, L., Zorzano, A., Palacin, M., Estevez, R., & Bertran, J. (2005). Identification of LAT4, a novel amino acid transporter with system L activity. *J Biol Chem*, *280*(12), 12002-12011. https://doi.org/10.1074/jbc.M408638200

Bone, D. B., Robillard, K. R., Stolk, M., & Hammond, J. R. (2007). Differential regulation of mouse equilibrative nucleoside transporter 1 (mENT1) splice variants by protein kinase CK2. *Mol Membr Biol*, *24*(4), 294-303. https://doi.org/10.1080/09687860701210617

Borea, P. A., Gessi, S., Merighi, S., Vincenzi, F., & Varani, K. (2018). Pharmacology of Adenosine Receptors: The State of the Art. *Physiol Rev*, *98*(3), 1591-1625. https://doi.org/10.1152/physrev.00049.2017

Boswell-Casteel, R. C., & Hays, F. A. (2017). Equilibrative nucleoside transporters-A review. *Nucleosides Nucleotides Nucleic Acids*, *36*(1), 7-30. https://doi.org/10.1080/15257770.2016.1210805

Bradford, K., & Shih, D. Q. (2011). Optimizing 6-mercaptopurine and azathioprine therapy in the management of inflammatory bowel disease. *World J Gastroenterol*, *17*(37), 4166-4173. https://doi.org/10.3748/wjg.v17.i37.4166

Breslow, J. L., Sloan, H. R., Ferrans, V. J., Anderson, J. L., & Levy, R. I. (1973). Characterization of the mouse liver cell line FL83B. *Exp Cell Res*, *78*(2), 441-453. https://doi.org/10.1016/0014-4827(73)90089-x

Brown, C. H., & Achkar, E. (1970). Azathioprine therapy for inflammatory bowel disease. A preliminary report. *Am J Gastroenterol*, *54*(4), 363-377. https://www.ncbi.nlm.nih.gov/pubmed/5478849

Burchenal, J. H., Murphy, M. L., Ellison, R. R., Sykes, M. P., Tan, T. C., Leone, L. A., Karnofsky, D. A., Craver, L. F., Dargeon, H. W., & Rhoads, C. P. (1953). Clinical evaluation of a new antimetabolite, 6-mercaptopurine, in the treatment of leukemia and allied diseases. *Blood*, *8*(11), 965-999. https://www.ncbi.nlm.nih.gov/pubmed/13105700

Chambers, E. K., Stratulat, E., Judge, G., Shafique, S., & Ladel, L. (2023). Stomach Pain Upon Stomach Pain: Medication-Induced Pancreatitis. *Cureus*, *15*(2), e35554. https://doi.org/10.7759/cureus.35554

Chan, G. L., Erdmann, G. R., Gruber, S. A., Matas, A. J., & Canafax, D. M. (1990). Azathioprine metabolism: pharmacokinetics of 6-mercaptopurine, 6-thiouric acid and 6-thioguanine nucleotides in renal transplant patients. *J Clin Pharmacol*, *30*(4), 358-363. https://doi.org/10.1002/j.1552-4604.1990.tb03606.x

Chen, L., Yan, H. X., Liu, X. W., & Chen, W. X. (2020). Clinical efficacy and safety of 6-thioguanine in the treatment of childhood acute lymphoblastic leukemia: A protocol for systematic review and meta-analysis. *Medicine (Baltimore)*, *99*(18), e20082. https://doi.org/10.1097/MD.0000000000020082

Chen, Y., Yuan, X., Xiao, Z., Jin, H., Zhang, L., & Liu, Z. (2018). Discovery of novel multidrug resistance protein 4 (MRP4) inhibitors as active agents reducing resistance to anticancer drug 6-Mercaptopurine (6-MP) by structure and ligand-based virtual screening. *PLoS One*, *13*(10), e0205175. https://doi.org/10.1371/journal.pone.0205175

Cheng, Y., & Prusoff, W. H. (1973). Relationship between the inhibition constant (K1) and the concentration of inhibitor which causes 50 per cent inhibition (I50) of an enzymatic reaction. *Biochem Pharmacol*, *22*(23), 3099-3108. https://doi.org/10.1016/0006-2952(73)90196-2

Christensen, H. N., & Riggs, T. R. (1952). Concentrative uptake of amino acids by the Ehrlich mouse ascites carcinoma cell. *J Biol Chem*, *194*(1), 57-68. https://www.ncbi.nlm.nih.gov/pubmed/14927593

Christensen, H. N., Riggs, T. R., Fischer, H., & Palatine, I. M. (1952). Amino acid concentration by a free cell neoplasm; relations among amino acids. *J Biol Chem*, *198*(1), 1-15. https://www.ncbi.nlm.nih.gov/pubmed/12999712

Christensen, H. N., Riggs, T. R., & Ray, N. E. (1952). Concentrative uptake of amino acids by erythrocytes in vitro. *J Biol Chem*, *194*(1), 41-51. https://www.ncbi.nlm.nih.gov/pubmed/14927591

Coe, I. R., Griffiths, M., Young, J. D., Baldwin, S. A., & Cass, C. E. (1997). Assignment of the human equilibrative nucleoside transporter (hENT1) to 6p21.1-p21.2. *Genomics*, *45*(2), 459-460. https://doi.org/10.1006/geno.1997.4928

Corzo, J. (2006). Time, the forgotten dimension of ligand binding teaching. *Biochem Mol Biol Educ*, *34*(6), 413-416. https://doi.org/10.1002/bmb.2006.494034062678

Crawford, C. R., Patel, D. H., Naeve, C., & Belt, J. A. (1998). Cloning of the human equilibrative, nitrobenzylmercaptopurine riboside (NBMPR)-insensitive nucleoside transporter ei by functional expression in a transport-deficient cell line. *J Biol Chem*, *273*(9), 5288-5293. https://doi.org/10.1074/jbc.273.9.5288

Curtis, J. E., Cowan, D. H., Bergsagel, D. E., Hasselback, R., & McCulloch, E. A. (1975). Acute leukemia in adults: assessment of remission induction with combination chemotherapy by clinical and cell-culture criteria. *Can Med Assoc J*, *113*(4), 289-294. https://www.ncbi.nlm.nih.gov/pubmed/1056807

Damaraju, V. L., Kuzma, M., Cass, C. E., & Sawyer, M. B. (2015). Inhibition of sodium-independent and sodium-dependent nucleobase transport activities by tyrosine kinase inhibitors. *Cancer Chemother Pharmacol*, *76*(5), 1093-1098. https://doi.org/10.1007/s00280-015-2859-8

Drew, D., North, R. A., Nagarathinam, K., & Tanabe, M. (2021). Structures and General Transport Mechanisms by the Major Facilitator Superfamily (MFS). *Chem Rev*, *121*(9), 5289-5335. https://doi.org/10.1021/acs.chemrev.0c00983

Dubinsky, M. C., Lamothe, S., Yang, H. Y., Targan, S. R., Sinnett, D., Theoret, Y., & Seidman, E. G. (2000). Pharmacogenomics and metabolite measurement for 6-mercaptopurine therapy in inflammatory bowel disease. *Gastroenterology*, *118*(4), 705-713. https://doi.org/10.1016/s0016-5085(00)70140-5

Eckle, T., Krahn, T., Grenz, A., Kohler, D., Mittelbronn, M., Ledent, C., Jacobson, M. A., Osswald, H., Thompson, L. F., Unertl, K., & Eltzschig, H. K. (2007). Cardioprotection by ecto-5'-nucleotidase (CD73) and A2B adenosine receptors. *Circulation*, *115*(12), 1581-1590. https://doi.org/10.1161/CIRCULATIONAHA.106.669697

Eguchi, Y., Makanae, K., Hasunuma, T., Ishibashi, Y., Kito, K., & Moriya, H. (2018). Estimating the protein burden limit of yeast cells by measuring the expression limits of glycolytic proteins. *Elife*, *7*. https://doi.org/10.7554/eLife.34595

Elion, G. B. (1986). Historical background of 6-mercaptopurine. *Toxicol Ind Health*, *2*(2), 1-9. https://doi.org/10.1177/074823378600200201

Elwi, A. N., Damaraju, V. L., Baldwin, S. A., Young, J. D., Sawyer, M. B., & Cass, C. E. (2006). Renal nucleoside transporters: physiological and clinical implications. *Biochem Cell Biol*, *84*(6), 844-858. https://doi.org/10.1139/o06-198

Fernandez-Ramos, A. A., Marchetti-Laurent, C., Poindessous, V., Antonio, S., Laurent-Puig, P., Bortoli, S., Loriot, M. A., & Pallet, N. (2017). 6-mercaptopurine promotes energetic failure in proliferating T cells. *Oncotarget*, *8*(26), 43048-43060. https://doi.org/10.18632/oncotarget.17889

Fountain, J. R. (1956). Treatment of chronic myeloid leukaemia with mercaptopurine. *Br Med J*, *2*(5005), 1345-1348. https://doi.org/10.1136/bmj.2.5005.1345

Furukawa, J., Inoue, K., Maeda, J., Yasujima, T., Ohta, K., Kanai, Y., Takada, T., Matsuo, H., & Yuasa, H. (2015). Functional identification of SLC43A3 as an equilibrative nucleobase transporter involved in purine salvage in mammals. *Sci Rep*, *5*, 15057. https://doi.org/10.1038/srep15057

Gearry, R. B., Barclay, M. L., Burt, M. J., Collett, J. A., & Chapman, B. A. (2004). Thiopurine drug adverse effects in a population of New Zealand patients with inflammatory bowel disease. *Pharmacoepidemiol Drug Saf*, *13*(8), 563-567. https://doi.org/10.1002/pds.926

Girard, N. (2022). New Strategies and Novel Combinations in EGFR TKI-Resistant Non-small Cell Lung Cancer. *Curr Treat Options Oncol*, *23*(11), 1626-1644. https://doi.org/10.1007/s11864-022-01022-7

Giverhaug, T., Loennechen, T., & Aarbakke, J. (1999). The interaction of 6-mercaptopurine (6-MP) and methotrexate (MTX). *Gen Pharmacol*, *33*(4), 341-346. https://doi.org/10.1016/s0306-3623(99)00022-1

Goldstein, F. (1987). Immunosuppressant therapy of inflammatory bowel disease. Pharmacologic and clinical aspects. *J Clin Gastroenterol*, *9*(6), 654-658. https://doi.org/10.1097/00004836-198712000-00009

Gray, J. H., Owen, R. P., & Giacomini, K. M. (2004). The concentrative nucleoside transporter family, SLC28. *Pflugers Arch*, *447*(5), 728-734. https://doi.org/10.1007/s00424-003-1107-y

Griffiths, M., Yao, S. Y., Abidi, F., Phillips, S. E., Cass, C. E., Young, J. D., & Baldwin, S. A. (1997). Molecular cloning and characterization of a nitrobenzylthioinosine-insensitive (ei) equilibrative nucleoside transporter from human placenta. *Biochem J*, *328 (Pt 3)*(Pt 3), 739-743. https://doi.org/10.1042/bj3280739

Gupta, R., & Brunak, S. (2002). Prediction of glycosylation across the human proteome and the correlation to protein function. *Pac Symp Biocomput*, 310-322. https://www.ncbi.nlm.nih.gov/pubmed/11928486

Hall, B. E., Richards, M. D., Willett, F. M., Feichtmeir, T. V., & Aggeler, P. M. (1953). Evaluation of 6-mercaptopurine in the treatment of leukemia; a preliminary report. *Stanford Med Bull*, *11*(4), 237-240. https://www.ncbi.nlm.nih.gov/pubmed/13122302

He, J., & Liu, L. (2019). [Significance of NUDT15 gene in individualized treatment with 6-mercaptopurine in children with acute lymphoblastic leukemia]. *Zhongguo Dang Dai Er Ke Za Zhi*, *21*(1), 100-104. https://doi.org/10.7499/j.issn.1008-8830.2019.01.018

Headrick, J. P., Peart, J. N., Reichelt, M. E., & Haseler, L. J. (2011). Adenosine and its receptors in the heart: regulation, retaliation and adaptation. *Biochim Biophys Acta*, *1808*(5), 1413-1428. https://doi.org/10.1016/j.bbamem.2010.11.016

Hill, J. M., & Lajous, J. (1954). 6-Mercaptopurine therapy in leukemia. *Ann N Y Acad Sci*, *60*(2), 461-465. https://doi.org/10.1111/j.1749-6632.1954.tb40040.x

Huang, Q. Q., Yao, S. Y., Ritzel, M. W., Paterson, A. R., Cass, C. E., & Young, J. D. (1994). Cloning and functional expression of a complementary DNA encoding a mammalian nucleoside transport protein. *J Biol Chem*, *269*(27), 17757-17760. https://www.ncbi.nlm.nih.gov/pubmed/8027026

Jackson, P. J. (1983). Determination of 6-thiouric acid in human urine. *Clin Biochem*, *16*(5), 285-286. https://doi.org/10.1016/s0009-9120(83)94053-5

Jarvis, S. M., & Young, J. D. (1987). Photoaffinity labelling of nucleoside transporter polypeptides. *Pharmacol Ther*, *32*(3), 339-359. https://doi.org/10.1016/0163-7258(87)90080-5

Jimenez-Sanchez, M., Licitra, F., Underwood, B. R., & Rubinsztein, D. C. (2017). Huntington's Disease: Mechanisms of Pathogenesis and Therapeutic Strategies. *Cold Spring Harb Perspect Med*, *7*(7). https://doi.org/10.1101/cshperspect.a024240

Kahn, J. M., Stevenson, K., Beauchemin, M., Koch, V. B., Cole, P. D., Welch, J. J. G., Gage-Bouchard, E., Karsenty, C., Silverman, L. B., Kelly, K. M., & Bona, K. (2023). Oral Mercaptopurine Adherence in Pediatric Acute Lymphoblastic Leukemia: A Survey Study From the Dana-Farber Cancer Institute Acute Lymphoblastic Leukemia Consortium. *J Pediatr Hematol Oncol Nurs*, *40*(1), 17-23. https://doi.org/10.1177/27527530221122685

Kanai, Y., Segawa, H., Miyamoto, K., Uchino, H., Takeda, E., & Endou, H. (1998). Expression cloning and characterization of a transporter for large neutral amino acids activated by the heavy chain of 4F2 antigen (CD98). *J Biol Chem*, *273*(37), 23629-23632. https://doi.org/10.1074/jbc.273.37.23629

Karner, S., Shi, S., Fischer, C., Schaeffeler, E., Neurath, M. F., Herrlinger, K. R., Hofmann, U., & Schwab, M. (2010). Determination of 6-thioguanosine diphosphate and triphosphate and nucleoside diphosphate kinase activity in erythrocytes: novel targets for thiopurine therapy? *Ther Drug Monit*, *32*(2), 119-128. https://doi.org/10.1097/FTD.0b013e3181d12f19

Karran, P., & Attard, N. (2008). Thiopurines in current medical practice: molecular mechanisms and contributions to therapy-related cancer. *Nat Rev Cancer*, *8*(1), 24-36. https://doi.org/10.1038/nrc2292

Kenakin, T. (1997). Differences between natural and recombinant G protein-coupled receptor systems with varying receptor/G protein stoichiometry. *Trends Pharmacol Sci*, *18*(12), 456-464. https://doi.org/10.1016/s0165-6147(97)01136-x

Khoo, X. H., Wong, S. Y., Ibrahim, N. R. W., Ng, R. T., Chew, K. S., Lee, W. S., Wong, Z. Q., Raja Ali, R. A., Shahrani, S., Leow, A. H., & Hilmi, I. N. (2022). Nudix Hydroxylase 15 Mutations Strongly Predict Thiopurine-Induced Leukopenia Across Different Asian Ethnicities: Implications for Screening in a Diverse Population. *Front Med (Lausanne)*, *9*, 880937. https://doi.org/10.3389/fmed.2022.880937

Kingston, R. E., Chen, C. A., & Okayama, H. (2003). Calcium phosphate transfection. *Curr Protoc Cell Biol*, *Chapter 20*, Unit 20 23. https://doi.org/10.1002/0471143030.cb2003s19

Kingston, R. E., Chen, C. A., & Rose, J. K. (2003). Calcium phosphate transfection. *Curr Protoc Mol Biol*, *Chapter 9*, Unit 9 1. https://doi.org/10.1002/0471142727.mb0901s63

Kockerols, C., Valk, P. J. M., Blijlevens, N. M. A., Cornelissen, J. J., Dinmohamed, A. G., Geelen, I., Hoogendoorn, M., Janssen, J., Daenen, L. G. M., Reijden, B. A. V., & Westerweel, P. E. (2023). BCR::ABL1 kinase domain mutation testing and clinical outcome in a nationwide chronic myeloid leukemia patient population. *Eur J Haematol*. https://doi.org/10.1111/ejh.14107

Kumar, S., Josan, V., Sanger, K. C., Tewari, K. K., & Krishnan, P. S. (1967). Studies on guanine deaminase and its inhibitors in rat tissue. *Biochem J*, *102*(3), 691-704. https://doi.org/10.1042/bj1020691

Lancaster, D. L., Lennard, L., Rowland, K., Vora, A. J., & Lilleyman, J. S. (1998). Thioguanine versus mercaptopurine for therapy of childhood lymphoblastic leukaemia: a comparison of haematological toxicity and drug metabolite concentrations. *Br J Haematol*, *102*(2), 439-443. https://doi.org/10.1046/j.1365-2141.1998.00812.x

Larsen, R. H., Hjalgrim, L. L., Grell, K., Kristensen, K., Pedersen, L. G., Brunner, E. D., Als-Nielsen, B., Schmiegelow, K., & Nersting, J. (2020). Pharmacokinetics of tablet and liquid formulations of oral 6-mercaptopurine in children with acute lymphoblastic leukemia. *Cancer Chemother Pharmacol*, *86*(1), 25-32. https://doi.org/10.1007/s00280-020-04097-x

Lennard, L., Davies, H. A., & Lilleyman, J. S. (1993). Is 6-thioguanine more appropriate than 6-mercaptopurine for children with acute lymphoblastic leukaemia? *Br J Cancer*, *68*(1), 186-190. https://doi.org/10.1038/bjc.1993.311

Lin, W., & Buolamwini, J. K. (2007). Synthesis, flow cytometric evaluation, and identification of highly potent dipyridamole analogues as equilibrative nucleoside transporter 1 inhibitors. *J Med Chem*, *50*(16), 3906-3920. https://doi.org/10.1021/jm070311l

Livak, K. J., & Schmittgen, T. D. (2001). Analysis of relative gene expression data using real-time quantitative PCR and the 2(-Delta Delta C(T)) Method. *Methods*, *25*(4), 402-408. https://doi.org/10.1006/meth.2001.1262

Lonnerholm, G., Kreuger, A., Lindstrom, B., Ludvigsson, J., & Myrdal, U. (1986). Plasma and erythrocyte concentrations of mercaptopurine after oral administration in children. *Pediatr Hematol Oncol*, *3*(1), 27-35. https://doi.org/10.3109/08880018609031198

Luber, R. P., Honap, S., Cunningham, G., & Irving, P. M. (2019). Can We Predict the Toxicity and Response to Thiopurines in Inflammatory Bowel Diseases? *Front Med (Lausanne)*, *6*, 279. https://doi.org/10.3389/fmed.2019.00279

Mason, M., Currey, H. L., Barnes, C. G., Dunne, J. F., Hazleman, B. L., & Strickland, I. D. (1969). Azathioprine in rheumatoid arthritis. *Br Med J*, *1*(5641), 420-422. https://doi.org/10.1136/bmj.1.5641.420

Minowada, J., Onuma, T., & Moore, G. E. (1972). Rosette-forming human lymphoid cell lines. I. Establishment and evidence for origin of thymus-derived lymphocytes. *J Natl Cancer Inst*, *49*(3), 891-895. https://www.ncbi.nlm.nih.gov/pubmed/4567231

Oliver, J. M., & Paterson, A. R. (1971). Nucleoside transport. I. A mediated process in human erythrocytes. *Can J Biochem*, *49*(2), 262-270. https://doi.org/10.1139/o71-038

Osman, A. E. G., & Deininger, M. W. (2021). Chronic Myeloid Leukemia: Modern therapies, current challenges and future directions. *Blood Rev*, *49*, 100825. https://doi.org/10.1016/j.blre.2021.100825

Oxender, D. L., & Christensen, H. N. (1963). Distinct Mediating Systems for the Transport of Neutral Amino Acids by the Ehrlich Cell. *J Biol Chem*, *238*, 3686-3699. https://www.ncbi.nlm.nih.gov/pubmed/14109206

Paproski, R. J., Visser, F., Zhang, J., Tackaberry, T., Damaraju, V., Baldwin, S. A., Young, J. D., & Cass, C. E. (2008). Mutation of Trp29 of human equilibrative nucleoside transporter 1 alters affinity for coronary vasodilator drugs and nucleoside selectivity. *Biochem J*, *414*(2), 291-300. https://doi.org/10.1042/BJ20080074

Patel, D. H., Crawford, C. R., Naeve, C. W., & Belt, J. A. (2000). Cloning, genomic organization and chromosomal localization of the gene encoding the murine sodium-dependent, purine-selective, concentrative nucleoside transporter (CNT2). *Gene*, *242*(1-2), 51-58. https://doi.org/10.1016/s0378-1119(99)00521-1

Pickard, M. A., & Paterson, A. R. (1972). Nucleoside transport in human erythrocytes: equilibrium exchange diffusion of uridine. *Can J Biochem*, *50*(6), 704-705. https://doi.org/10.1139/o72-096

Poppe, D., Tiede, I., Fritz, G., Becker, C., Bartsch, B., Wirtz, S., Strand, D., Tanaka, S., Galle, P. R., Bustelo, X. R., & Neurath, M. F. (2006). Azathioprine suppresses ezrin-radixin-moesin-dependent T cell-

APC conjugation through inhibition of Vav guanosine exchange activity on Rac proteins. *J Immunol*, *176*(1), 640-651. https://doi.org/10.4049/jimmunol.176.1.640

Quistgaard, E. M., Low, C., Guettou, F., & Nordlund, P. (2016). Understanding transport by the major facilitator superfamily (MFS): structures pave the way. *Nat Rev Mol Cell Biol*, *17*(2), 123-132. https://doi.org/10.1038/nrm.2015.25

Reichel, C. (2011). The overlooked difference between human endogenous and recombinant erythropoietins and its implication for sports drug testing and pharmaceutical drug design. *Drug Test Anal*, *3*(11-12), 883-891. https://doi.org/10.1002/dta.388

Reid, G., Wielinga, P., Zelcer, N., De Haas, M., Van Deemter, L., Wijnholds, J., Balzarini, J., & Borst, P. (2003). Characterization of the transport of nucleoside analog drugs by the human multidrug resistance proteins MRP4 and MRP5. *Mol Pharmacol*, *63*(5), 1094-1103. https://doi.org/10.1124/mol.63.5.1094

Ribera, J. M., Garcia, O., Montesinos, P., Brunet, S., Abella, E., Barrios, M., Gonzalez-Campos, J., Bravo, P., Amigo, M. L., & Hernandez-Rivas, J. M. (2012). Treatment of young patients with Philadelphia chromosome-positive acute lymphoblastic leukaemia using increased dose of imatinib and deintensified chemotherapy before allogeneic stem cell transplantation. *Br J Haematol*, *159*(1), 78-81. https://doi.org/10.1111/j.1365-2141.2012.09240.x

Richardson, R. B., Allan, D. S., & Le, Y. (2014). Greater organ involution in highly proliferative tissues associated with the early onset and acceleration of ageing in humans. *Exp Gerontol*, *55*, 80-91. https://doi.org/10.1016/j.exger.2014.03.015

Ritzel, M. W., Ng, A. M., Yao, S. Y., Graham, K., Loewen, S. K., Smith, K. M., Hyde, R. J., Karpinski, E., Cass, C. E., Baldwin, S. A., & Young, J. D. (2001). Recent molecular advances in studies of the concentrative Na+-dependent nucleoside transporter (CNT) family: identification and characterization of novel human and mouse proteins (hCNT3 and mCNT3) broadly selective for purine and pyrimidine nucleosides (system cib). *Mol Membr Biol*, *18*(1), 65-72. https://doi.org/10.1080/09687680010026313

Ritzel, M. W., Yao, S. Y., Huang, M. Y., Elliott, J. F., Cass, C. E., & Young, J. D. (1997). Molecular cloning and functional expression of cDNAs encoding a human Na+-nucleoside cotransporter (hCNT1). *Am J Physiol*, *272*(2 Pt 1), C707-714. https://doi.org/10.1152/ajpcell.1997.272.2.C707

Ritzel, M. W., Yao, S. Y., Ng, A. M., Mackey, J. R., Cass, C. E., & Young, J. D. (1998). Molecular cloning, functional expression and chromosomal localization of a cDNA encoding a human Na+/nucleoside cotransporter (hCNT2) selective for purine nucleosides and uridine. *Mol Membr Biol*, *15*(4), 203-211. https://doi.org/10.3109/09687689709044322

Rose, J. B., Naydenova, Z., Bang, A., Eguchi, M., Sweeney, G., Choi, D. S., Hammond, J. R., & Coe, I. R. (2010). Equilibrative nucleoside transporter 1 plays an essential role in cardioprotection. *Am J Physiol Heart Circ Physiol*, *298*(3), H771-777. https://doi.org/10.1152/ajpheart.00711.2009

Ruan, W., Li, J., Choi, S., Ma, X., Liang, Y., Nair, R., Yuan, X., Mills, T. W., & Eltzschig, H. K. (2023). Targeting myocardial equilibrative nucleoside transporter ENT1 provides cardioprotection by enhancing myeloid Adora2b signaling. *JCI Insight*, *8*(11). https://doi.org/10.1172/jci.insight.166011

Ruel, N. M., Nguyen, K. H., Kim, C. S., Andrade, L. P. S., & Hammond, J. R. (2022). Impact of SLC43A3/ENBT1 Expression and Function on 6-Mercaptopurine Transport and Cytotoxicity in

Human Acute Lymphoblastic Leukemia Cells. *J Pharmacol Exp Ther*, *382*(3), 335-345. https://doi.org/10.1124/jpet.122.001155

Ruel, N. M., Nguyen, K. H., Vilas, G., & Hammond, J. R. (2019). Characterization of 6-Mercaptopurine Transport by the SLC43A3-Encoded Nucleobase Transporter. *Mol Pharmacol*, *95*(6), 584-596. https://doi.org/10.1124/mol.118.114389

Saeki, N., Eguchi, Y., Kintaka, R., Makanae, K., Shichino, Y., Iwasaki, S., Kanno, M., Kimura, N., & Moriya, H. (2020). N-terminal deletion of Swi3 created by the deletion of a dubious ORF YJL175W mitigates protein burden effect in S. cerevisiae. *Sci Rep*, *10*(1), 9500. https://doi.org/10.1038/s41598-020-66307-z

Sauve, S., Williamson, J., Polasa, A., & Moradi, M. (2023). Ins and Outs of Rocker Switch Mechanism in Major Facilitator Superfamily of Transporters. *Membranes (Basel)*, *13*(5). https://doi.org/10.3390/membranes13050462

Schaefer, M. H., Wanker, E. E., & Andrade-Navarro, M. A. (2012). Evolution and function of CAG/polyglutamine repeats in protein-protein interaction networks. *Nucleic Acids Res*, *40*(10), 4273-4287. https://doi.org/10.1093/nar/gks011

Seidel, K., Siswanto, S., Fredrich, M., Bouzrou, M., Brunt, E. R., van Leeuwen, F. W., Kampinga, H. H., Korf, H. W., Rub, U., & den Dunnen, W. F. (2016). Polyglutamine aggregation in Huntington's disease and spinocerebellar ataxia type 3: similar mechanisms in aggregate formation. *Neuropathol Appl Neurobiol*, *42*(2), 153-166. https://doi.org/10.1111/nan.12253

Shaye, O. A., Yadegari, M., Abreu, M. T., Poordad, F., Simon, K., Martin, P., Papadakis, K. A., Ippoliti, A., Vasiliauskas, E., & Tran, T. T. (2007). Hepatotoxicity of 6-mercaptopurine (6-MP) and Azathioprine (AZA) in adult IBD patients. *Am J Gastroenterol*, *102*(11), 2488-2494. https://doi.org/10.1111/j.1572-0241.2007.01515.x

Sheu, H. S., Chen, Y. M., Liao, Y. J., Wei, C. Y., Chen, J. P., Lin, H. J., Hung, W. T., Huang, W. N., & Chen, Y. H. (2022). Thiopurine S-Methyltransferase Polymorphisms Predict Hepatotoxicity in Azathioprine-Treated Patients with Autoimmune Diseases. *J Pers Med*, *12*(9). https://doi.org/10.3390/jpm12091399

Shin, J. Y., Wey, M., Umutesi, H. G., Sun, X., Simecka, J., & Heo, J. (2016). Thiopurine Prodrugs Mediate Immunosuppressive Effects by Interfering with Rac1 Protein Function. *J Biol Chem*, *291*(26), 13699-13714. https://doi.org/10.1074/jbc.M115.694422

Singh, M., Bhatia, P., Khera, S., & Trehan, A. (2017). Emerging role of NUDT15 polymorphisms in 6-mercaptopurine metabolism and dose related toxicity in acute lymphoblastic leukaemia. *Leuk Res*, *62*, 17-22. https://doi.org/10.1016/j.leukres.2017.09.012

Skipper, H. E. (1954). On the mechanism of action of 6-mercaptopurine. *Ann N Y Acad Sci*, *60*(2), 315-321. https://doi.org/10.1111/j.1749-6632.1954.tb40022.x

Smith, K. M., Slugoski, M. D., Loewen, S. K., Ng, A. M., Yao, S. Y., Chen, X. Z., Karpinski, E., Cass, C. E., Baldwin, S. A., & Young, J. D. (2005). The broadly selective human Na+/nucleoside cotransporter (hCNT3) exhibits novel cation-coupled nucleoside transport characteristics. *J Biol Chem*, *280*(27), 25436-25449. https://doi.org/10.1074/jbc.M409454200

Sousa, P., Estevinho, M. M., Dias, C. C., Ministro, P., Kopylov, U., Danese, S., Peyrin-Biroulet, L., & Magro, F. (2020). Thiopurines' Metabolites and Drug Toxicity: A Meta-Analysis. *J Clin Med*, *9*(7). https://doi.org/10.3390/jcm9072216

Stuart, R. O., Pavlova, A., Beier, D., Li, Z., Krijanovski, Y., & Nigam, S. K. (2001). EEG1, a putative transporter expressed during epithelial organogenesis: comparison with embryonic transporter expression during nephrogenesis. *Am J Physiol Renal Physiol*, *281*(6), F1148-1156. https://doi.org/10.1152/ajprenal.2001.281.6.F1148

Suarez-Almazor, M. E., Spooner, C., & Belseck, E. (2000). Azathioprine for treating rheumatoid arthritis. *Cochrane Database Syst Rev*(4), CD001461. https://doi.org/10.1002/14651858.CD001461

Takenaka, R., Yasujima, T., Furukawa, J., Hishikawa, Y., Yamashiro, T., Ohta, K., Inoue, K., & Yuasa, H. (2020). Functional Analysis of the Role of Equilibrative Nucleobase Transporter 1 (ENBT1/SLC43A3) in Adenine Transport in HepG2 Cells. *J Pharm Sci*, *109*(8), 2622-2628. https://doi.org/10.1016/j.xphs.2020.04.013

Tanaka, Y., Manabe, A., Fukushima, H., Suzuki, R., Nakadate, H., Kondoh, K., Nakamura, K., Koh, K., Fukushima, T., Tsuchida, M., Koike, K., Kiyokawa, N., Noguchi, E., Sumazaki, R., & Komiyama, T. (2015). Multidrug resistance protein 4 (MRP4) polymorphisms impact the 6-mercaptopurine dose tolerance during maintenance therapy in Japanese childhood acute lymphoblastic leukemia. *Pharmacogenomics J*, *15*(4), 380-384. https://doi.org/10.1038/tpj.2014.74

Tay, B. S., Lilley, R. M., Murray, A. W., & Atkinson, M. R. (1969). Inhibition of phosphoribosyl pyrophosphate amidotransferase from Ehrlich ascites-tumour cells by thiopurine nucleotides. *Biochem Pharmacol*, *18*(4), 936-938. https://doi.org/10.1016/0006-2952(69)90069-0

Thul, P. J., Akesson, L., Wiking, M., Mahdessian, D., Geladaki, A., Ait Blal, H., Alm, T., Asplund, A., Bjork, L., Breckels, L. M., Backstrom, A., Danielsson, F., Fagerberg, L., Fall, J., Gatto, L., Gnann, C., Hober, S., Hjelmare, M., Johansson, F., . . . Lundberg, E. (2017). A subcellular map of the human proteome. *Science*, *356*(6340). https://doi.org/10.1126/science.aal3321

Toksvang, L. N., Lee, S. H. R., Yang, J. J., & Schmiegelow, K. (2022). Maintenance therapy for acute lymphoblastic leukemia: basic science and clinical translations. *Leukemia*, *36*(7), 1749-1758. https://doi.org/10.1038/s41375-022-01591-4

Toksvang, L. N., Schmidt, M. S., Arup, S., Larsen, R. H., Frandsen, T. L., Schmiegelow, K., & Rank, C. U. (2019). Hepatotoxicity during 6-thioguanine treatment in inflammatory bowel disease and childhood acute lymphoblastic leukaemia: A systematic review. *PLoS One*, *14*(5), e0212157. https://doi.org/10.1371/journal.pone.0212157

Tsukaguchi, H., Tokui, T., Mackenzie, B., Berger, U. V., Chen, X. Z., Wang, Y., Brubaker, R. F., & Hediger, M. A. (1999). A family of mammalian Na+-dependent L-ascorbic acid transporters. *Nature*, *399*(6731), 70-75. https://doi.org/10.1038/19986

Uhlen, M., Fagerberg, L., Hallstrom, B. M., Lindskog, C., Oksvold, P., Mardinoglu, A., Sivertsson, A., Kampf, C., Sjostedt, E., Asplund, A., Olsson, I., Edlund, K., Lundberg, E., Navani, S., Szigyarto, C. A., Odeberg, J., Djureinovic, D., Takanen, J. O., Hober, S., . . . Ponten, F. (2015). Proteomics. Tissue-based map of the human proteome. *Science*, *347*(6220), 1260419. https://doi.org/10.1126/science.1260419

van Asseldonk, D. P., Seinen, M. L., de Boer, N. K., van Bodegraven, A. A., & Mulder, C. J. (2012). Hepatotoxicity associated with 6-methyl mercaptopurine formation during azathioprine and 6-mercaptopurine therapy does not occur on the short-term during 6-thioguanine therapy in IBD treatment. *J Crohns Colitis*, *6*(1), 95-101. https://doi.org/10.1016/j.crohns.2011.07.009

Varadi, M., Anyango, S., Deshpande, M., Nair, S., Natassia, C., Yordanova, G., Yuan, D., Stroe, O., Wood, G., Laydon, A., Zidek, A., Green, T., Tunyasuvunakool, K., Petersen, S., Jumper, J., Clancy, E., Green, R., Vora, A., Lutfi, M., . . . Velankar, S. (2022). AlphaFold Protein Structure Database: massively expanding the structural coverage of protein-sequence space with high-accuracy models. *Nucleic Acids Res*, *50*(D1), D439-D444. https://doi.org/10.1093/nar/gkab1061

Vauquelin, G. (2016). Effects of target binding kinetics on in vivo drug efficacy: koff , kon and rebinding. *Br J Pharmacol*, *173*(15), 2319-2334. https://doi.org/10.1111/bph.13504

Vilpo, J. A., Vilpo, L. M., Szymkowski, D. E., O'Donovan, A., & Wood, R. D. (1995). An XPG DNA repair defect causing mutagen hypersensitivity in mouse leukemia L1210 cells. *Mol Cell Biol*, *15*(1), 290-297. https://doi.org/10.1128/MCB.15.1.290

Wang, Q., & Holst, J. (2015). L-type amino acid transport and cancer: targeting the mTORC1 pathway to inhibit neoplasia. *Am J Cancer Res*, *5*(4), 1281-1294. https://www.ncbi.nlm.nih.gov/pubmed/26101697

Wielinga, P. R., Reid, G., Challa, E. E., van der Heijden, I., van Deemter, L., de Haas, M., Mol, C., Kuil, A. J., Groeneveld, E., Schuetz, J. D., Brouwer, C., De Abreu, R. A., Wijnholds, J., Beijnen, J. H., & Borst, P. (2002). Thiopurine metabolism and identification of the thiopurine metabolites transported by MRP4 and MRP5 overexpressed in human embryonic kidney cells. *Mol Pharmacol*, *62*(6), 1321-1331. https://doi.org/10.1124/mol.62.6.1321

Wu, K. H., Wu, H. P., Weng, T., Peng, C. T., & Chao, Y. H. (2015). Dasatinib for a child with Philadelphia chromosome-positive acute lymphoblastic leukemia and persistently elevated minimal residual disease during imatinib therapy. *Curr Oncol*, *22*(4), 303-306. https://doi.org/10.3747/co.22.2719

Wu, S. G., & Shih, J. Y. (2018). Management of acquired resistance to EGFR TKI-targeted therapy in advanced non-small cell lung cancer. *Mol Cancer*, *17*(1), 38. https://doi.org/10.1186/s12943-018-0777-1

Yamamoto, S., Inoue, K., Murata, T., Kamigaso, S., Yasujima, T., Maeda, J. Y., Yoshida, Y., Ohta, K. Y., & Yuasa, H. (2010). Identification and functional characterization of the first nucleobase transporter in mammals: implication in the species difference in the intestinal absorption mechanism of nucleobases and their analogs between higher primates and other mammals. *J Biol Chem*, *285*(9), 6522-6531. https://doi.org/10.1074/jbc.M109.032961

Yan, N. (2015). Structural Biology of the Major Facilitator Superfamily Transporters. *Annu Rev Biophys*, *44*, 257-283. https://doi.org/10.1146/annurev-biophys-060414-033901

Yanagida, O., Kanai, Y., Chairoungdua, A., Kim, D. K., Segawa, H., Nii, T., Cha, S. H., Matsuo, H., Fukushima, J., Fukasawa, Y., Tani, Y., Taketani, Y., Uchino, H., Kim, J. Y., Inatomi, J., Okayasu, I., Miyamoto, K., Takeda, E., Goya, T., & Endou, H. (2001). Human L-type amino acid transporter 1 (LAT1): characterization of function and expression in tumor cell lines. *Biochim Biophys Acta*, *1514*(2), 291-302. https://doi.org/10.1016/s0005-2736(01)00384-4

Yang, C., & Leung, G. P. (2015). Equilibrative Nucleoside Transporters 1 and 4: Which One Is a Better Target for Cardioprotection Against Ischemia-Reperfusion Injury? *J Cardiovasc Pharmacol*, *65*(6), 517-521. https://doi.org/10.1097/FJC.0000000000000194

Yang, H., Li, X., Li, G., Huang, H., Yang, W., Jiang, X., Sen, M., Liu, J., Liu, Y., Pan, Y., & Wang, G. (2021). Accurate quantitative determination of affinity and binding kinetics for tight binding inhibition

of xanthine oxidase. *Biomed Pharmacother*, *139*, 111664. https://doi.org/10.1016/j.biopha.2021.111664

Yao, S. Y., Ng, A. M., Muzyka, W. R., Griffiths, M., Cass, C. E., Baldwin, S. A., & Young, J. D. (1997). Molecular cloning and functional characterization of nitrobenzylthioinosine (NBMPR)-sensitive (es) and NBMPR-insensitive (ei) equilibrative nucleoside transporter proteins (rENT1 and rENT2) from rat tissues. *J Biol Chem*, *272*(45), 28423-28430. https://doi.org/10.1074/jbc.272.45.28423

Yoneda, K., Imanishi, N., Ichiki, Y., & Tanaka, F. (2019). Treatment of Non-small Cell Lung Cancer with EGFR-mutations. *J UOEH*, *41*(2), 153-163. https://doi.org/10.7888/juoeh.41.153

Yoshimaru, R., & Minami, Y. (2023). Genetic Landscape of Chronic Myeloid Leukemia and a Novel Targeted Drug for Overcoming Resistance. *Int J Mol Sci*, *24*(18). https://doi.org/10.3390/ijms241813806

Young, J. D., Yao, S. Y., Baldwin, J. M., Cass, C. E., & Baldwin, S. A. (2013). The human concentrative and equilibrative nucleoside transporter families, SLC28 and SLC29. *Mol Aspects Med*, *34*(2-3), 529-547. https://doi.org/10.1016/j.mam.2012.05.007

Yuasa, H., Yasujima, T., & Inoue, K. (2020). Current Understanding of the Intestinal Absorption of Nucleobases and Analogs. *Biol Pharm Bull*, *43*(9), 1293-1300. https://doi.org/10.1248/bpb.b20-00342

Zaza, G., Cheok, M., Krynetskaia, N., Thorn, C., Stocco, G., Hebert, J. M., McLeod, H., Weinshilboum, R. M., Relling, M. V., Evans, W. E., Klein, T. E., & Altman, R. B. (2010). Thiopurine pathway. *Pharmacogenet Genomics*, *20*(9), 573-574. https://doi.org/10.1097/FPC.0b013e328334338f

Zhu, J., & Thompson, C. B. (2019). Metabolic regulation of cell growth and proliferation. *Nat Rev Mol Cell Biol*, *20*(7), 436-450. https://doi.org/10.1038/s41580-019-0123-5

Zimm, S., Collins, J. M., Riccardi, R., O'Neill, D., Narang, P. K., Chabner, B., & Poplack, D. G. (1983). Variable bioavailability of oral mercaptopurine. Is maintenance chemotherapy in acute lymphoblastic leukemia being optimally delivered? *N Engl J Med*, *308*(17), 1005-1009. https://doi.org/10.1056/NEJM198304283081705

Zou, Y., Gao, W., Jin, H., Mao, C., Zhang, Y., Wang, X., Mei, D., & Zhao, L. (2023). Cellular Uptake and Transport Mechanism of 6-Mercaptopurine Nanomedicines for Enhanced Oral Bioavailability. *Int J Nanomedicine*, *18*, 79-94. https://doi.org/10.2147/IJN.S394819

Appendix

The following work is unpublished data that several Hammond laboratory members contributed towards, which will be compiled into a single manuscript and published. Data obtained by each contributor is to be presented in its entirety in their perspective thesis manuscript. Data that I did not produce with my own hands, but is relevant to this thesis, will only be mentioned and cited as personal communications.

Introduction

Tyrosine kinase inhibitors (TKI) have emerged as a revolutionary class of drugs in the field of cancer therapy, offering targeted treatment options for a variety of malignancies. These inhibitors work by binding to the tyrosine kinase ATP-binding domain and blocking phosphorylation of Bcr-Abl substrates, therefore preventing activation of downstream pathways that are crucial for cell growth and proliferation (Yoshimaru and Minaami, 2023). By disrupting these signaling pathways, TKIs effectively impede the proliferation and spread of cancer cells (Osman and Deininger, 2021; Yoshimaru and Minaami, 2023). One of the most notable applications of TKIs is in the treatment of CML and Philadelphia chromosome-positive (Ph+) ALL, which are variants of leukemia characterized by expression of the Bcr-Abl fusion oncogene. Also synonymously referred to as the Philadelphia chromosome, Bcr-Abl is the consequence of the fusion of the break point cluster (Bcr) gene at chromosome 22 and the Abelson (Abl) tyrosine kinase gene at chromosome 9. This fusion oncogene contains a constitutively activated tyrosine kinase that when targeted by TKIs, leads to decreased cell proliferation and cell survival. Bcr-Abl TKI drugs such as imatinib, dasatinib, and nilotinib demonstrate remarkable efficacy and are a prime example of precision medicine and tailoring treatments to the unique molecular characteristics of an individual's cancer (Osman and Deininger, 2021; Yoshimaru and Minaami, 2023). Beyond CML, TKIs have also found utility in several other cancer types, such as non-small cell lung cancer (NSCLC) (Wu et al., 2018; Yoneda et al., 2019). Epidermal growth factor receptor (EGFR) TKI drugs such as gefitinib and erlotinib have shown significant benefits in NSCLC patients, as a targeted therapy that offers a more favorable side effect profile compared to traditional chemotherapy, resulting in improved quality of life for patients undergoing treatment (Yoneda et al., 2019).

While TKIs have revolutionized cancer therapy, their usage is not without challenges, such as the development of TKI resistance in CML patients, through Bcr-Abl kinase domain mutations (Kockerols et al., 2023; Yoshimaru and Minaami, 2023) or EGFR kinase domain mutations (Wu et al., 2018; Yoneda et al., 2019; Girard N., 2022). Furthermore, Damaraju and colleagues, (2015) exhibited that various TKIs can interfere with sodium-independent nucleobase cellular accumulation in human renal proximal tubule epithelial cells (RPTEC). The identity of the affected sodium-independent nucleobase transporter was not stated, however, Damaraju and colleagues, (2015) [^{3}H]adenine inhibition kinetic data suggested ENBT1 was a strong candidate. In order of relative inhibitory potency of [^{3}H]adenine uptake, some TKIs investigated by Damaraju and colleagues, (2015) were gefitinib (IC_{50}: 0.7 ± 0.1 μM), erolotinib (IC_{50}: 15 ± 6 μM), imatinib (IC_{50}: 60 ± 14 μM), and dasatinib (IC_{50}: >100 μM). Bcr-Abl TKI drugs such as imatinib and dasatinib are utilized alongside 6-MP in Ph+ ALL combination therapy (Ribera et al., 2012; Wu et al., 2015). Interactions between drugs are of concern as co-treatment may potentially lead to inhibition of ENBT1-mediated 6-MP cellular accumulation, thus blunting the efficacy 6-MP and negatively affecting Ph+ ALL combination therapy.

Results

The Hammond laboratory replicated Damaraju and colleagues, 2015 work in HEK293-hSLC43A3 cells and confirmed significant inhibition of ENBT1-mediated [^{3}H]adenine uptake, relative to 100% control, by 10 μM TKI: gefitinib ($p<0.001$, n=7), dasatinib ($p=0.004$, n=6), and imatinib ($p=0.015$, n=6). Erlotinib (n=6) and nilotinib (n=6) were also assessed but shown to have no significant effect, stats were obtained via ordinary one-way ANOVA multiple comparisons (NM. Ruel, personal communication, February 15, 2019). Subsequently, gefitinib was followed up on as the highest potency inhibitor and gefitinib inhibition kinetics were

assessed in K562 cells, which is a human leukemia cell line derived from an adult CML patient, in the same manner as described in section 4.2.d, utilizing 30 μM [^{3}H]6-MP and concentrations of gefitinib ranging from 30 nM – 100 μM. Gefitinib exhibited concentration-dependent inhibition of ENBT1-mediated [^{3}H]adenine uptake relative to the 100% uptake control, reaching near complete inhibition at 100 μM gefitinib. Gefitinib K_i value was calculated to be 2.5 ± 0.9 μM in K562 cells (NM. Ruel, personal communication, September 20, 2019). Based on these preliminary results, we hypothesized that relative to 6-MP mono-treatment, 6-MP co-treatment with a sub-cytotoxic concentration of gefitinib would result in a rightward shifted 6-MP EC_{50} value due to gefitinib inhibiting ENBT1-mediated 6-MP uptake and blunting 6-MP effect on cell viability.

This hypothesis was tested on K562 cells via 6-MP cell viability assays in presence or absence of gefitinib. To better assess hypothesized antagonistic effect of 6-MP and gefitinib co-treatment, gefitinib effect on cell viability was minimized by determining a sub-cytotoxic concentration of gefitinib/concentration of gefitinib that does not affect cell viability, that also adequately inhibited ENBT1-mediated [^{3}H]adenine uptake. Compound-mediated response, 100% cell viability, 0% cell viability, and % reduced MTT were obtained and calculated as described previously in section 3.7, in K562 cells utilizing gefitinib (3 nM – 50 μM). Gefitinib exhibited an incomplete cell viability curve with an extrapolated EC_{50} value of 90.4 ± 30.5 μM (Figure 21.A). Based on this gefitinib cell viability curve, 3 μM gefitinib (dotted line) was determined to be sub-cytotoxic in K562 cells (Figure 21.A). When compared to the previously described gefitinib inhibition profile performed in K562 cells, 3 μM gefitinib produced roughly 50% inhibition of ENBT1-mediated [^{3}H]adenine uptake relative to the 100% uptake control (NM. Ruel, personal communication, March 29, 2019). Subsequently, K562 cells were co-treated with 6-MP (80 nM

– 1.28 mM) in presence of 3 μM gefitinib or equal volumes of solvent (DMSO). K562 cells exhibited a biphasic 6-MP cell viability curve with first-phase EC_{50} values of 1.26 ± 0.23 μM and 0.65 ± 0.09 μM for 6-MP gefitinib(-) and 6-MP gefitinib(+) conditions, respectively. F-test analysis of 6-MP gefitinib(-) and 6-MP gefitinib(+), 6-MP first-phase EC_{50} values determined a significant difference (Extra sum-of-squares F-test, $F_{1,198}$=16.42, p<0.0001, n=7). These results exhibited a leftward shifted 6-MP EC_{50} value in presence of gefitinib, suggesting gefitinib actually potentiated 6-MP effect on cell viability (Figure 21.B). However, these results were not replicable and further experiments suggested gefitinib did not affect 6-MP effect on cell viability (NM. Ruel, personal communication, November 20, 2019).

Much like 6-MP, TKI drugs require transport into cells to interact with intracellular tyrosine kinase domains, however, there is no known transporter for gefitinib. To indirectly determine whether gefitinib is an ENBT1 substrate and acted as a competitive inhibitor, gefitinib cell viability assays were performed in transfected-HEK293 cells. We hypothesized that if ENBT1 mediated the cellular accumulation of a compound that has cytotoxic properties or is otherwise detrimental to cellular mitochondria function, HEK293-hSLC43A3 and HEK293-mslc43a3 cells which express hENBT1 and mENBT1, should upon treatment exhibit higher sensitivity or a leftward shift in cell viability, relative to HEK293-EV cells which do not express either transporter. Compound-mediated response, 100% cell viability, 0% cell viability, and % reduced MTT were obtained and calculated as described previously in section 3.7, utilizing gefitinib (12 nM – 200 μM). HEK293 cells exhibited a single-phase 6-MP cell viability curve with first-phase EC_{50} values of 24 ± 3 μM, 25 ± 2 μM and 23 ± 6 μM for HEK293-EV, HEK293-hSLC43A3, and HEK293-mslc43a3 cells, respectively. F-test analysis of HEK293 cell first-phase EC_{50} values determined no significant difference (Extra sum-of-squares F-test, $F_{2,216}$=1.417, p=0.245,

n=5), suggesting that hENBT1 and mENBT1 do not mediate gefitinib effect on cell viability, therefore gefitinib is not an ENBT1 substrate (Figure 21.C).

Summary

Data described and presented in this appendix display **(1):** in order of relative potency, 10 μM TKI: gefitinib, dasatinib, and imatinib significantly inhibit ENBT1-mediated [^{3}H]adenine uptake, in order of relative potency (NM. Ruel, personal communication, February 15, 2019). **(2):** gefitinib inhibition of ENBT1-mediated [^{3}H]adenine uptake is concentration-dependent with a K_i value of 3.2 ± 1.0 μM in HEK293-hSLC43A3 cells (NM. Ruel, personal communication,). **(3):** 3 μM gefitinib is sub-cytotoxic to K562 cells and inhibits roughly 29% of ENBT1-mediated [^{3}H]adenine uptake (Figure 21.A) (NM. Ruel, personal communication, March 29, 2019). **(4)**: K562 cell co-treatment with 6-MP and gefitinib shifted 6-MP EC_{50} to the left, suggesting an increase in 6-MP sensitivity (Figure 21.B). However, these results have not been replicable (NM. Ruel, personal communication, November 20, 2019). **(5):** HEK293-EV, HEK293-hSLC43A3, and HEK293-mslc43a3 are functionally similar in mediating gefitinib effect on cell viability (Figure 21.C).

Limitations

Despite investigating Bcr-Abl TKI drugs in context of combination therapy with 6-MP for the treatment of CML and Ph+ ALL, this work focused on the EGFR TKI drug gefitinib, which is utilized for treatment of NSCLC and is not administrated alongside 6-MP. Thus, this

work currently has no direct clinical relevance. Additionally, it is possible that the sub-cytotoxic concentration of gefitinib is not adequate to sufficiently inhibit ENBT1-mediated 6-MP uptake to impact 6-MP EC_{50} values in K562 cells. Instead, a concentration of gefitinib that fully inhibits ENBT1-mediated 6-MP uptake should be utilized rather than a sub-cytotoxic concentration. At the time, there was value in utilizing a sub-cytotoxic concentration of gefitinib. However, gefitinib effect on cell viability could instead, be accounted for by subtracting the cell viability of a gefitinib treated group, from a co-treated group. This would be necessary to determine whether gefitinib has no effect on 6-MP efficacy or is not high enough concentration to have an effect on 6-MP efficacy.

Closing Remarks

TKI drugs such as gefitinib, dasatinib, and imatinib have been shown to interfere with the nucleobase flux capacity of ENBT1 (NM. Ruel, personal communication, February 15, 2019). 6-MP and gefitinib co-treatment potentiated 6-MP effect on cell viability rather than blunting it as hypothesized (Figure 21.B). Gefitinib inhibition of XO was proposed as the mechanism of action for increased 6-MP, through shunting 6-MP metabolism away from the XO pathway and towards the TPMT and HGPRT pathways. However, K562 cells are known to have low XO expression levels and co-treatment of 6-MP and allopurinol, an XO inhibitor, did not affect 6-MP effect on cell viability (NM. Ruel, personal communication, October 9, 2019; NM. Ruel, personal communication, November 20, 2019). Due to lack of a mechanism of action and overall inability to replicate initial findings of gefitinib potentiating 6-MP effect on cell viability, investigating potential drug-drug interactions between 6-MP and gefitinib at ENBT1 were put on hold. Instead, the relationship between ENBT1 and gefitinib was explored to investigate how gefitinib

is transported into cells to act on intracellular EGFR tyrosine kinases. It was indirectly determined that gefitinib is not an ENBT1 substrate/competitive inhibitor (Figure 21.C), and thus inhibits ENBT1 through a non-competitive or uncompetitive mechanism. The Hammond laboratory has also observed that TKI drugs relatively potently (<100 μM range) interfere with the nucleoside flux capacity of ENT2 (N. Shahid, personal communication, August 31, 2022). Therefore, the ENTs may be a more promising candidate transporter system for mediating gefitinib uptake.

Figure 21. Gefitinib cell viability in K562 and transfected-HEK293 ►

Gefitinib cell viability curves in K562, HEK293-hSLC43A3, HEK293-mslc43a3, and HEK293-EV cells plated in complete media, treated with 3 nM – 1.28 mM of various compounds for 48 hours. **A:** K562 cells gefitinib cell viability curve showing single-phase nature of gefitinib response. 3 μM gefitinib was determined as a sub-cytotoxic concentration (n=5). **B:** K562 cells 6-MP + gefitinib cell viability curve showing biphasic nature of 6-MP ± gefitinib response and a ~2-fold leftward 6-MP EC50 value shift in presence of 3 μM gefitinib (n=7). **C:** Transfected-HEK293 cells gefitinib cell viability curve showing single-phase nature of gefitinib response and no HEK293-hSLC43A3 and HEK293-mslc43a3 curve shift, relative to HEK293-EV (n=5). Data are shown as mean ± SD.

Figure 21.

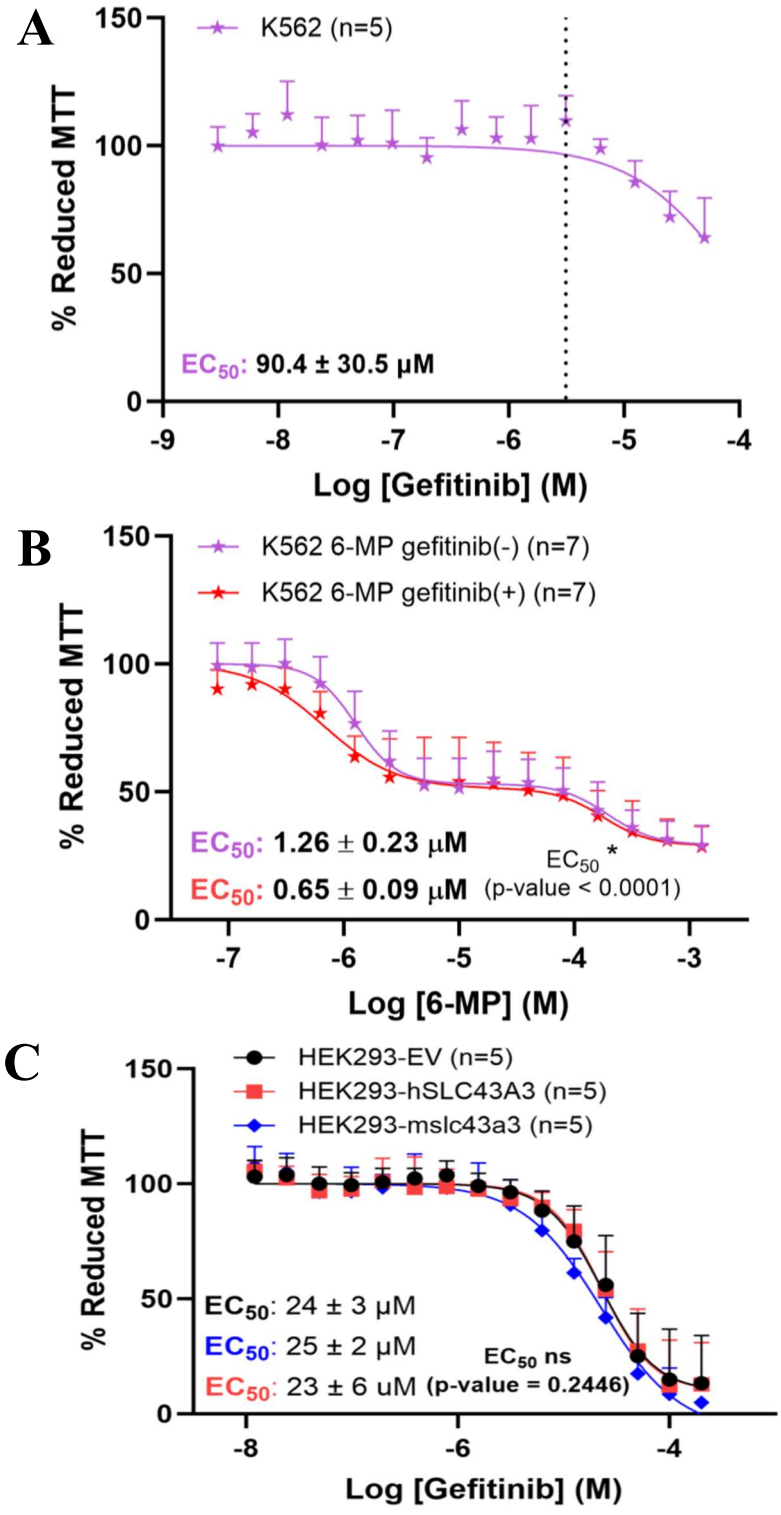
A
K562 (n=5)
% Reduced MTT
150
100
50
0
EC50: 90.4 ± 30.5 µM
-9
-8
-7
-6
-5
-4
Log [Gefitinib] (M)
B
K562 6-MP gefitinib(-) (n=7)
K562 6-MP gefitinib(+) (n=7)
% Reduced MTT
EC50: 1.26 ± 0.23 µM
EC50 *
EC50: 0.65 ± 0.09 µM (p-value < 0.0001)
-7
-6
-5
-4
-3
Log [6-MP] (M)
C
HEK293-EV (n=5)
HEK293-hSLC43A3 (n=5)
HEK293-mslc43a3 (n=5)
% Reduced MTT
EC50: 24 ± 3 µM
EC50: 25 ± 2 µM
EC50 ns
EC50: 23 ± 6 uM (p-value = 0.2446)
-8
-6
-4
Log [Gefitinib] (M)